POLITECNICO
MILANO 1863

SCUOLA DI INGEGNERIA INDUSTRIALE
E DELL'INFORMAZIONE

Techno-Economic and Environmental Assessment of an Autonomous Desalination System powered with Hybrid Renewable Energy Sources and Design of a Reverse Osmosis plant with a capacity of 2,000 m^3/day

TESI DI LAUREA MAGISTRALE IN
ENERGY ENGINEERING-INGEGNERIA ENERGETICA

Author: **Alberto Pilato Colomar**

Student ID: 935893
Advisor: Giampaolo Manzolini
Academic Year: 2020-2021

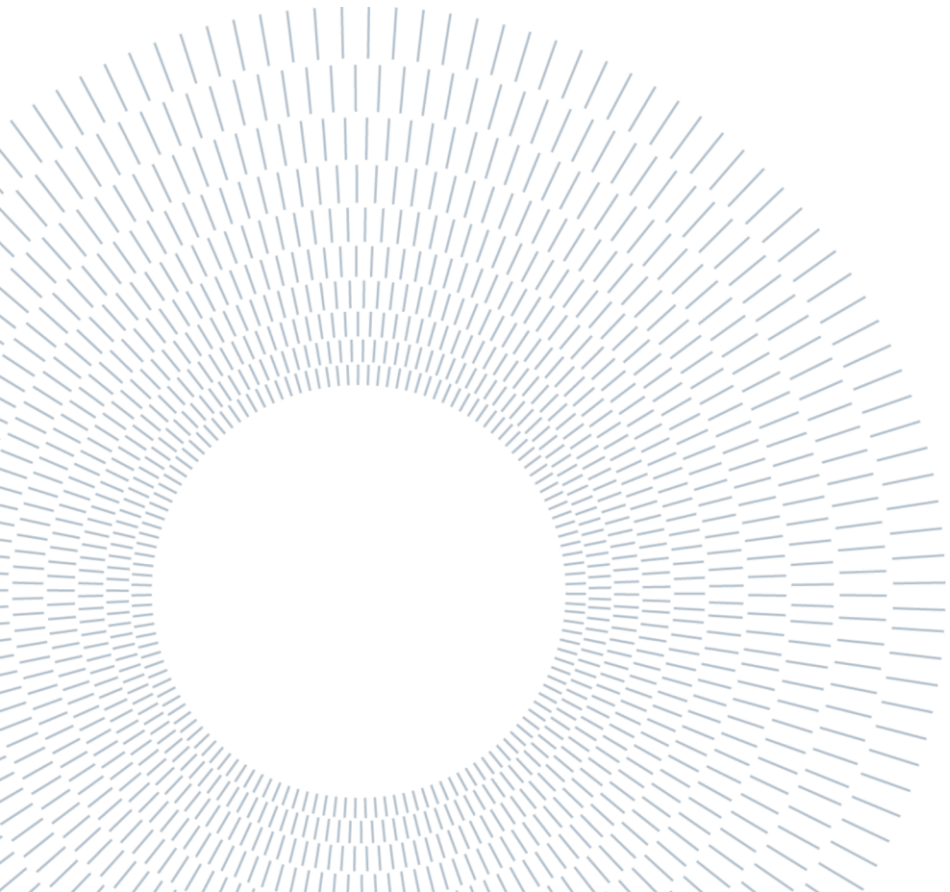

Abstract

Freshwater scarcity is one of the most important problems facing the world today. The rapid growth in energy and water demand is having a strong impact on climate change and thus the depletion of freshwater reserves. Seawater desalination is a viable solution to produce fresh water, especially in coastal areas. However, its sustainability is constrained by the high energy consumption of current technologies. Renewable energy is an attractive solution to power desalination plants to reduce costs and carbon emissions. The aim of this work is to design a seawater reverse osmosis desalination plant with a capacity of 2,000 m^3/day and then hybrid renewable energy system to meet the electrical load demand of the autonomous desalination plant that will be in the island El Hierro, Spain.

In this way, the procedure is to find the optimal sizing through a techno-economic and environmental assessment of different off-grid hybrid energy configurations by means of the HOMER Pro™ software. Two off-grid scenarios (with and without diesel generator) with different energy system configurations were proposed and compared to each other. In both scenarios, the energy power systems are a combination of a photovoltaic, wind turbine, and batteries. On the other hand, it is necessary to design the seawater reverse osmosis plant which consist of the pre-treatment where the ultrafiltration stage is made with the WAVE™ software, the reverse osmosis process and post-treatment by means of the IMSDesign™ software. In addition, thanks to the incorporation of an energy recovery device, the specific energy consumption of the plant is reduced to a value of 2.18 kWh/m^3. Besides, the optimization results of the hybrid renewable energy systems shows that the best configuration which minimizes the net present cost consisted of the 550-kW diesel generator, 274-kW photovoltaic system, 28 wind turbines, 518 batteries of 1.02 kWh, and 341-kW DC/AC converter based on the site power resources and the profile of electricity demand. Furthermore, the implementation of a water tank replacing the batteries has also been considered. This resulted in a 10% reduction of the NPC. Finally, the whole system showed reduced water production cost values compared to other similar technologies.

Keywords: Seawater reverse osmosis desalination, hybrid renewable energy system, autonomous desalination plant, off-grid hybrid energy configurations, specific energy consumption, energy recovery device.

Abstract in lingua italiana

La scarsità di acqua dolce è uno dei problemi più importanti che il mondo deve affrontare oggi. La rapida crescita della domanda di energia e di acqua sta avendo un forte impatto sul cambiamento climatico e quindi sull'esaurimento delle riserve di acqua dolce. La desalinizzazione dell'acqua di mare è una soluzione praticabile per produrre acqua dolce, specialmente nelle aree costiere. Tuttavia, la sua sostenibilità è limitata dall'alto consumo energetico delle tecnologie attuali. L'energia rinnovabile è una soluzione attraente per alimentare gli impianti di dissalazione per ridurre i costi e le emissioni di carbonio. Lo scopo di questo lavoro è quello di progettare un impianto di desalinizzazione ad osmosi inversa dell'acqua di mare con una capacità di 2.000 m^3/giorno e poi un sistema ibrido di energia rinnovabile per soddisfare la domanda di carico elettrico dell'impianto di desalinizzazione autonomo che sarà nell'isola El Hierro, Spagna.

In questo modo, la procedura è quella di trovare il dimensionamento ottimale attraverso una valutazione tecnico-economica e ambientale di diverse configurazioni di energia ibrida off-grid per mezzo del software HOMER Pro™. Sono stati proposti e confrontati tra loro due scenari off-grid (con e senza generatore diesel) con diverse configurazioni di sistema energetico. In entrambi gli scenari, i sistemi di alimentazione energetica sono una combinazione di fotovoltaico, turbina eolica e batterie. D'altra parte, è necessario progettare l'impianto di osmosi inversa dell'acqua di mare che consiste nel pre-trattamento dove la fase di ultrafiltrazione è fatta con il software WAVE™, il processo di osmosi inversa e il post-trattamento per mezzo del software IMSDesign™. Inoltre, grazie all'incorporazione di un dispositivo di recupero energetico, il consumo energetico specifico dell'impianto è ridotto a un valore di 2,18 kWh/m^3. Inoltre, i risultati dell'ottimizzazione dei sistemi ibridi di energia rinnovabile mostrano che la migliore configurazione che minimizza il costo attuale netto consisteva in un generatore diesel da 550 kW, un impianto fotovoltaico da 274 kW, 28 turbine eoliche, 518 batterie da 1,02 kWh e un convertitore DC/AC da 341 kW in base alle risorse energetiche del sito e al profilo della domanda elettrica. Inoltre, è stata considerata anche l'implementazione di un serbatoio d'acqua in sostituzione delle batterie. Questo ha portato a una riduzione del 10% dell'NPC. Infine, l'intero sistema ha mostrato valori di costo di produzione dell'acqua ridotti rispetto ad altre tecnologie simili.

Parole chiave: Dissalazione ad osmosi inversa dell'acqua di mare, sistema ibrido di energia rinnovabile, impianto di dissalazione autonomo, configurazioni energetiche ibride

Contents

1. An Overview of Seawater Desalination Technologies

1.1 The need of Desalination

Water is a crucial resource for the existence of humankind (60% of the mass of the human body is water) on the earth and is relevant to promote socio-economic development. Only 0.5% of the total world's water corresponds to fresh water. The rest is salt water. But only fresh water is required for agricultural, community and domestic uses. Today, unfortunately, 25% of the world's total population is suffering from inadequate and precarious fresh water supply [1]. According to the *Comprehensive Assessment of Water Management in Agriculture,* 1/3 people today are dealing with water shortages in Developing Countries (DCs) [2]. The rapid population growth which is shown in the Figure 1.1 fostered by an improvement of standards of living will cause an increase of global freshwater demand (See **¡Error! No se encuentra el origen de la referencia.**) and severe water outages over the next decades. Most countries in the Middle East and North Africa suffer from water scarcity, as well as more developed countries such as Mexico, Pakistan, and large parts of China and India [3]. The lack of fresh water damages the economic development, threatens human health, leads to environmental degradation, and foments political instability. Thus, Goal 6 from the agenda 2030 was created to ensure availability and sustainable management of water and sanitation for all. Therefore, it is crucial to find out alternative energy sources to obtain fresh water to cope up the increasing demand. As a result, different seawater desalination techniques have emerged as the keys to sustain future generations from all over the world.

Desalination is a term used to remove salts and dissolved solids from seawater, brackish water, or wastewater to produce freshwater. Freshwater is obtained when water contains less than 1000 mg/L of salts or other dissolved solids [4]. Desalination technologies might reduce water scarcity by using large part of seawater that appear to be available into new sources of water supply.

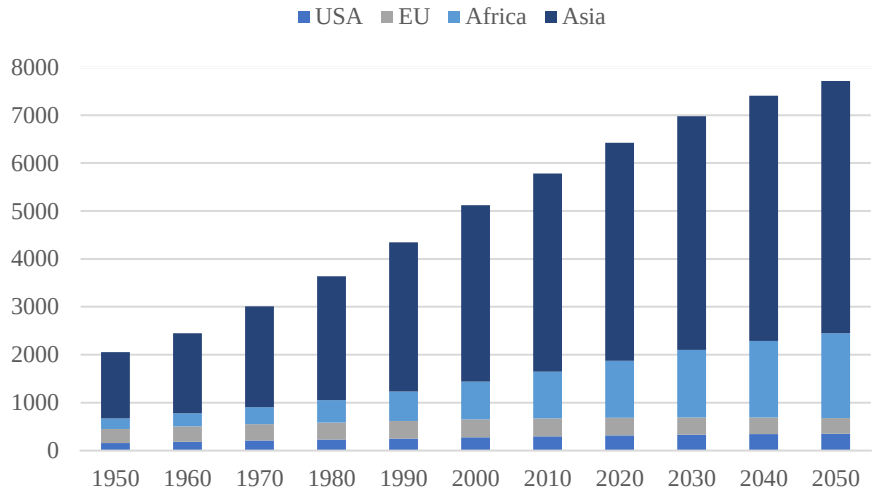

Figure 1.1: Expected distribution of population worldwide during the years 1950-2050 (millions of inhabitants). Extracted data from Food and Agricultural Organization of the United Nations database.

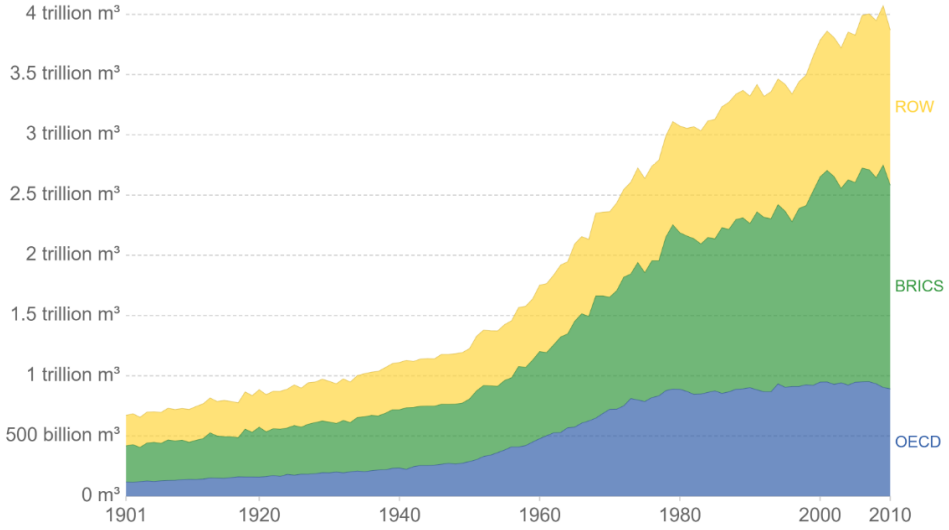

Figure 1.2: Freshwater use by aggregated region, 1901 to 2010. Courtesy of Global International Geosphere-Biosphere Program (IGB)[1]

[1] Global freshwater withdrawals for agricultural, industrial, and domestic uses by aggregated regional groups. Organisation for Economic Co-operation and Development (OECD) countries which are most European countries. BRICS countries are Brazil, Russia, India, China, and South Africa. ROW refers to the rest of the World

1.2 Water Resource and data

Water is one of the most abundant and important resources present on the planet; Whereas seawater represents the 97,5% of the total available water, only a 0,5 % corresponds to the available freshwater found in lakes, rivers, and aquifers. The rest is constituted by underground and surface waters.

The water experiments a renewable cycle that makes the total amount of water constant over time. Firstly, water close to seashore evaporates into the atmosphere due to the difference in temperatures between the land surface and the sea. The steam is accumulated in clouds from which rainfall originates. Thus, precipitated water in turns feed into underground and surface waters. Obviously, the local availability depends on the level of precipitations. The higher the level of precipitation, the higher the local availability of freshwater is.

The main difference between freshwater and seawater is related to the relative amount of salt found in them. In the Table 1.1 is shown all the water variety according to the amount of the total dissolved solids (TDS) measured in ppm. Thus, the reference average salinity of seawater is about 35000 ppm. Then, the Table 1.2 includes the typical seawater composition which is essentially constant throughout the world but differs from that one from the river, which is shown in the Table 1.3. The main highlight is that sodium chloride content in the river water is much lower than in the seawater but, conversely, calcium and bicarbonate content is far higher.

Type	Total dissolved solids (TDS) in ppm
Freshwater	Up to 1,500
Brackish water	1,500-10,000
Salt water	>10,000
Seawater	10,000-45,000
Standard seawater	35,000

Table 1.1: Available water classification based on salinity content

Chemical ion	Concentration [ppm]	Percentage of salt content [%]
Chloride Cl^-	19,345	55
Sodium Na^+	10,752	30.6
Sulphate SO_4^{2-}	2,701	7.6
Magnesium Mg^{2+}	1,295	3.7
Calcium Ca^{2+}	416	1.2
Potassium K^+	390	1.1
Bicarbonate HCO_3^-	145	0.4
Bromide Br^-	66	0.2
Borate BO_3^3	27	0.08
Strontium Sr^{2+}	13	0.04
Fluoride F^-	1	0.003

Table 1.2: Chemical composition of seawater including concentration of total dissolved solids (TDS)

Chemical ion	Salt content in river water [%]	Salt content in seawater [%]
Chloride Cl^-	8.6	55
Sodium Na^+	6.9	30.6
Sulphate SO_4^{2-}	12.4	7.6
Magnesium Mg^{2+}	4.6	3.7
Calcium Ca^{2+}	16.6	1.2
Potassium K^+	2.6	1.1
Bicarbonate HCO_3^-	31.9	0.4
Bromide Br^-	-	0.2
Borate BO_3^3	-	0.08
Strontium Sr^{2+}	-	0.04
Silica SiO_2	14.6	-
Iron Fe^{2+}	0.7	-
Nitrate NO_3^-	1.1	-
Fluoride F^-	-	0.003

Table 1.3: Comparison of the percentage of salt content between river and seawater.

As a result of the high content of dissolved solids present in seawater, the thermodynamic properties of it differs far from that of the freshwater. Table 1.4 shows the typical properties of seawater at standard conditions which are fundamental in the design and operation of desalination processes. Osmotic pressure

in linked to the relative number of dissolved salts and strongly influences the water to pass through the membranes. On the other hand, boiling point elevation describes the increase in boiling temperature of a solution and is causally linked to the salt concentration in the solution, but weakly dependent on its temperature.

Osmotic pressure [bar]	27
Boiling Point Elevation, at 20°C [°C]	0.32
Density [kg/m^3]	1,024
Viscosity [kg/m·s]	1.074x10^{-3}
Specific Heat [kJ/kg °C]	35,000

Table 1.4: Thermodynamic properties of standard seawater.

1.3 History of Desalination

The idea of separating salt from water was first used, not because of the need to get fresh water but because salt was an expensive resource at the time. Researchers and investigators started to find out ways of producing freshwater in remote location and, specially, on naval ships at sea. In 1790, United States Secretary of States Thomas Jefferson received a request to sell a desalination process, to convert saltwater to freshwater.

Desalination technologies started to grow over the past 50 years (See Figure 1.3 which represents the overall installed capacity worldwide with time), being the result of a long history of research and development efforts. In order to satisfy freshwater needs in remote locations during World War II, a huge part of investment and research was destinated to promote desalination techniques [5]. After the war, in 1960, desalination technologies based on thermal processes were commercially available. Inside this category, multi-stage flash distillation processes (See section 1.6.1 in detailed) became popular in the Arabian Gulf, which was the main area of many commercial plants set up [6]. Later, other processes used for desalination such as membrane techniques were discovered and initially used only for brackish water treatment. Desalination became a commercial technology in both membrane and thermal processes by the end of 1980s which enable to a rapid growth in world desalination capacity.

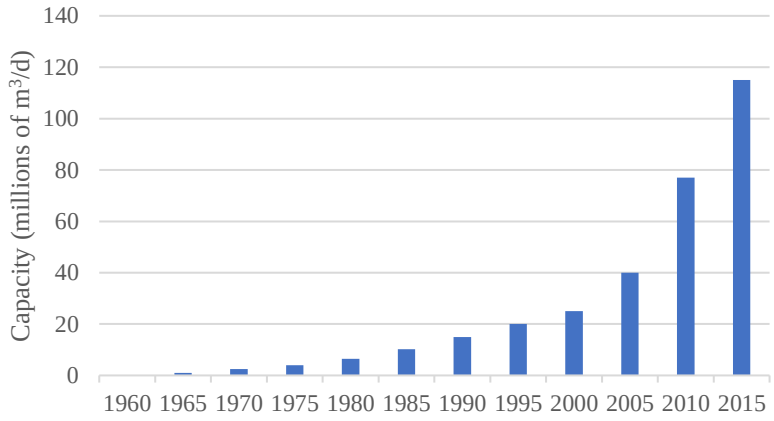

Figure 1.3: Worldwide desalination installed capacity from 1960-2015. Data extracted from [7].

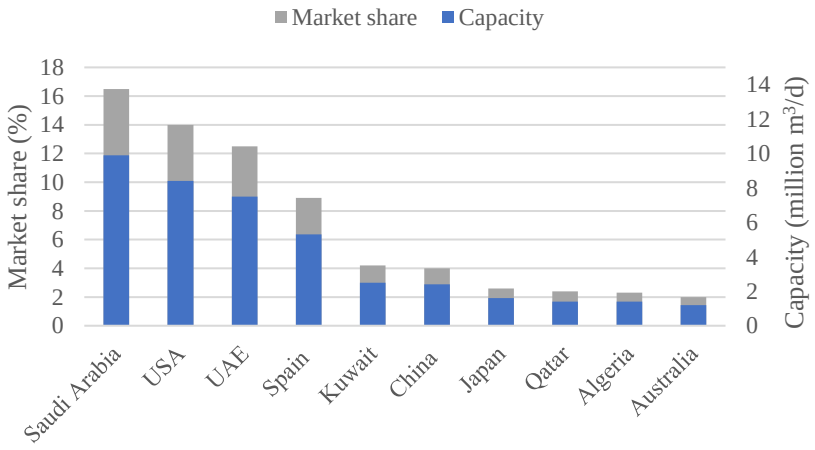

Figure 1.4: Worldwide distribution of desalination capacities. Top 10 countries using desalination technologies. Data extracted from [8].

Figure 1.4 shows that many countries of the world use desalination technologies but no other region of the world has utilized desalination techniques on as large scale as the Middle East. However, in Spain and Italy are implementing large number of desalination plants [9]. Spain has been using desalination technologies since 1964 to provide drinking water in the Canary Islands, the Balearic Islands, and along coasts [10], [11].

1.4 Water Desalination Fundamentals

Water desalination is a chemical process that separates dissolved salts and other minerals from water. Brackish water, seawater, wells, rivers and wastewater are feedwater sources used in desalination water processes to obtain potable water [12].

There are two main types of seawater desalination processes: Membrane separation and thermal evaporation (See Figure 1.5).

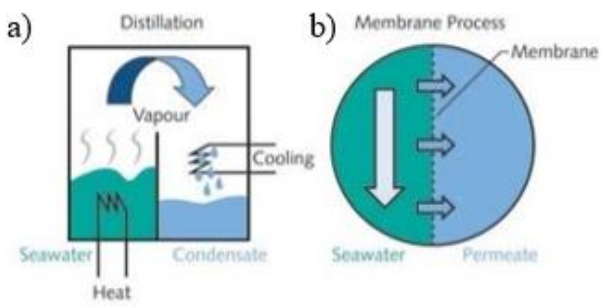

Figure 1.5: . a) Thermal evaporation, b) Membrane separation.

Membrane processes are used increasingly often for the creation of potable water from seawater, groundwater, or wastewater. Membrane separation requires driving forces including pressure, electric potential, and concentration to overcome the osmotic pressures and force brackish or seawater through membrane processes [12]. The membrane acts as a specific filter that will let water flow through, while it avoids the passage of suspended solids and other substances. On the other hand, ***thermal desalination or phase-change processes*** employs heat to evaporate the water from a salt solution, and the water vapor is then condensed and recovered [13].

The three most applied desalination processes are: Reverse Osmosis (RO), Multi-stage Flash (MSF), and Multi-effect Distillation (MED). In 2013, RO was 65% of the total installed desalination capacity, while MSF accounted for 22% and MED for only 8%, as shown in Figure 1.6 [14].

The Table 1.5 represents the most commercial and available methods inside both categories; phase-change processes and membrane processes to desalinate brackish or seawater.

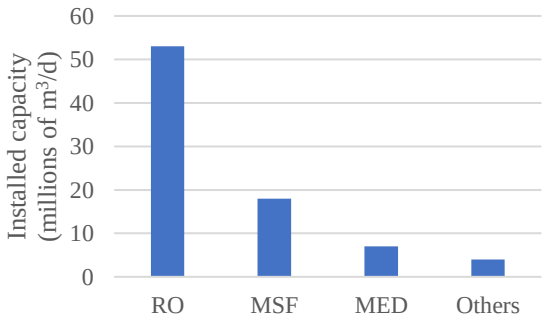

Figure 1.6: Worldwide installed capacity of desalination technologies by 2013. Data extracted from [14]

Thermal	Membrane
Multi-stage flash (MSF)	Reverse Osmosis (RO)
Multi-effect distillation (MED)	Electrodialysis (ED)
Vapor compression (VC)	

Table 1.5: Commercially available desalination technologies.

1.5 Membrane Processes

1.5.1 Reverse Osmosis (RO)

1.5.1.1 Osmosis principles

Osmosis is a process where a weaker saline solution tends to migrate to a strong saline solution. In other words, a solution that is less concentrated will have a natural tendency to migrate to a solution with a higher concentration. For instance, if you have two containers full of water with different salt concentration and separated by a semi-permeable membrane, then the water with the lower salt concentration will begin to migrate towards the water with the higher salt concentration. Figure 1.7 shows how osmosis works.

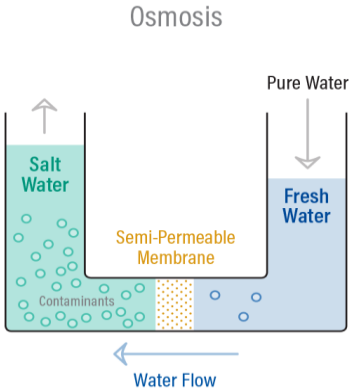

Figure 1.7: Graphical representation of osmotic process [15].

1.5.1.2 Reverse Osmosis principles

Reverse osmosis is the same process of osmosis but in reverse. Whereas osmosis is a natural phenomenon that occurs without energy, to reverse the process of osmosis you need to apply energy to the more saline solution. The membrane allows the water to pass through it, except most dissolved salts and other substances. However,

pressure is needed to allow the passage of the water through the membrane to desalinate water in the process and to hold back most contaminants.

A high-pressure pump is used to increase the pressure on the higher salt concentration side of the RO. The pump forces the water across the membrane leaving around 95% of dissolved salts behind in the concentrate or reject stream [15]. The amount of pressure required depends on the salt concentration of the feed water. The more concentrated the feed water, the more pressure is required to overcome the osmotic pressure. Below is an ideal representation of how reverse osmosis works.

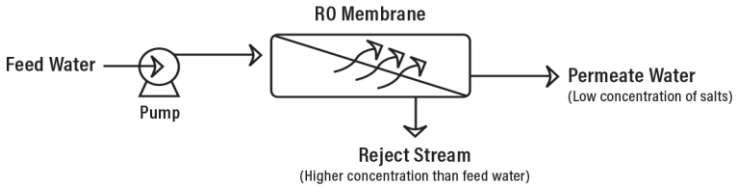

Figure 1.8: Diagram of the functioning of reverse osmosis [15].

The feed water enters the RO membrane thanks to the pressure of the pump so the water molecules cross the semi-permeable membrane avoiding the passage of salts and other contaminants, so are discharged through the reject stream, which goes to drain or can be fed back into the feed water supply to be recycled through the RO system to save water. The water that crosses the membrane is called the permeate water with 95% to 99% of the dissolved salts removed from it [16]. There are two types of membrane filtration:

Dead-end filtration or direct filtration involves all the feed water passing through the membrane, leaving the solids behind Figure 1.9. **Dead-end filtration** is a batch process meaning that the filter will accumulate particles such that water can no longer pass through. Thus, the filter will need to be replaced or cleaned.

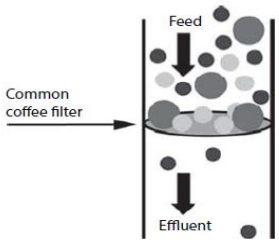

Figure 1.9: Dead-end filtration with a coffee filter [16].

On the other hand, in **crossflow filtration**, feed water goes tangentially over the membrane surface rather than perpendicularly to it. In contrast to dead-end filtration, crossflow filtration has one influent stream and two effluent streams; concentrate of dissolved salts and permeate. It reduces fouling and scaling issues of

the RO membrane, and it is due to that the tangential flow across the membrane surface provides shear forces scouring the surface to keep it clean.

Crossflow is a continuous operation, due to that the scouring process keeps the membrane free of foulants but, periodically the membrane will need to be cleaned because always there are solids accumulated at the surface.

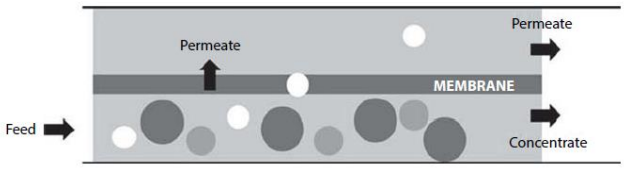

Figure 1.10: Crossflow filtration [16].

1.5.1.3 Basic Terms and Definitions

1.5.1.3.1 Recovery

Recovery or conversion is a term that describes what volume percentage of water is collected as permeate. Most of the systems are designed to recover a 75% of influent water [16]. Recovery is calculated by the following equation (1.1) :

$$\%\text{Recovery} = (\text{permeate flow}/\text{feed flow})*100 \qquad (1.1)$$

The higher the recovery the lower the need to dispose reject water, but also the lower the purity of permeate water is. Thus, higher recovery results in lower product purity.

The recovery of a RO system is not a property of the membrane, it is the designer who selects the recovery for the system adjusting it with control valve located in the concentrate or reject stream. If the valve is partially closed, part of the feed water is forced to pass through the membrane resulting in higher recovery. However, exceeding the design recovery can result in accelerated fouling and scaling of the membrane, because if more water is passing through the membrane, it will accumulate foulants and other substances in that region. On the contrary, if the recovery is lower, it will not impact the membrane fouling, but will result in higher quantity of wastewater from RO system [16].

1.5.1.3.2 Rejection

Rejection is the opposite of recovery, a term used to describe what percentage of influent species a membrane retains [16]. Recovery is calculated by the following equation (1.2):

$$\%Rejection=[(Cf-Cp)/Cf]*100 \quad (1.2)$$

Where:

Cf= influent concentration of a specific component.

Cp= Permeate concentration of a specific component.

1.5.1.3.3 Flux

Flux is the volumetric flow rate of a fluid passing through a given surface. In this case, the fluid is water, and the surface is the membrane. The flux of water passing through the membrane is proportional to the net pressure driving force applied to the water [16]. It is calculated by the following equation (1.3):

$$J = K(\Delta P - \Delta \Pi) \quad (1.3)$$

Where:

J= Flux of water in the RO membrane.

K= Water transport coefficient, equal to permeability/thickness of the membrane.

ΔP= Pressure variation across the membrane.

ΔΠ= Osmotic pressure variation across the membrane.

The flux is not a property of the membrane since the designer select it. The higher the flux, the faster the membrane fouling, and scaling occurs. Therefore, if the feed water quality is low, the operating flux should be low too.

The specific flux or permeability is generally compared between different membranes measuring their performances. Since not all the membranes are at the same operating pressure.

$$\text{Specific Flux} = \frac{\text{Flux}}{\text{Applied Pressure}} \quad (1.4)$$

The higher the specific flux the lower the driving pressure required to operate the RO system.

1.5.1.3.4 Concentration polarization

Before defining this concept, it is necessary a bit of theory. Firstly, the flow of water passing through the RO membrane is similar to the flow passing through a pipe (See Figure 1.11). There are three regions in the pipe; The biggest one is the bulk flow, which is convective, while the others are called boundary layers which are diffusive and perpendicular to the convective flow of the bulk solution. The slower velocity of water passing through the pipe, the thicker the boundary layer is.

The same occurs with the flow through a membrane. However, there is a net flow out through the membrane, so there is a convective flow, but only diffusional flow crosses the membrane. Since diffusive flow is slower than convective flow, solids that should be rejected tend to build up on the boundary layer. Therefore, the concentration of solids and other substances at the membrane surface is higher than in the bulk region and it is called "concentration polarization."

This phenomenon has several negative effects on the performance of the RO membrane. The solid species creates a barrier acting as a hydraulic resistance to water flow through the membrane; This barrier increases the osmotic pressure within the boundary layer meaning that the operating pressure should increase to permit the passage of the water through the membrane.

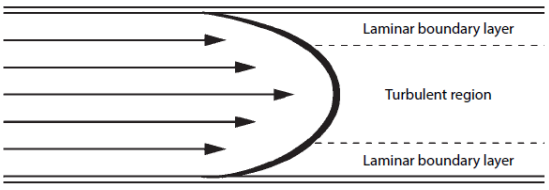

Figure 1.11: One-dimensional flow differentiating turbulent and laminar zone [16]

1.5.1.4 RO Membrane technologies

The selection of membrane configuration is determined by technical and economic aspects. Membrane will never be as one flat plate, because this large surface would result in high investment costs. That is the reason systems are built as enrolled tubes, to enable a large membrane surface minimizing the volume. Therefore, reverse

osmosis membranes are typically modularized using configurations that pack a large amount of membrane area into a relatively small volume. There are divided in four basic types: Tubular membrane system, plate & frame membrane system, spiral wound, and hollow fine fibber.

1.5.1.4.1 Tubular Modules

Tubular-shaped membranes are located inside of a tube which is the supporting layer of the membrane. The feed stream goes across the length of the membrane tube and is filtered out into the outer shell while concentrate collects at the opposite end of the membrane tube. A drawback of tubular membranes is that the density is low, which increases the investment cost per module.

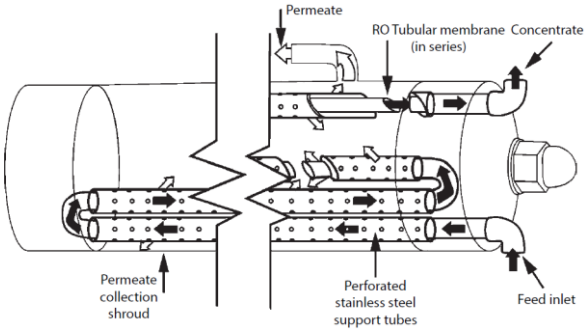

Figure 1.12: Tubular membrane module [16]

1.5.1.4.2 Plate & frame membrane systems

This kind of membrane system is usually used for high suspended solids applications but not in water purification facilities. These modules are composed by packs of two membrane layers placed over the permeate channel where the water flow through. (See Figure 1.13).

These membrane modules are expensive because the complexity of the systems needs a lot of devices. They are easy to clean but tend to foul and scale.

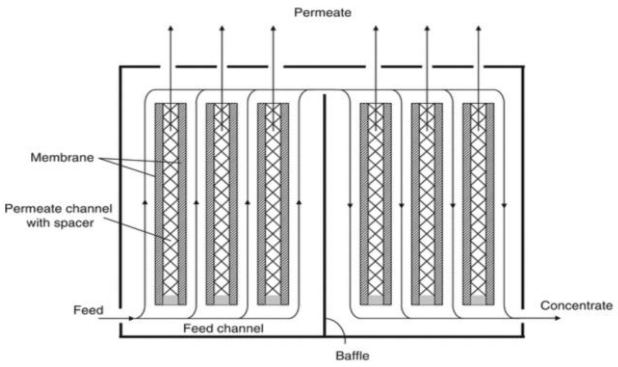

Figure 1.13: Plate and Frame Membrane Module. Courtesy of [17]

1.5.1.4.3 Spiral Wound membranes

Spiral Wound membrane modules are the most typical one used for RO applications. This technology consists of a central tube and several sheets in which the membrane is placed coaxial to it. The feed water gets into the latest layers and passes through the membrane till arrive to the central tube and become to the permeate stream. Solids and other substances remain in the membrane layer and forms the concentrate stream which can be recirculated or not. The major advantage of a spiral wound module is that the packing density is higher than the other technologies.

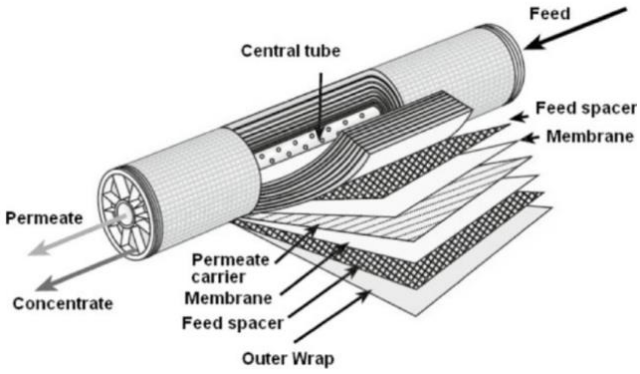

Figure 1.14: Spiral wound membrane [18].

If a transversal cut is done, the module has the shape of a spiral (See Figure 1.15) where the inlet flows through the outer layers crossing tangentially the feed spacer and membrane layer leading the path to the permeate tube.

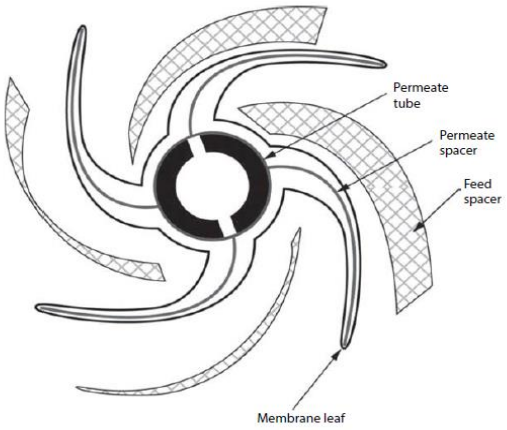

Figure 1.15: Cross-section of a Spiral wound RO membrane. Courtesy of [16].

1.5.1.4.4 Hollow Fine fiber membrane modules

Hollow fiber membrane module is composed by millions of long, porous filaments from 1-3,5 mm diameter, which are in a PVC shell. The fiber is flexible. Its function is simple; Hollow fiber works like tubular systems but uses a small tube diameter which allows for flexibility.

A drawback of this system would be irreversible fouling and fiber breakage. Then, the investment cost in not that expensive as the plate & frame modules but it is higher in terms of operation and maintenance costs. However, presents a higher packing density than tubular membranes.

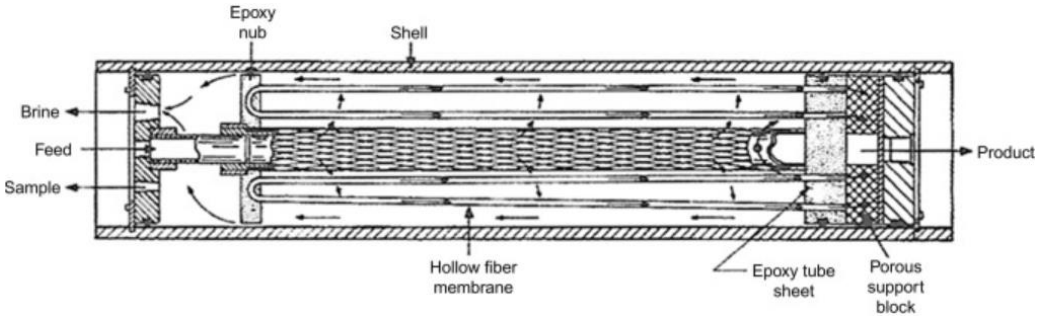

Figure 1.16: Hollow fiber membrane module [18].

1.5.2 Electrodialysis

ED is a mature technology method which is used for seawater desalination since more than 50 years [19]. Electrodialysis uses ion-selective membranes and an electrical potential as a driving force to separate charged species from water. ED process is driven by direct current (DC) in which ions flow through the cation and anion selective membranes to electrodes of opposite charge [15]. In contrast to RO, ED is only able to remove ionic components like dissolved minerals since the driving force for the separation is an electric field. The separation of minerals occurs in the membrane module called cell pair. A cell pair is composed by a cation and anion selective membrane and two spacers. (See Figure 1.17). The number of cells depends on the system. A drawback is that ED will need a higher driving force (energy required) if the concentration of dissolved salts increases. Therefore, if dissolved minerals are only a few thousand of ppm, ED could not work. Another one is that ED is only suitable for separating ionic components, it is not able to remove the organic matter, suspended solids, and colloids. On the other hand, ED systems separate ionic substances without phase change which results in low energy consumption.

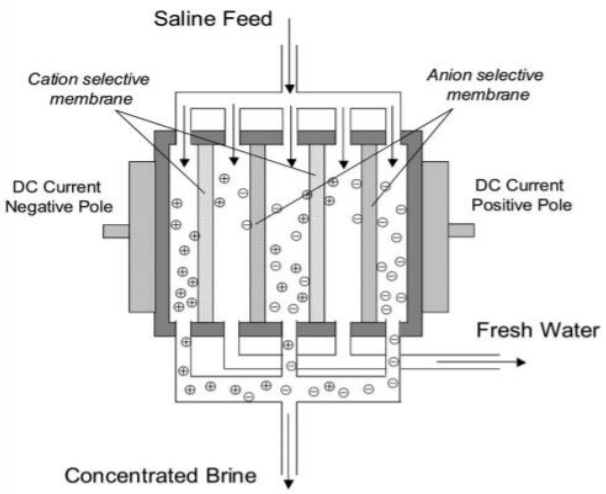

Figure 1.17: Schematic diagram of Electrodialysis process [9].

1.6 Thermal Processes

1.6.1 Multi-stage Flash (MSF)

Multi-stage Flash Distillation was introduced in 1957 by Silver R.S. optimizing the number of stages and the heat transfer area [20]. This accounts for the major portion of desalinated municipal potable water produced in the world [21]. MSF systems are widely used in the Middle East and they account for over 22% of the world´s desalination capacity [14] and have increased from 500 m^3/day in the 60s to 75000 m^3/day in the 90s [22]. During years, MSF have added the use of demisters resulting in a decrease of product salinity which is maintained below 10 ppm.

MSF is a phase-change or thermal process which involves water evaporation and condensation inside the flashing chamber. These effects are combined to recover the latent heat of evaporation for reuse by preheating the incoming water. (See Figure 1.18). The saline feed water flows inside the pipe, then it is preheated into the brine heater and goes back to the flashing chamber. Thus, the water evaporates leaving dissolved salts on the bottom of the vessel (brine pool) supported by the demister. The flashed water condenses thanks to the tube bundle of condenser/pre-heater tubes and is collected in trays. A detailed schematic of the MSF flashing stage is shown in (Figure 1.19)

MSF is a multi-stage process because it has more than one vessel (between 15 and 25 stages) that operates at a successively low pressure to maximize water recovery. The range of recoveries for conventional MSF desalination processes is limited to about 10 to 30 % for seawater desalination [13].

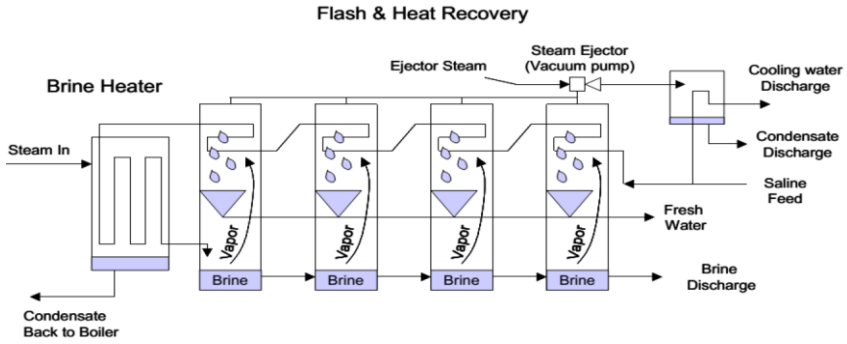

Figure 1.18: Multi-stage flash distillation process [9].

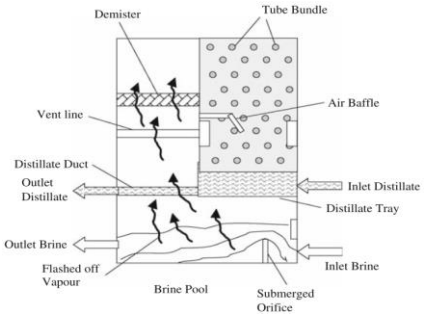

Figure 1.19: Detailed schematic flashing stage of MSF distillation process [23].

The main problems linked to MSF processes are the followings:

1) Scale formation due to precipitation of Ca and Mg salts on the heat exchanger tubes [24].
2) Corrosion in the flash chambers due to their operation in aggressive environment consisting of seawater and non-condensable gases like O_2 and CO_2. They are affected by chloride ref14. But also, corrosion is observed in condenser tubes, resulting from formation of small micro galvanic cells [25].
3) MSF plants require a huge amount of material and land [26].
4) MSF processes require both electrical and thermal energy with high specific energy consumption as compared to other processes.

1.6.2 Multiple Effect Distillation (MED)

The multiple effect distillation plants can be found in various industries, but they started with the desalination industries with a capacity of 500 m^3/day in the 60s. In 2006, MED capacity increased to a value of 36.000 m^3/day [27]. However, it lost importance respect to MSF in the past due to that the heat exchanger tubes can have scale problems. Now it is gaining attention due to the better thermal performance compared to MSF. Moreover, to solve the problem of scaling, MED processes operate

at low temperatures, less than 70°C. This is due to those evaporators adopt a horizontal film configuration, where the saline feed water is sprayed on the outer surface of the heater tubes and because typically, 8 to 16 effects are used in MED to minimize the temperature and thus, the energy consumption and the overall electrical power consumption. As a result, energy costs for MED are lower than that of the MSF.

The operation process is simple; Saline feed water is distributed on the evaporator vessel which has been heated from the boiler. The steam formed passes through the second vessel (second effect) at a lower temperature and so on. The steam generated in the final effect is typically at a temperature and pressure too low to be further use, so systems are coupled with a final vessel to condense this steam.

MED systems can have different configurations according to:

- Type of heat transfer surface: Horizontal tube falling film (See Figure 1.20), vertical climbing film tube and rising film vertical tube.
- Direction of brine flow respect to the vapor flow direction: Forward, backward, or parallel feed [28].

The two main drawbacks associated with this technology are corrosion and scaling. A clear example is the deposition of calcium carbonate on the condenser tubes. It leads to a reduction of the efficiency and an increase of specific heat consumption.

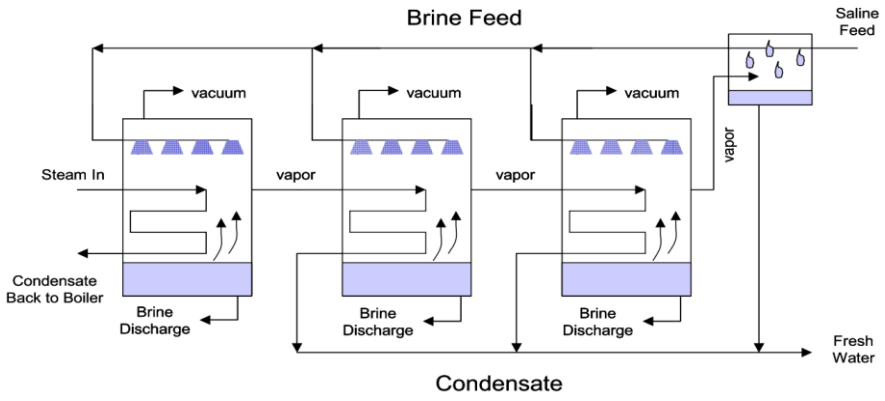

Figure 1.20: Schematic of Multi-effect distillation process (MED) [9].

1.6.3 Vapor Compression (VC)

Vapor compression systems are similar to MED technologies. In fact, MED systems can be coupled with them. VC processes rely on low pressure operation to drive evaporation. The heat of evaporation can be supplied by one of two approaches: mechanical vapor compression (MVC) which is shown in Section 1.6.3

and thermal vapor compression (TVC). Typically, VC systems are used in small/medium installations [21]. MVC systems generally have a capacity of 3000 m^3/day and a single stage, while TVC units sizing are about 20000 m^3/day and have several stages or effects. It is due to that MVC systems have the same specific power consumption regardless the number of effects, while TVC units can increase the thermal efficiency by adding additional stages [29].

The MVC system is composed by horizontal tube evaporator, spray nozzles, a vapor compressor, pumps, and a preheater. As shown in Figure 1.21, compressed steam flows within the tubes and then is mixed with the brine that is sprayed on the outside surface of the tubes. Thus, more vapor is generated to be recycled and the compressed steam condenses. Scale formation on the outside surface of the tubes is reduced by limiting the maximum temperature of the compressed vapor (<70°C).

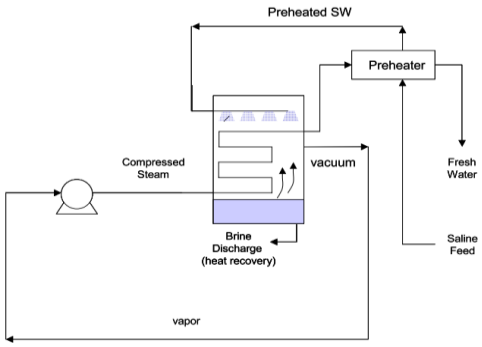

Figure 1.21: Schematic of single stage mechanical vapor compression (MVC) distillation process [9]

2. Desalination coupled with Renewable Energies

2.1 Renewables in Spain

According to the last IEA (International Energy Agency) report, Spain has shown a key role and leadership on clean energy transitions. The Spanish energy and climate framework is based on a 2050 target of climate neutrality and 97% share of renewable energies in the total energy mix. Its principal aim is to reduce CO_2 emissions increasing the share of renewables in the electricity sector, since Spain's total energy mix is still heavily dominated by fossil fuels [30].

A 72% of total primary energy supply (TPES) and 68% of total final consumption (TFC) are met with fossil fuels and only one-fourth of TES was produced domestically in 2019. The rest was imported.

Domestic production mostly relies on nuclear, bioenergy and waste, and other renewables, notably wind and solar. Production of renewable energy has increased a 47% the last 10 years and it represents a 55% of the total domestic production in 2019. Unfortunately, 42% and 25% of TPES correspond to oil and gas. See Figure 2.1.

On the other hand, Spain is centered to recover from the COVID-19 induced global economic crisis. Therefore, the state will bring forward the investments in its clean energy transition over the upcoming years

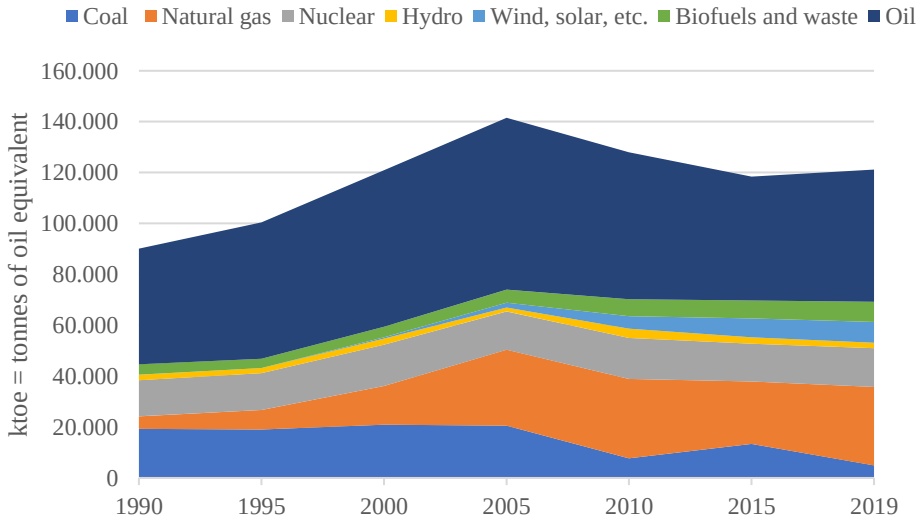

Figure 2.1: Total energy supply (TES) by source, Spain 1990-2019. Extracted data from International Energy Agency (IEA) [30].

A huge percentage of renewable energy in total final consumption (TFC) leads to renewable electricity, more than 50%. The rest is used for heat and transport. Wind was the technology leader of the renewable electricity generation in Spain (2019) and it was coupled with hydro and solar energy, which all have brought the share of renewables in

electricity up to 37% that year [30]. In contrast, bioenergy was predominantly used for heat and transport sector.

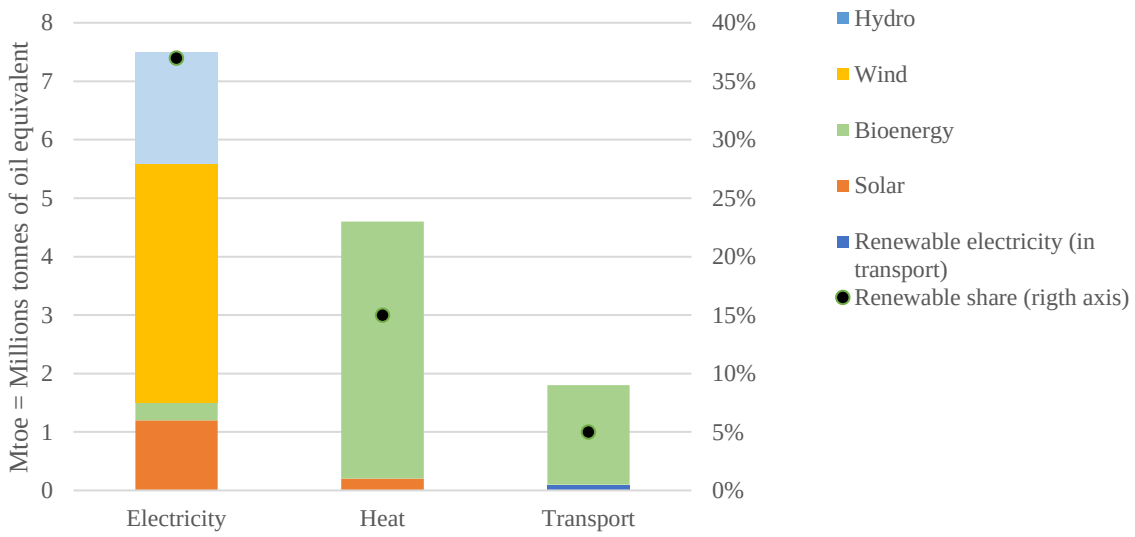

Figure 2.2: Renewable energy in total final energy consumption in Spain, 2019. Adapted from IAE statistics [30].

In the image below (Figure 2.3), it is clearly seen that a significant increase in wind and solar energy has occurred over the last decade, so they and the installation of many PV plants have doubled the share of renewable electricity generation, from 20% in 2005 to 40% in 2010.

The installed capacity of wind generation exponentially increased more than 20 GW between 2000 to 2010 and occurred with solar energy, which grew up 9 GW in the recent years.

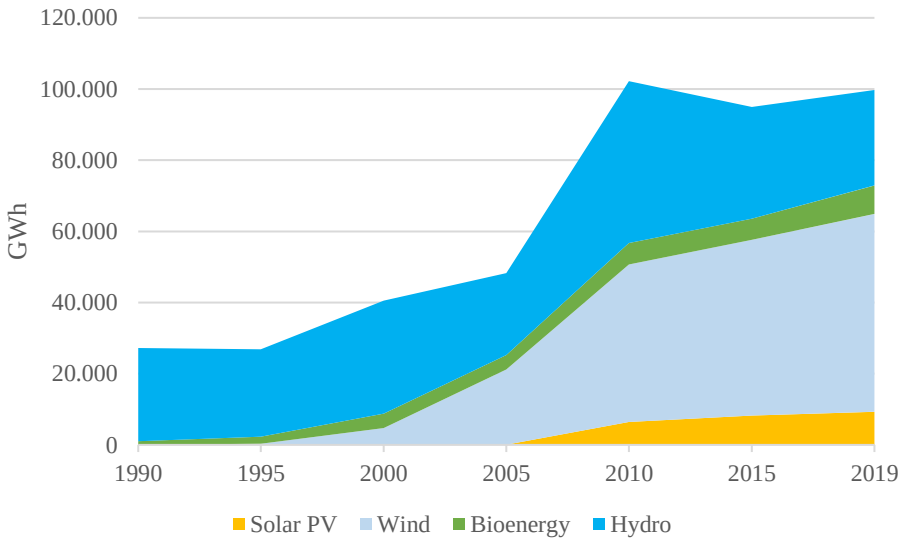

Figure 2.3: Renewable energy in electricity generation in Spain, 1990 to 2019. Adapted from IEA *World Energy Statistics and balances* [30].

2.2 Renewable Energy Technologies for Water Desalination

Water Desalination based on the use of renewable energy technologies enable to achieve a sustainable way to produce fresh water. Renewable energy is an attractive solution not only to reduce desalination plants 'carbon footprint but also as the investment cost of the plants continue to decline and the price of fossil fuels continue to increase [31].

There are numerous studies of profitable and feasible small-scale RE-DES (renewable powered desalination) project pilots (<1.000 m^3/d), that are applicable for remote and arid region. Nowadays, large-scale RE-DES power plants are being studied with connection to the grid to ensure a constant water production. For example, Al Khafji solar saline water reverse osmosis (Solar SWRO) Desalination plant is the biggest desalination plant coupled with renewable energy. It supplies more than 60.000 m^3 of potable water per day to the city of Al Khafji in north-eastern Saudi Arabia, providing a regular supply of water to the city throughout the year [32].

Currently, there are many configurations of RE-DES technologies which are techno-economically feasible (See Figure 2.5). So, selecting the most suitable combination system depends on several variables, such as location, capacity of the plant, salt concentration of feed water, access of an electric grid and the renewable source and its availability [31]. As shown in Figure 2.4, PV-RO and wind-RO are the

most widely exploited RE-DES configurations corresponding to 32% and 19% of the field respectively [33].

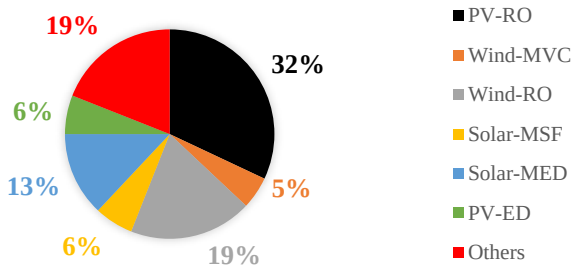

Figure 2.4: Landscape of RE-DES worldwide plant configurations. Data adapted from Ref. [33]

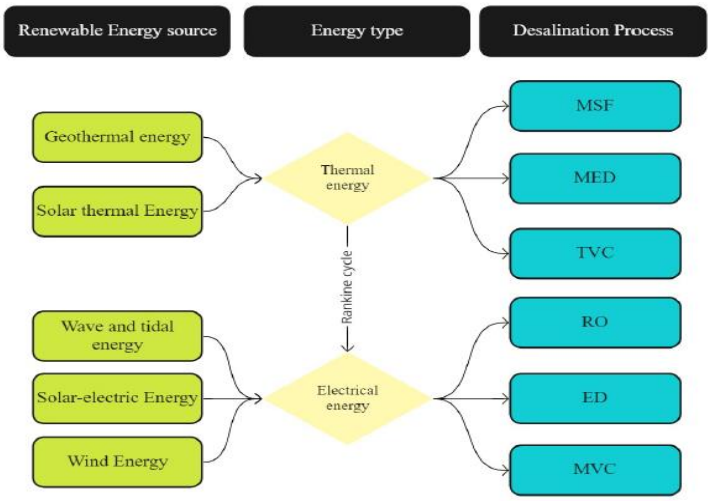

Figure 2.5: Possible RE-DES configuration; Renewable energy sources with conventional and innovative desalination processes. Own elaboration.

2.3 Energy analysis of commercial renewable powered desalination technologies

The aim of this section is to compare the most relevant renewable energy powered desalination technologies by means of desalination energy consumption process and economic analysis of both renewable energy (solar thermal, solar PV, and wind) and desalination technologies (MSF, MED, RO, and ED) as shown in Table 2.1.

RE-Thermal	RE-Membrane
Solar-MED	PV-RO, Wind-RO
Solar-MSF	PV-ED

Table 2.1: Most common renewable powered desalination technologies.

Desalination is an energy-intensive process, which consumes more energy per liter than other water supply [34]. The energy required depends on:

- Technology employed
- Design of the plant
- Quality and temperature of the inlet feed water
- The application of energy recovery devices
- Intended quality of the produced potable water

The minimum energy consumption required to separate dissolved salts and other minerals from water under ideal conditions is common to all desalination processes, irrespective of the technology used and the number of stages. This minimum energy required is determined by the difference between the free energy of the inflow and outflow.

Therefore, according to the Van't Hoff equation and the variation of the Gibbs free energy, it can be determined that in order to desalinate water, at 25º C and with a salinity of 33,000 ppm, the minimum work required is 0.77 kWh/m³ [35].

However, this is not true. The energy consumption is much higher, around five to thirty times higher than the minimum required. It depends on the type of technology and the energy source, and it is due to that desalination processes have losses during their performance, such as, pump, thermal and pipe losses, or membrane losses.

In membrane desalination processes (RO, ED) only electricity is needed as no heat energy is required, whereas in thermal distillation both energies are needed. Electricity is needed for pumps and control systems and heat energy is needed to evaporate water.

Therefore, electricity could be generated from renewable energy sources to reduce CO_2 emissions instead of fossil fuel or other conventional and pollutant energy sources.

2.3.1 Energy consumption in membrane processes

For RO process, AC (Alternating Current) is consumed to drive all the pumps and control system, whereas for ED, DC (Direct Current) is consumed by electrodes and AC or DC electricity by pumps.

2.3.1.1 Energy consumption in Reverse Osmosis (RO) process

Electricity is the only energy type required in the **RO process**. The energy consumption of the RO device mainly depends on the salinity and recovery rate of the feed water. Osmotic pressure is related to the total dissolved solids concentration

of the influent; thus, high salinity water requires more energy to overcome a higher osmotic pressure [36].

RO plants range in size from quite small unit scales from 0.1 m^3/d to 395,000 m^3/d, which have an energy consumption between 3.7 to 8 kWh_e/m^3. Although, in small scale plants, it may exceed 15 kWh_e/m^3. For instance, a SWRO plant with a capacity of 24,000 m^3/d, has an energy consumption around 5 kWh_e/m^3 with an energy recovery device (ER) for seawater. When brackish water is presented, the pressure of the pump is lower than the previous case, therefore, it makes the energy consumption low, which oscillates from 1.5 to 2.5 kWh_e/m^3 [36]. In contrast, according to a review by Shalaby, the specific energy consumption for experimental PV-RO configuration plants ranges from 1.1 to 16.3 kWh_e/m^3 for capacity size from 50,000 to 250 m^3/d, depending on system size, use of batteries, feed source, pretreatment and type of electrical recovery device (ERD) [37].

Figure 2.6 shows that the electric energy consumption of pumps and control systems for SWRO and BWRO desalination technologies has decreased over the years as the efficiency of these systems continue to improve. Currently, as mentioned above, the SEC (Specific Energy Consumption) would be around 3-5 kWh/m^3 depending on the plant capacity (m^3/d) and its location (3 in the Mediterranean Sea and 5 in other regions) due to the amount of salinity in the sea. As shown in Figure 2.6, SEC is not only from pumps. It comes through all steps and treatments of the plant. However, it is worth noting that the decline in SEC has been slowing down, and it has become increasingly difficult to achieve more efficient energy systems.

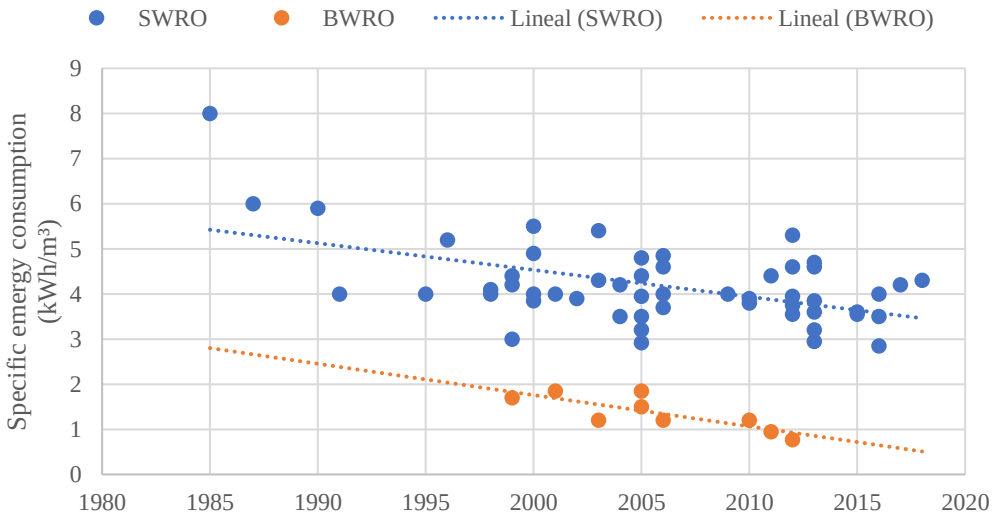

Figure 2.6: Energy consumption trends in sea and brackish water reverse osmosis desalination.

Furthermore, if an energy recovery device (ERD) is included in the RO process, it can make use of the residual energy of the concentrated stream to pressurize the feed to recover energy and to lower water production costs Another important variable to reduce energy consumption is to increase the efficiency of the pumps. Even a slightly rise of 3% can lead to a significant reduction of SEC, especially in the case of seawater [38].

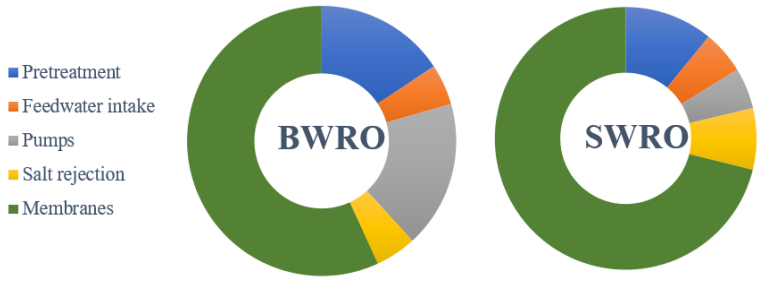

Figure 2.7: Specific energy consumption of main steps and treatments of BW and SW RO desalination process. Data extracted from [39].

2.3.1.2 *Energy consumption in Electrodialysis (ED)*

For **ED process**, electricity is also the only type of energy required. Electricity consumption generally ranges from 0.7 to 2.5 kWh_e/m^3 for low salinity ED water desalination units (<2,500 ppm), and 2.64 to 5.5 kWh_e/m^3 for medium salinity levels (2,500-5,000 ppm) [35]. However, when comparing the two membrane desalination technologies, the average energy consumption is lower in ED process than RO. This is due to the fact that ED is mainly used in brackish water where energy consumption is lower, since in seawater desalination, as the concentration of salt is higher, energy consumption increases, being higher than in RO [35], [40].

2.3.2 Energy Consumption in thermal distillation

There are two types of energy in thermal distillation processes:

- Thermal energy in which the low temperature heat corresponds to the main portion of the energy input
- Electricity is used to drive the pumps and control systems

Both are required for processes such as MSF, MED, and TVC. Whereas in MVC process only electricity is required. All processes can be divided in many stages to increase their efficiency and consume less energy. The simplest distillation technique, single-stage evaporation, consumes a huge amount of energy, around 650 kWh/m^3. So, the main evaporation processes (MSF and MED) have overcome this problem by reusing the energy consumption through multiple stages.

On the other hand, the efficiency of distillation processes can be measured by two equivalent parameters:

- Gain Output Ratio (GOR). It is a measure of how much thermal energy is consumed in desalination process, and it is defined as the ratio of the mass of distillate or latent heat of evaporation ($\Delta h_{evap}\dot{m}_{distillate}$) associated with the mass of the input steam in kg. The GOR (2.1) is a dimensionless parameter which reveals how much energy is consumed for water production [41]:

$$GOR = {\Delta h_{evap}\dot{m}_{distillate}}/{\dot{Q}_{in}} \qquad (2.1)$$

The higher the GOR value is, the better is the performance of the process. But higher GORs than the optimal ones may incorporate larger heat transfer areas, which then increases capital costs. Higher capital costs are only cost-effective when energy costs are reduced or when they are justified if greater demand for water suitably impacts the economics. The trade-off between operating and maintenance cost (OPEX) and capital cost (CAPEX) is shown in Figure 2.8, where it can be seen the relationship with GOR [42]. The optimal value will be reached by the meet of capital cost and O&M cost.

- Performance Ratio (PR): It can be defined as the ratio of the mass of distillate to the energy input 2326 KJ.

$$PR = {\Delta h_{evap}\dot{m}_{distillate}}/{2326} \qquad (2.2)$$

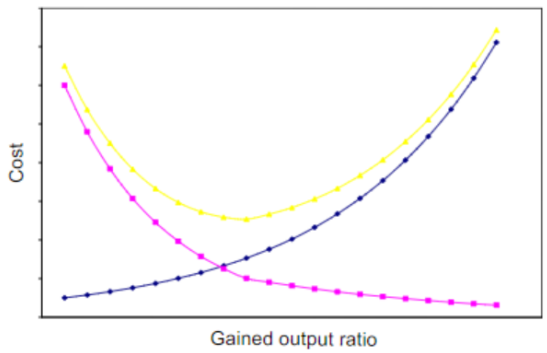

Figure 2.8: Trade-off between CAPEX (Purple) and OPEX (Blue); Total cost (Yellow) [42].

2.3.2.1 *Energy consumption in MSF*

The energy consumption is affected by several factors, such as, the brine heater, number of stages, the percentage of salts in flashing brine solution, the maximum temperature of heat source, the geometrical configuration of the flash stage and the design configuration of heat exchange devices. Thus, the MSF unit energy consumption can be reduced by boosting the number of stages, GOR or PR parameter, and the heat transfer area.

The MSF process works at a maximum operating brine temperature (TBT) between 90 ºC and 110 ºC. The more TBT is the higher is the flash range, which, increases the production rate and improves the performance. Nevertheless, TBT is limited due to scaling effects. The general GOR and PR values from commercial MSF processes range between 8 and 12 $kg_{distillate}/kg_{steam}$; 3.5 and 4.5 $kg_{distillate}/MJ$, but it also depends on the steam feed temperature. Moreover, the electrical energy equivalent of the power plant that supplies MSF process oscillates between 15.83 and 23.5 kWh_e/m^3 and the electrical energy consumption of pumps and control systems ranges between 2.5 and 5 kWh_e/m^3. Thus, the total energy consumption of the MSF unit ranges between 19.58 and 27.25 kWh_e/m^3 [43].

2.3.2.2 *Energy consumption in MED process*

MED units, as the MSF plants, requires both type of energy input, thermal and electrical energy. MED process works at a lower TBT (from 64 ºC to 70 ºC) than MSF. Generally, GOR design ranges between 10 to 16, so the thermal energy consumption corresponds to 145 MJ/m^3 (GOR=16) and 230 MJ/m^3 (GOR=10). The electrical energy equivalent of the power plant that supplies MED process ranges from 12.2 to 19.1 kWh_e/m^3 and the total electricity consumption of the pumps and control systems oscillates between 2 to 2.5 kWh_e/m^3. Therefore, the total equivalent energy consumption of MED processes ranges from 14.45 to 21.35 kWh_e/m^3.

In the picture below, it can be seen that MSF plants usually are designed bigger than MED units leading to a higher total energy consumption.

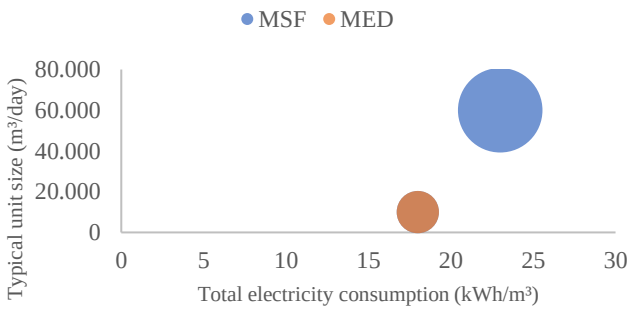

Figure 2.9: Total energy consumption of typical MSF and MED units.

2.3.2.3 *Energy consumption in TVC and MVC processes*

As mentioned in Section 1.6.3, there two approaches for these processes:

- Mechanical Vapor Compression (MVC), which needs electrical or mechanical energy input, operates at a TBT around 74 ºC, with an electrical energy consumption ranging from 7 to 12 kWh_e/m^3.
- Thermal Vapor Compression (TVC) in contrast needs both, electrical and mechanical energy sources and TBT oscillates between 63 to 70 ºC. For this temperature, GOR value is around 12, a heat input of 14.56 kWh_e/m^3 equivalent electrical to thermal energy, and an electricity consumption of 1.6-1.8 kWh_e/m^3. Therefore, the total energy consumption is equal to 16.26 kWh/m^3.

2.3.2.4 *Comparison of energy consumption between commercial desalination technologies*

All these processes have in common that strongly depend on the materials and devices used, size of the plant, unit design, and the seawater feed stream quality to the unit except that the energy consumption in thermal distillation processes is not influenced by the salt concentration in the feed water. This is the opposite of reverse osmosis and electrodialysis processes which are strongly dependent on salt concentration.

Once the energy consumption of all technologies seen above has been obtained, it is concluded that the most used thermal distillation processes (MSF and MED) require more energy than SWRO process. This is due to the high thermal energy need for water evaporation, and the continuous improvement in RO technology and devices, which resulted in lower power consumption. Table 2.2 shows the reported average consumption of the main desalination technologies.

	MSF	MED	SWRO	BWRO	ED
Capacity size (m^3/d)	50,000-70,000	5,000-15,000	Up to 128,000	Up to 98,000	2-145,000
Electrical E_{cons} (kWh/m^3)	2.5-5	2-2.5	4-6 with ER	1.5-2.5	2.64-5.5
Equivalent Electrical to Thermal E_{cons} (kWh/m^3)	15.83-23.5	12.2-19.1	None	None	None
Total E_{cons} (kWh/m^3)	19.58-27.25	14.45-21.35	4-6 with ER	1.5-2.5	2.64-5.5
GHG emissions (kg CO_2/m^3 H_2O	18.3-26	13.7-19.2	4.8-5.3		2.5-5.3

Table 2.2: Specific energy consumption of the most commercial desalination technologies. Extracted data from [35-39]. Total equivalent specific energy consumption is equal to the sum of kilowatt-hours (electric) and kilowatt-hours (thermal), converted based on assumed 30% efficiency of a modern power station.

In addition, the energy required for desalination systems is typically generated from conventional fossil fuels, having two environmental impacts: The dumping of by-products, CO_2 emissions, acid rain gases (NOX; SO_2) and fine particulate matter. Table 2.3 also summarizes the resulted greenhouses gas emissions emitted by desalination processes [44]. Therefore, it is obvious that among the mentioned desalination methods, the RO process has less negative effect on the environment

Besides, even for reverse osmosis process, the carbon dioxide emissions are high and in literature, some studies show that renewable powered desalination processes can be a good option, as they can be used in a variety of ways emitting less carbon emissions. (See Table 2.3).

Renewable powered desalination technology	**CO_2 emissions (kg CO_2/kWh$_e$**
Grid-RO	0.913-0.94
Wind-RO	0.024
PV-RO	0.15

Table 2.3: CO_2 emissions from RO desalination process using several energy sources. Adapted from [45].

2.4 Economic analysis of commercial renewable powered desalination technologies

This section deals with the different elements that make up the financial cost of production and operation of the different desalination plants coupled with renewable energies.

In recent decades, the average costs per unit of water produced in desalination plants has fallen in line with decreasing energy consumption (See Figure 2.10). Energy consumption is a fundamental part of the cost of the desalination process and its reduction is associated with a reduction in the cost production. Since 1970, when the first plant to produce drinking water from salt water (Lanzarote) was installed, the evolution of the cost has been linked to technological improvements and a reduction in energy consumption.

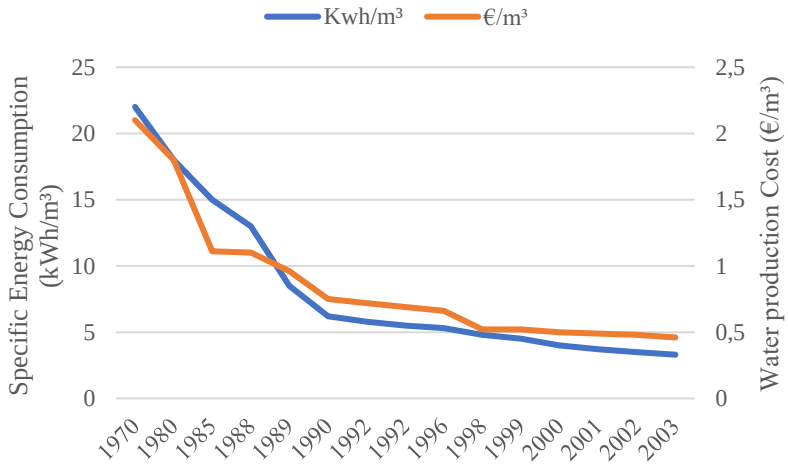

Figure 2.10: Evolution of the unit cost of water production through desalination plants [46].

When analyzing the economics of a desalination plant, costs can be influenced into factors according to their nature such as, intake water quality, plant capital cost, energy cost, labor, and maintenance cost, concentrate disposal cost, and financing interest rate. The total cost estimation of the plant is given by the sum of the total investment cost (CAPEX) of the plant, which are all the initial costs in year zero, indirect capital costs, which are based on a percentage of direct capital costs (Freight and insurance, construction overhead, owner's direct expense and contingency), depreciating capital costs that are amortized over the life of the plant (Land cost and working capital) and, operation and maintenance costs (OPEX) for chemicals, energy, supplies and maintenance materials, replacement parts and membranes, insurance and fixed charges.

Energy is the largest water production cost component of all desalination systems. The most relevant membrane processes (RO and ED) strongly depend on electrical energy, and their costs accounts for approximately 44% of the total water cost. The same occurs with thermal distillation processes (MED and MSF), which use low temperature heat for evaporation and electricity for pumps and control systems. The energy cost of a thermal distilled water plant represents around the 60% of the total cost of water production.

The water production cost from desalination systems coupled with renewable energy sources is highly linked to their energy costs. Despite the free cost of renewable energy, its capital cost is still high, this makes the water production cost high. However, these costs are increasingly being reduced since these technologies are constantly improving and reducing the cost of materials, and also because many governments are trying to encourage the use of renewable energy by subsidizing part of the installations. The economics of commercial RE-DES will be briefly

discussed, and Table 2.4-Table 2.5 present the average reported water production cost.

Phase change or thermal distilled processes, which use conventional fossil fuels, are more expensive than membrane distilled processes and it is due to the huge amount of fuel required to vaporize salt water [43]. A detailed cost comparison is illustrated in the next section.

2.4.1 Solar powered Thermal Desalination economics

Firstly, thermal desalination plants operated by fossil fuels are mainly used for seawater and have a large capacity. For MED plants, which produces more than 90,000 m^3/d of potable water, the estimated water cost oscillates between 0.44 and 0.85 €[2]/m^3. If water production of MED plants is around 30,000 m^3/d, the cost would rise up to 1.66 €/m^3. In contrast, MSF plants usually are bigger than MED plants, with a production capacity between 23,000 and 528,000 m^3/d, the reported water production cost was between 0.44 and 1.49 €/m^3. VC is generally used for small-scale water production with a capacity of around 1,000 m^3/d and it reported a water production cost between 1.7 and 2.21 €/m^3 [35]. The Table 2.4 summarizes the water production cost difference between these three technologies

Process	Size of the plant (m^3/d)	Water production cost (€/m^3)
MED	30,000	1.66-1.95
	>90,000	0.44-0.85
MSF	23,000-528,000	0.44-1.49
VC	1,000-1,500	1.7-2.21

Table 2.4: Cost of desalinated water in main thermal processes.

It should be noted that the above data has been analyzed from past projects where a Rankine cycle efficiency of around 0.3 provided the energy needed for the desalination process. There are other configurations that could reduce the total costs such as concentrating solar power (parabolic trough, linear Fresnel, or parabolic disc) and solar humidification and de-humidification. Currently, solar collectors have a thermal efficiency between 60% and 75% and their levelized cost $(LCOE)_{th}$ from solar

[2] Calculation is based on the assumption that 1$ = 0.85€

to thermal systems is between 0.042-0.077 €/kWh$_{th}$ (not taking into account desalination systems), but mainly depends on the type of the collector, unit price, efficiency, taxes and government subsidies [47]. These technologies are described and analyzed below.

There is also another category of solar thermal systems called direct systems in which the heat gaining, and desalination processes take place naturally in the same device. The main technologies are solar stills in which the still works as a trap for solar radiation that passes through a transparent cover. But this project analysis is only focused on commercial desalination technologies (MED).

2.4.1.1 Solar thermal-MED desalination process

Solar thermal process extracts heat energy from the sun's radiation and then it can be used in low-temperature heating or to drive a heat engine to generate electricity. Thus, a solar thermal collector absorbs solar radiation and transfers the thermal energy to a fluid passing through [48]. Concentrating solar power (CSP) is the main form of solar thermal energy that is used for electricity generation and can be perfectly fitted with MSF or MED desalination technologies. The most relevant technologies used in CSP are power towers and parabolic trough collectors. In a general CSP system, the collector absorbs solar radiation and heats a heat transfer fluid. Then, the heat can be used to drive a turbine and generate electricity or can be stored in thermal energy storages (TES) [49]. The performance of these technologies is measured by the conversion efficiency of irradiation-to-heat and mainly depends on the maximum temperature of the collector fluid, technology used, ambient temperature and incident irradiation.

MED desalination technology can be powered with CSP systems such as parabolic trough configuration as shown in Figure 2.11: Detailed configuration of CSP/MED system [50]., where superheated steam (>360 ºC) is generated. Then, combined with an organic Rankine cycle (ORC), the steam passes through a turbine to reduce the temperature until reaches a value of 70 ºC. Thus, it can be connected to the MED plant. The rest of the electricity generated by the turbine can supply the pumps and the control system of the MED plant. This RE-DES configuration system is still expensive. The reported water production cost oscillates between 2.04 and 2.38 €/m^3 [50].

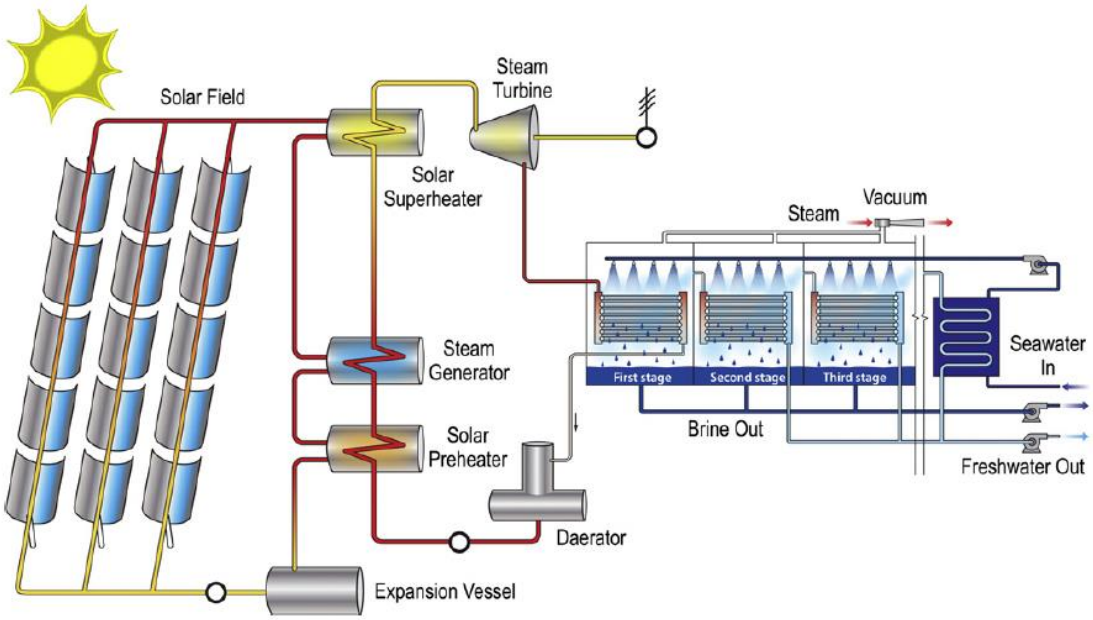

Figure 2.11: Detailed configuration of CSP/MED system [50].

Another typical and direct solar configuration is to use solar stills in which, seawater is evaporated directly by solar energy and condenses as distilled water (See Figure 2.12) [51]. This technology is simple, the capital costs is low and there is no need to be coupled with fossil fuels to evaporate water. However, the cost of water production is quite high because of the low productivity of the still. The reported average daily production rate of the still oscillates between 4 and 6 l/m^3, which is the same as ranging from 0.02 to 0.03 m^3/d if the still sizes 5 m^2. And for this daily production, water cost ranges from 1.11 to 5.3 €/m^3

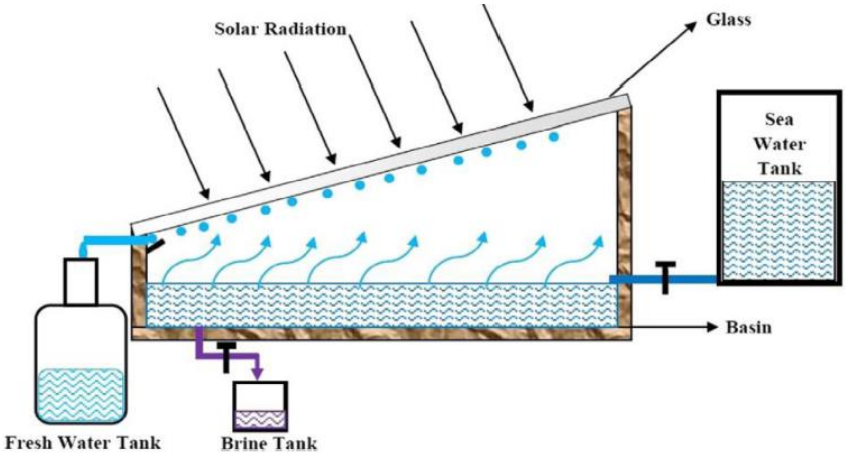

Figure 2.12: A schematic diagram of a solar still. Courtesy of [52].

2.4.2 Membrane Desalination economics

Membrane RO processes are a developed technology that have achieved a reduced water production cost. As mentioned in other sections, they can desalinate seawater, brackish water, or wastewater. For large SWRO plants with capacities oscillating between 100,000 and 350,000 m^3/d, the water production cost ranges between 0.38 and 0.56 €/m^3. When the size of the plant is around 30,000 m^3/day, water production cost is around 0.89 €/m^3 and, for units that are smaller than 1,000 m^3/day the water cost ranges from 0,6 to 1.46 €/m^3. On the other hand, for brackish water (when the intake water quality is less than 10,000 ppm), RO and ED are the most economic technologies for water desalination. RO is more economic than ED when the total dissolved solids are higher than 5,000 ppm. However, ED is the more cost-effective desalination system for lower ppm, unless high recovery is required. Then, the water production cost of more than 40,000 m^3/d BWRO plants is around 0.22 €/m^3 [35], whereas in ED plants the water production cost is around 0.51 €/m^3 [35]. All these data are illustrated in the Table 2.5.

Process	Size of the plant (m^3/d)	Water production cost (€/m^3)
SWRO	100,000-350,000	0.38-0.56
	15,000-60,000	0.41-1.38
	<1,000	0.6-1.46
BWRO	>40,000	0.22-0.46
	20-1,200	0.66-1.13
	<10	0.48-11.04
ED	>40,000	0.51
	1,000-10,000	0.89

Table 2.5: Average water production cost of the main membrane desalination processes. Data extracted from [35].

Comparing both Table 2.4 and Table 2.5, it is concluded that membrane processes, specifically **RO technology is more cost-effective compared to thermal distillation processes**, even though, these latter systems produce water with very low TDS compared to in the RO system. This is due to the improvement of this technology. It requires less pressure, has longer life, and a reduced water production cost [35]. The only case in which thermal distillation systems would be profitable is when the low-temperature heat is supplied from the by-product of the electricity power plant, any

waste heat, when there is an economically available solar source, or when the salt concentration is more than 60,000 ppm.

2.4.2.1 *Photovoltaic Reverse Osmosis (RO) desalination economics*

The combination of PV-RO system (Figure 2.13) has been developed extensively for small isolated systems. The biggest drawback is the huge initial investment and land availability, although the cost of photovoltaic solar panels has decrease within the last few years [53] (See Figure 2.14). All innovative technologies of solar modules oscillate between 0.3-0.8 USD/W or 0.26-0.68 €/W. Many of these systems use batteries or energy backup to run the system 24 hours a day but it leads to a higher cost of the water production.

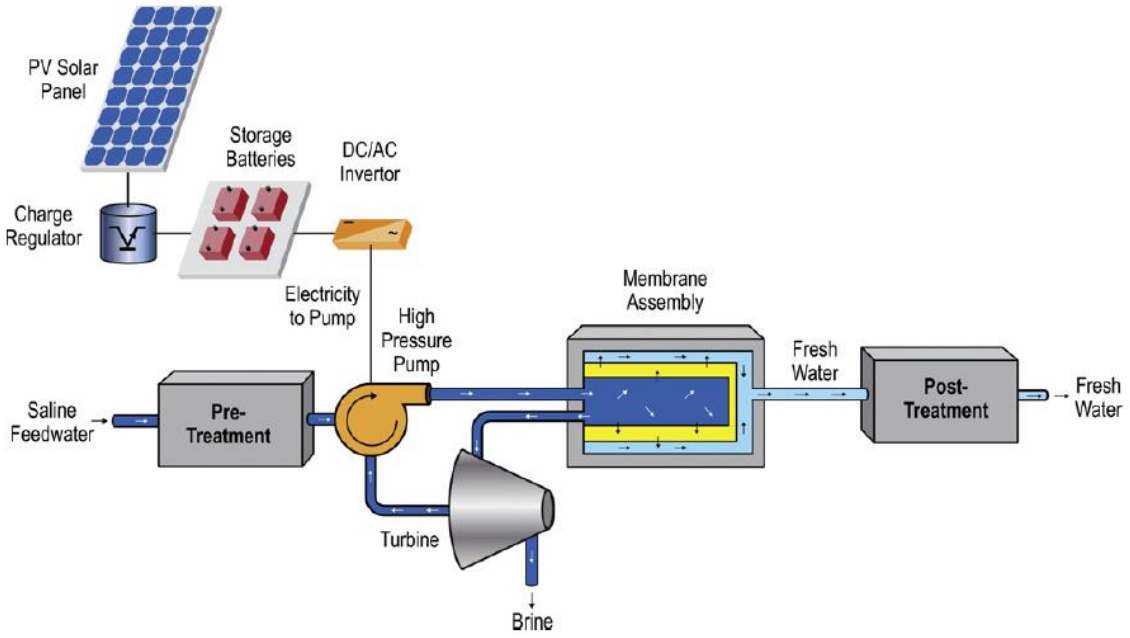

Figure 2.13: Detailed configuration of PV/RO system [36].

RO plants range in size from quite small unit scales from 0.1 m³/d to 395,000 m³/d whereas, renewable powered RO plants are mostly used in arid zones sparsely populated, remotely situated from large scale sources of potable water and electricity, with a capacity desalination less than 1,000 m³/day according to several scientific studies in the past years. However, this kind of technologies has also been evaluated for large water production capacity. A clear example is the PV powered SWRO plant located in Saudi Arabia, the largest PV-RO desalination plant in the world that has recently been installed It supplies more than 60,000 m³/d of desalinated seawater to the city of Al Khafji and it has an installed capacity of 15 MW connected to the desalination plant and the national grid. It produces enough power

during the peak hours that will be sufficient to sustain the energy requirement of the desalination plant.

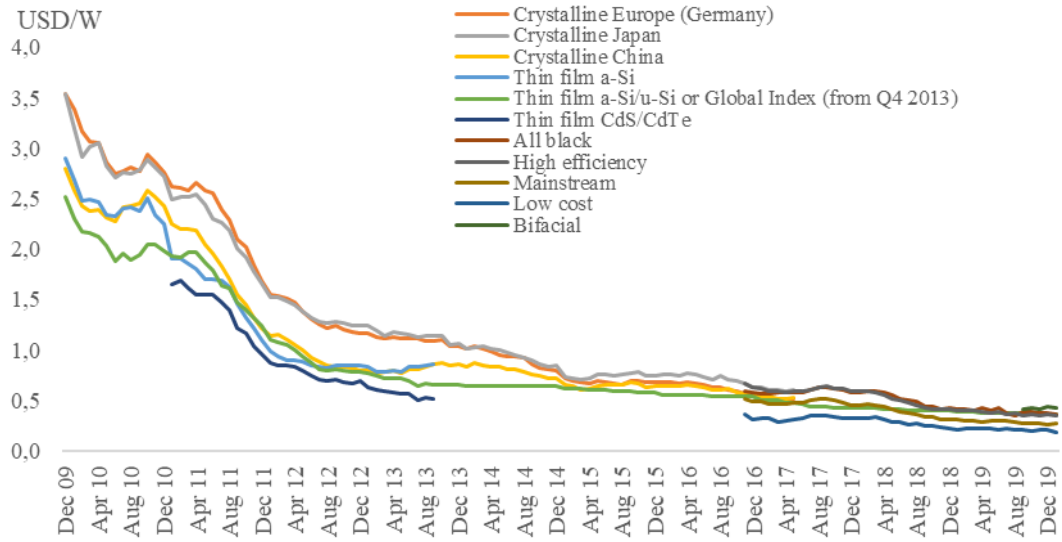

Figure 2.14: Average monthly solar PV module prices by technology and manufacturing country sold in Europe, 2010-2020. Data extrated from International Energy Agency (IRENA).

There is no doubt that PV-powered reverse osmosis is considered one of the most promising and attractive configurations of renewable energy powered desalination and it is due to several factors such as:

- The modularity of photovoltaic system provides different scales of reverse osmosis implementation, and its capacity can be increase after installation.
- The ease of predicting the solar radiation intensity curve compared to the random variation of wind power.
- The minimal maintenance required for PV modules and their long lifetime.
- Areas that demand high water consumption usually have high solar radiation.

Directly coupled PV-RO produces the most water competitive price. PV-RO systems are found to be more economically viable than diesel-powered systems, provided that solar energy resources are sufficient. According to Manolakos et al. [54], a techno-economic study of both technologies was done, and water production cost for the PV-RO was significantly lower than that of the ORC at 7.77 €/m³ compared to 12.53 €/m³. Table 2.6 shows a vast number of projects that are done with this mix of technologies.

Location	PV power (kW)	Size of the plant (m³/d)	Feedwater (ppm)	SEC (kWh/m³)	Production cost (€/m³)
Massawa, Eritrea (2002)	2.4	3	40,000	3.5	2.36
Athens (2007)	0.85	0.35	32,738	4.6	7.8
United Arab Emirates (2008)	17.9	20	45,000	7.33	6.24
Thirasia island, Greece (2008)	0.846	2.4	22,000	3.8-6	7.77
USA (2011)	0.23	0.3	35,000	4.2-5	5.63
Al Khafji, Saudi Arabia (2019)	**15,000**	**60,000**	**45,000**	**-**	**5.04**
Fortaleza, Brazil (2014)	-	3,600	BW	-	-

Table 2.6: Summary of PV-RO desalination plants over the world

2.4.2.2 *Photovoltaic Electrodialysis economics*

ED uses direct current on the electrodes of the battery stack, so it can use the energy supply from the photovoltaic technology without major modifications using inverters. PV/ED is the most competitive in low concentration brackish water. Figure 2.15 shows a schematic diagram of this kind of systems.

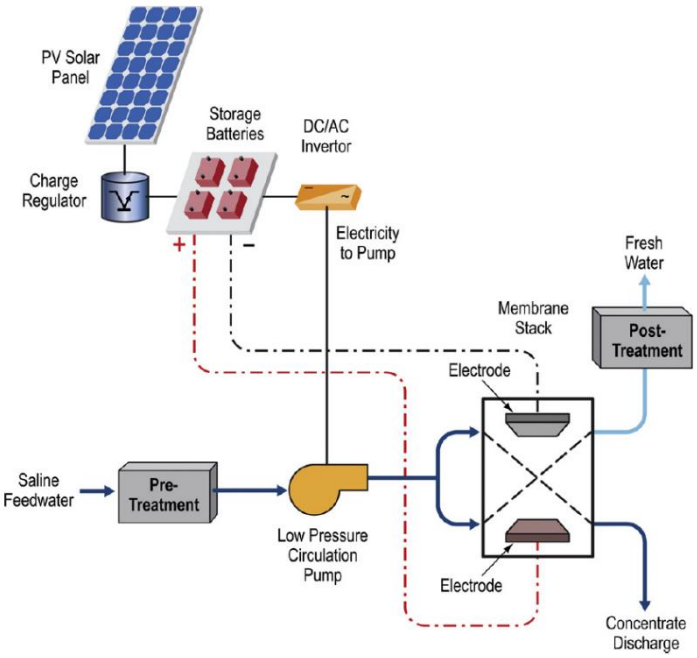

Figure 2.15: Schematic diagram of PV/ED. Courtesy of [36].

2.4.2.3 *Wind-RO desalination economics*

Wind-RO and PV-RO are the most widely deployed technologies for renewable energy desalination contributing 19% and 32% of the field respectively (Figure x) and it is due to their availability, affordability, technological maturity, and zero CO_2 emissions [33]. Wind turbines play an important role of achieving sustainability goals of many countries [55]. They have low operating costs and high efficiency, energy availability making wind turbines a successful and clean option for powering RO plants [45],[56], reducing carbon footprint and water production costs [57].

The major drawbacks of wind turbines are their strong dependence on air velocity. It must be range from 10 to 25 m/s. If the speed of wind is less than 5 m/s, the turbine will not supply energy because of there will no movement of it and if the velocity value is more than 25 m/s, the control system of the wind turbine will stop it, otherwise the wind could damage the blades. Furthermore, wind turbines must gain social acceptance and improved public perception due to their aerodynamic noise and visual impact.

In some regions, the cost of wind power that drives desalination is getting increasingly competitive with other conventional energy costs in water supply. The onshore wind power system cost oscillates between 5 and 9 cents/kWh and 10 to 20 cents/kWh offshore. However, these costs are planned to fall to approximately 2-3 cents/kWh by 2022, which will be close to fossil fuels. The cost of natural gas is estimated to be 2-4 cents/kWh and 3-5 cents/kWh of coal. Table 2.7 shows a comparison of the water production cost between both renewable powered RO and conventional energy sources powered RO plants. Although the cost of wind-RO is more attractive than PV-RO, traditional powered reverse osmosis plants are still considered to be the most cost-effective, with a cost advantage over wind energy. However, with the increasing scarcity of fossil fuels and rising prices, wind and solar power capacity will be expanded, and the use of technologies will become more mature [22], [58].

	PV-RO	Wind-RO	Wind-RO	Conventional
Size capacity (m^3/d)	<100	<100	1,000-2,000	1,000
Water production cost (€/m^3)	BW: 5-7	BW: 3-5	1.5-4	BW: 0.21-1.06
	SW: 3.14-9	SW: 5-7		SW: 0.35-2.7

Table 2.7: Comparative costs for RO water production [22], [58].

3. Optimal Sizing of a HRES powered desalination plant

The aim of this section is to design a renewable energy system, to meet the electrical load demand of a reverse osmosis plant, and to figure out the optimal sizing and techno-economic evaluation of several off-grid power systems such as photovoltaic, wind, and diesel generator technologies. These simulations will be analysed with HOMER Pro™ software to identify the best performance and the optimal plant configuration.

The case study is based on a typical SWRO that will be in the Canary Islands, Spain specifically in El Hierro, which is the smallest island of the archipelago with only 10,000 inhabitants. The Canary Islands are an archipelago located on the Atlantic Ocean, near the Southern coast of Morocco. It is autonomous community of Spain consisting of the following main islands: El Hierro, La Gomera, La Palma, Tenerife, Gran Canaria, Lanzarote and Fuerteventura [59] (See Figure 3.1).

The main limitation of desalination is its high energy requirement, and the increase in environmental pollution due to the use of fossil fuels. About 98% of the primary energy consumption of the archipelago comes from imported fuel. Due to its remote location and high fuel prices, it is obvious that the isolated power system has increase the difficulty of its optimization [60]–[62].The energy required for desalination of public facilities in the Canary Islands may account for 5% to 10% of the island's total electricity generation [59].

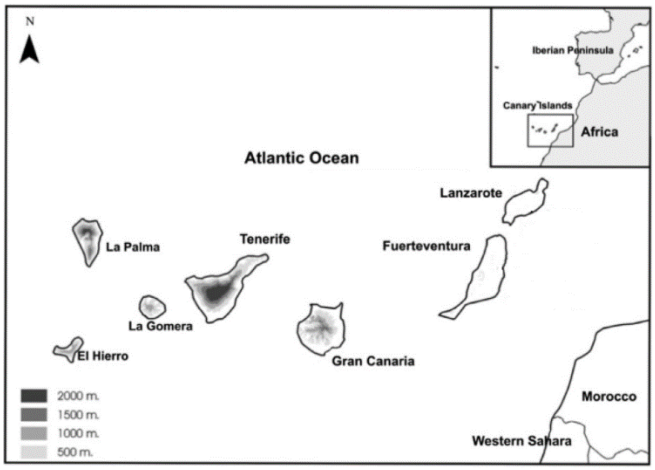

Figure 3.1: Canary Islands and El Hierro location [59].

The use of renewable energies (RES) production for fresh water from sea has produced an innovative technology that can minimize the possible environmental impact of the desalination process due to the huge energy consumption produced by fossil fuels. Thus, RES also allow avoiding external dependence of the fossil fuels [63]. In this case and mostly of islands that suffer from freshwater scarcity has usually good solar radiation and wind potential [59].

An autonomous desalination system (ADS) perfectly fits in this case. It is basically a desalination system powered with a hybrid renewable energy system (HRES). ADS is an excellent choice for regions which suffer from water scarcity or with a huge tourist volume that want to be environmentally friendly avoiding the pollution for the use of fossil fuels in the desalination. HRES could be combined with renewable and conventional energies and these systems can work off-grid or connected to the electrical grid in order to reach the highest efficiencies [64].

These ADS located in El Hierro consists of 10,000 inhabitants. A maximum daily consumption 200 L/d/inhabitant was assumed, also taking future water needs into consideration. Therefore, the maximum total water production needs are 2,000 m^3/day. So, for this production capacity, it is necessary to feed the plant with approximately 5,000 m^3/day, as the conversion rate of this type of plant is around 40%. In Section 4, the SWRO plant has been designed to go deeper into this type of technology.

3.1 Input data elaboration

In the following subsections, each HOMER Pro input variable is described in detail, including the evaluation of the load demand and REs activity.

3.1.1 Seawater Reverse Osmosis plant characteristics

The design, input and output characteristics of the plant located in “El Hierro” are calculated in the Section 4, and the SWRO specifications are listed in Table 3.1.

Parameter	Value
Size capacity	2,000 m³/d
Water intake capacity	5,081.51 m³/d
Permeate recovery	39.4%
Feedwater design temperature	25ºC
Feedwater TDS	35,984.11 mg/L
Feedwater pH	8.1
Operation period	12 h/d
Permeate TDS	305.68 mg/L
Peak power demand	496.19 kW
Average power demand	181.67 kW
Energy consumption	2.18 kWh/m³
Load factor	0.31
RO feed pressure	52.3 bar

Table 3.1: SWRO desalination plant characteristics.

3.1.2 Electrical load demand

As shown in the table above, the RO desalination plant with a capacity of 2,000 m³/d, consumes 4,360 kWh/day, with an average demand of 181.67 kW and a peak demand of 496.19 kW. The monthly average of electric load variation of the desalination plant is shown in Figure 3.2 The highest demand for electricity takes place in July, and the lowest one in January.

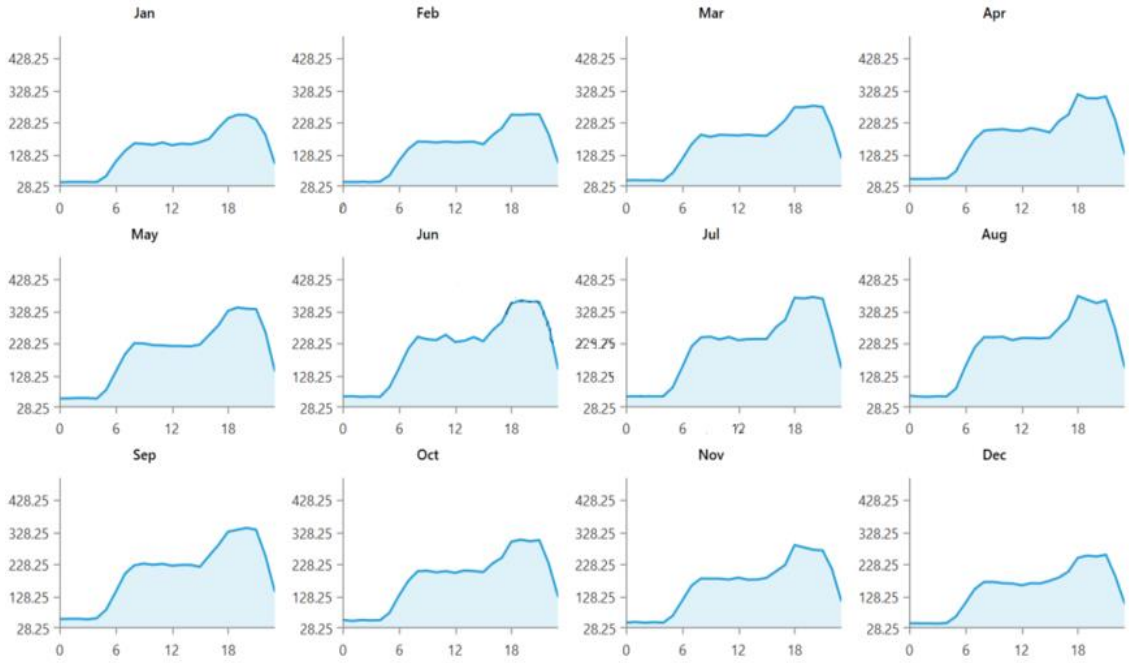

Figure 3.2: Monthly average of electric load variation of the SWRO desalination plant. Load demand in kW (X-axis) and hours per day (Y-Axis). Simulated in HOMER Pro™.

3.1.3 Solar radiation and wind speed in El Hierro, Canary Island

The monthly solar radiation values of El Hierro are obtained with the HOMER Pro software from NASA (National Aeronautics and Space Administrative) [65] (See Figure 3.3). The coordinates from El Hierro are: 27º46.1'N, 18º1.3'W and the average solar radiation value is 6.01 kWh/m²/day.

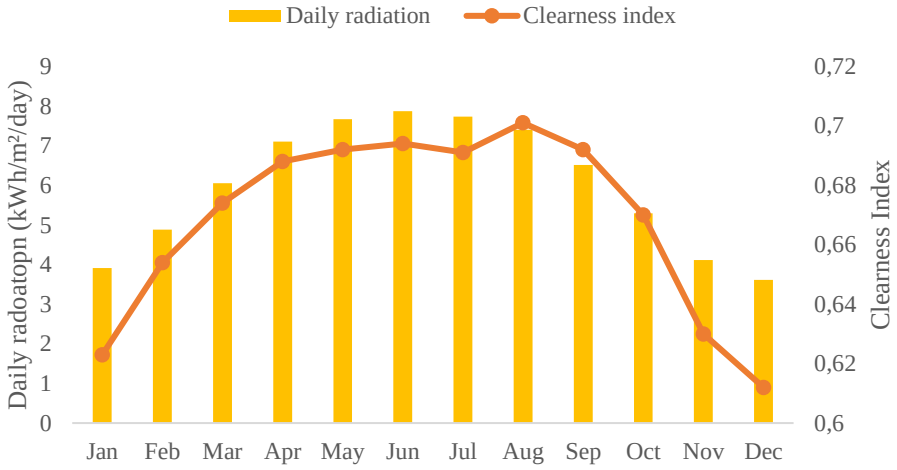

Figure 3.3: Monthly average Solar Global Horizontal Irradiance (GHI) Data over 22-year period (Jul 1083-Jun2005). Data extracted from NASA Prediction of Worldwide Energy resource (POWER) Database.

The coordinates from El Hierro are: 27º46.1'N, 18º1.3'W. The solar radiation at these coordinates varies from 3.91 kWh/m²/day in January to 3.61 kWh/m²/day in December hitting its maximum in July with 7.87 kWh/m²/day so the average solar radiation value is 6.01 kWh/m²/day.

On the other hand, a monthly average wind dataset from El Hierro (27º46.1'N, 18º1.3'W) was collected, at 190 m above sea level. As shown in Figure 3.4, wind speed has a minimum value of 5.24 m/s in October and a maximum value of 7.33 m/s in July with an annual average of 6.23 m/s. The temperature practically varies from 20 to 25 degrees during the entire year.

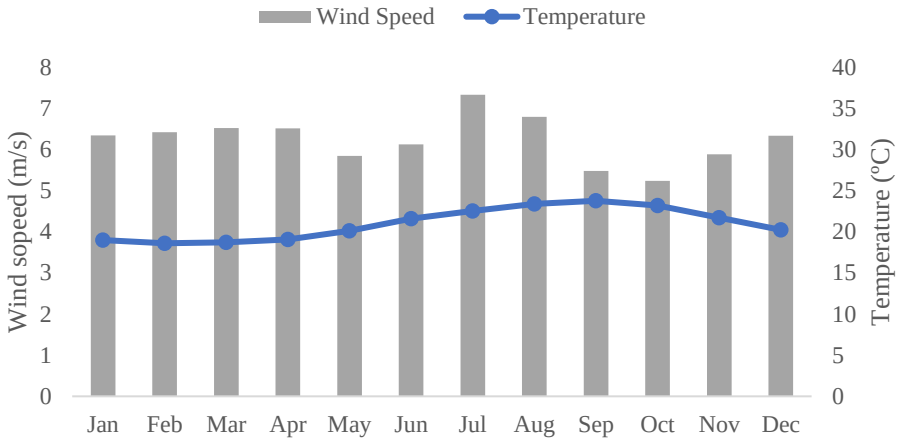

Figure 3.4: Monthly average Wind Speed Data over 30-year period (Jan 1984-Dec2013). Data extracted from NASA Prediction of Worldwide Energy resource (POWER) Database.

3.2 System structure, specifications, and mathematical model

The Hybrid Renewable Energy System (HRES) proposed in the present project is based on different off-grid combinations of photovoltaic (PV) modules and wind turbines supplemented with battery banks. In addition, it will be possible to add diesel generators, if necessary, shown in Figure 3.7. In this HRES, PV and wind turbines are the main power sources, and diesel is used as a backup to compensate for the random variation in solar and wind energy output.

Therefore, the objective of this HRES is to supply the necessary energy to provide power to an ADS with a production of 2,000 m^3/d with an energy consumption of 2.18 kWh/m^3 as it was calculated in chapter 4.

3.2.1 Photovoltaic system

Photovoltaics arrays are modelled in the software independently of the cell voltage and temperature. HOMER assumes that direct current (DC) output of PV module is linearly proportional to the incident global radiation upon it [66].

The power output of the PV array is calculated using the equation (3.1) which is a simplification considering the effect of ambient conditions on the power output:

$$P_{MPP} = \frac{G}{G_{ref}} * P_{sc,ref} * f_{PV} \quad (3.1)$$

Where, G is the global solar radiation (beam and diffuse) incident on the PV array surface expressed in kW/m², while G_{ref} is the maximum global solar radiation and its value is 1,000 W/m², $P_{sc,ref}$ is the rated capacity of the PV array in kW, and f_{PV} is the PV derating factor which accounts for effects of dust, wire losses, elevated temperatures on the panel and its value can be determined by the equations (3.2) and (3.3):

$$f_{PV} = 1 + \gamma * (T_c - T_{c,ref}) \quad (3.2)$$

Where $T_{c,ref}$ is the cell reference temperature provided by the manufacturer and T_c is the cell temperature and it is calculated by the equation (3.3).

$$T_c = T_{amb} + G * \frac{NOCT - T_{NOCT}}{G_{NOCT}} \quad (3.3)$$

In which T_{NOCT} is the nominal operating cell temperature.

The initial capital cost (ICC_{PV}) of the PV modules estimated in the software is 1,200 € per installed kilowatt [67], [68], [69], and the replacement cost (RC_{PV}) is slightly lower than the capital cost. In this case, it is considered a value of 700 €/kW [68]. These costs correspond to the PV panels, mounting hardware, wiring, installation, and so on. In addition, the operation and maintenance cost (OMC_{PV}) estimated is 0.015*ICC_{PV}. The PV size considered for the system can vary between 0 to 1,000 kW (Table 1). Finally, the lifetime of the PV array estimated is 25 years and there is no tracking system included.

The properties of the PV modules are included in the data sheet placed on the Appendix A.

3.2.2 Wind turbine

The function of a wind turbine is simple, the kinetic energy of wind converts into electricity thanks to the mechanical movement of the turbine. Thus, HOMER Pro

software determine the average wind turbine power based on the Weibull probability density function by means of the equation (3.4):

$$P_{wind} = \frac{1}{2}\tau * \rho * C_p * A * \sum_{x=1}^{j} f_{(v)} * v_x^3 \qquad (3.4)$$

Where τ is a determined period of time, ρ is the density of the air and it is equal to 1.225 kg/m³, C_p corresponds to the capacity factor of the wind turbine, v_x^3 is the velocity of the wind in which the power generation highly depends on it, and $f_{(v)}$ is the Weibull distribution [59].

The initial capital cost (ICC_{WT}) of the wind turbine selected in the software is 30,000 € per unit [70], [71], and the replacement cost (RC_{WT}) is slightly lower than the capital cost. In addition, the operation and maintenance cost (OMC_{WT}) estimated is 0.025*ICC_{WT} [59]. Finally, the lifetime of the wind turbines estimated is 20 years which is provided by the manufacturer. All data is shown in Table 3.2.

3.2.3 Battery Bank

The battery bank can be made by one or more batteries. A battery is a device that can store a part of the electricity generated by means of renewable energy or other conventional energy sources. In HOMER Pro, the main characteristics of a battery are its round-trip efficiency, minimum state of charge, lifetime, capacity curve, and maximum voltage [66], [59].

The battery bank considered in this project consists of generic 1 kWh Li-on [ASM][3] for 276 Ah in seven strings of 3.7 V provided by the software and it can store 2,430 kWh which is calculated by the formula (3.5):

[3] The generic Li-on [ASM] is an example battery of 1 kWh nominal capacity that uses HOMER's new Modified Kinetic Model. This example battery includes rate dependent losses, temperature dependence on capacity, cycle lifetime estimation using the Rainflow Counting, and temperature effects on calendar life.

$$E = \eta * D_d * V_0 * C_N \quad (3.5)$$

Where η is the efficiency of the batteries, D_d is the determined period in which the battery can store electrical energy, V_0 is the output voltage, and C_N is the capacity of the battery bank and is expressed in Ah.

Furthermore, a controller will be installed to control the generator and the battery bank in order to use energy better. There are three important dispatch strategies:

- HOMER Cycle Charging (CC). When a generator is required, it works at maximum capacity and all the energy excess charges the batteries.
- HOMER Load Following (LF). When a generator is required, it supplies only enough power to meet the load demand and does not charge the battery.
- HOMER Combined Dispatch (CD). It is a combination of the previous dispatch strategies in order to improve performance over both, by making more efficient use of the generator.

According to a similar case study [72], the three of them strategies were simulated in order to find the optimal configuration.

3.2.4 Converter

A converter is needed to convert electric power from DC to AC due to the PV array is in DC bus. The size of the converter normally is 1.25 times the peak power demand, which in this case is approximately 580 kW. Thus, the converter may vary from 0 to 750 kW [59]. Lifetime of a device is estimated to be 15 years and an efficiency of 95% as shown in Table 3.2.

3.2.5 Generator

A generator is a conventional power source that consumes fuel. In this case, the possibility of installing a diesel generator is being studied if RE systems do not cover the electrical demand at any given period.

HOMER Pro sets the fuel curve as linearly proportional for the generator's fuel consumption and uses the equation (3.6):

$$F = F_0 Y_{gen} + F_1 P_{gen} \quad (3.6)$$

Where Y_{gen} is the nominal capacity of the diesel generator in kW, P_{gen} is the power output of the generator, F_0 is the fuel curve y-intercept coefficient, and F_1 is the fuel curve slope. The units of F are in L/h, m³/h [66].

As the generator used is an internal combustion engine, diesel fuel is needed to feed the system and a price of 1€/liter is set in the software. Table 3.2 also resumes the capital, replacement, and O&M costs assumed for the generator. Consequently, HOMER calculates the fixed and marginal's cost of energy with the equations (3.7) and (3.8) [66]:

$$c_{gen,fixed} = c_{om,fixed} + \frac{C_{rep,gen}}{R_{gen}} + F_0 Y_{gen}\, c_{fuel,eff} \quad (3.7)$$

Where $c_{om,fixed}$ is the operational and maintenance cost in €/h, $C_{rep,gen}$ is the replacement in €, R_{gen} is the lifetime of the generator, F_0 is the fuel curve y-intercept coefficient in L/h/kW, Y_{gen} is the generator capacity in kW, and $c_{fuel,eff}$ is the effective price of fuel in €/L which includes the CO_2 emissions cost penalties [66].

$$c_{gen,marg} = F_1 c_{om,eff} \quad (3.8)$$

Where F_1 is the fuel curve slope in L/h/kWh [66].

Components	Model	Capital cost	Replacement cost	O&M cost	Lifetime	ref
PV modules	Canadian Solar MaxPower CS6X-325P	1,200 €/kW	700 €/kW	13 €/year	25 years	[67]-[69]
Wind turbine	Eocycle EO10	30,000 €/unit	15,300 €/unit	750 €/year	20 years	[70], [71]
Converter	Generic system	527 €/kW	154 €/kW	8 €/year	15 years	[59]
Batteries	Generic 1kWh Li-Ion [ASM]	641 €/unit	126 €/unit	15 €/year	25 years	[66], [59]
Generator	Diesel generic	760 €/kW	753 €/kW	0.03 €/op. hour	15,000 hours	[73]

Table 3.2: System components and input prices considered in the project based on literature review.

3.3 System constraints and other considerations

The HRES to be analyzed also has several system and user-imposed limitations. On one hand, the economic variables of the project have been considered such as the nominal discount rate, the expected inflation rate, the lifetime of the project, and penalties for capacity shortages. Table 3.3 shows all these values considered in this project.

On the other hand, constraints such us the maximum annual capacity shortage and the minimum fraction of renewables have also been considered, as well as other considerations regarding the operating reserve such as the minimum percentage of load in case demand suddenly increases exponentially, or the minimum percentage of solar and wind energy production.

Finally, it has also been considered carbon dioxide emissions penalties in € per ton possibly caused by the diesel generator. The value shown in the table below was estimated according to EU energy policies [74].

Constraints	Model	
Max. capacity shortage	0-5%	[74]
Min. RF	90%	-
Solar power output	80%	-
Wind power output	50%	-
Nominal discount rate	12.25%	[75]
Expected inflation rate	5.1%	[75]
Project lifetime	25 years	-
Capacity shortage penalty	10 €/kWh	[76]
CO_2 emission penalties	100 €/ton	[74]

Table 3.3: Project constraints and considerations over its lifetime.

It has been considered two different discount rates to perform a sensitivity analysis to know how affects this variable to the system.

3.4 Evaluation criteria

3.4.1 Total Net Present Value

Net present cost (NPC, €) of a project or HRE system is the difference between the present value of the whole costs of the system during its lifetime and the present value of all revenue it earns over its lifetime. It includes capital, replacement, operational and maintenance costs, fuel, and emissions penalty costs. In contrast, revenues include salvage and grid sales revenue if it is connected to the grid. HOMER calculates the NPC by summing the total discounted cash flows in each year of the project lifetime [77] and can be calculated by the following equation (3.9):

$$NPC = \frac{C_{tot}}{CRF(d_r, p)}, where\ CRF(d_r, p) = \frac{d_r(1+d_r)^p}{(1+d_r)^p - 1}\ and\ d_r = \frac{d_r' - f_r}{1+f_r} \quad (3.9)$$

Where CRF is the capital recovery factor, d_r is the real discount rate, d_r' is the interest rate, p is the lifetime of the project, C_{tot} is the total cost per year that includes all the costs mentioned above, and f_r is the inflation rate [78].

3.4.2 Levelized Cost of Water

Although the HOMER software only does an analysis of the HRES, the LCOW should also be considered since the purpose of the work is the production of water by means of ADS. So, the levelized cost of water is the average cost per m³ of freshwater production by the system. This parameter accounts for the capital and operating system of the whole project over its lifetime and allows for a comparison of other similar projects [79]. It is calculated by the equation (3.10).

$$LCOW = \frac{\sum_{i=1}^{n}(CRF(d_r, p)ICC_i) + RC_i + OMC_i}{Q_p} \quad (3.10)$$

Where Q_p is the total water production by the system during its lifetime, ICC_i.is the total capital cost, RC_i is the total replacement cost, and OMC_i is the total O&M cost.

3.4.3 Levelized Cost of Energy

The levelized cost of energy or LCOE is the average cost per kWh of useful electrical energy produced by the system. It is the rate of the total energy output of

the energy system to operate it over its lifetime to the average cost of the system over that lifetime. Thus, to calculate this value, HOMER uses the equation:

$$LCOE = \frac{\sum_{i=1}^{n}(CRF(d_r, p)ICC_i) + RC_i + OMC_i}{E_L} \quad (3.11)$$

Where E_L is the total energy production by the system during its lifetime, ICC_i.is the total capital cost, RC_i is the total replacement cost, and OMC_i is the total O&M cost [80].

3.4.4 Capacity Shortage Fraction

CSF is the fraction between the total capacity shortage and the total electrical demand during a determined period. A capacity shortage is a shortfall that occurs between the required operating capacity and the actual amount of operating capacity the system can provide [77]. If its value is equal to 0 means that the load demand is continually satisfied, and if it is one means that the load is never served [78].

$$CSF = \frac{E_{sh}}{E_{Load}} E_{sh} = E_{Load} - E_{gen} \quad (3.12)$$

Where E_{Load} is the total load served, E_{sh} is the capacity shortage, and E_{gen} is the total energy generated by the system.

3.4.5 Total Carbon emission

It represents the overall greenhouse gases (GHG) emitted in form of carbon dioxide produced (ton CO_2/year) by the HRES in a period. It is a frequent environmental indicator to evaluate the emission performance of the system, and it is directly linked to how much fuel is consumed [81].

$$TCE = \sum_{tT} TCO_2 E_{diesel} \quad (3.13)$$

Where TCO_2 is the total amount of carbon dioxide emissions expressed in ton/kWh, and E_{diesel} is the total energy production of the diesel generator expressed in kWh.

3.4.6 Renewable fraction

The renewable fraction is simply the total percentage of the renewable energy delivered to the load.

$$RF = \frac{E_{RES}}{E_{load}} \quad (3.14)$$

3.5 Selection methodology

As said above, the simulation and optimization process are conducted using the HOMER Pro software package. Therefore, the research framework can be divided into three stages: pre-HOMER evaluation, optimization analysis, and results evaluation. Figure 3.5 shows the graphical outline of the method used in this project. The pre-HOMER evaluation is first conducted through a case-by-case assessment of the existing renewable energy resources and the load requirements of the inspected site. For the time being, the limitations related to modern energies and climate conditions are also recognized. In the second stage, the selected energy technology configuration is accurately developed by the HOMER software, and then the technical, environmental, and economic optimization analysis is performed. In the current study, the system goal is to run different system costs, CO_2 emissions, and the possibility of power loss. The different combinations are rated according to energy cost and net present cost. In the last stage, the development and evaluation of best sustainable configuration with the lowest cost and emissions and maximum reliability is analyzed.

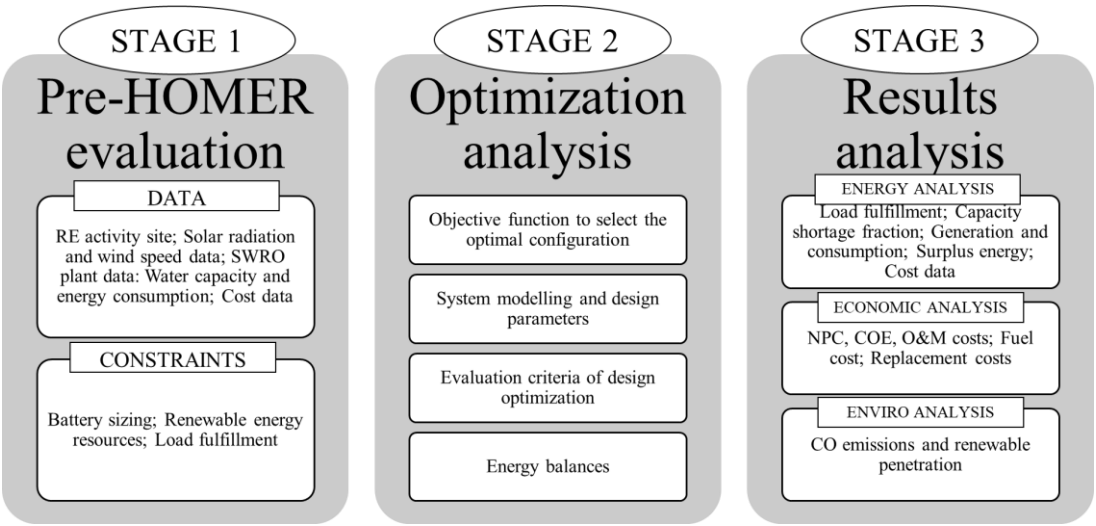

Figure 3.5: Schematic framework procedure for the case study. Own elaboration.

3.6 Model optimization and data

In this project, the techno-economic and environmental design of SWRO-HRES is formulated to optimize various evaluation criteria in terms of minimizing the net

present cost (NPC) of the system, capacity shortage fraction (CSF), cost of energy (COE), renewable penetration (RP), and minimizing the total CO_2 emissions (TCE). The input variables of the components are the capacity of the PV system, the size of the diesel generator, the size of the battery bank, the number of wind turbines, and the converter power. Figure 3.6 shows the schematic procedure to select the optimal combination and configuration of HRES to power the SWRO plant [78].

First, a pre-HOMER evaluation is performed by estimating the existing solar radiation and wind speed data from NASA, and the yearly, daily, and hourly electrical load demand required for the desalination plant. Once the financial requirements and design parameters of the components described above are collected for the case study, HOMER software starts to add a photovoltaic system to meet the electrical load demand and then checks if the total demand is satisfied. A converter is included in the case the PV system successfully meets the load demand as the PV array is in the DC bus. Otherwise, a wind turbine is also added to support the photovoltaic system. Subsequently, the software verifies the load demand fulfilment again. If the load is working properly, the software also includes a battery bank to store any excess of electrical energy in a period. Moreover, a conventional power source generator can be added as a backup system if the other renewable energy systems do not meet the load demand due to their random availability or a higher peak demand in a determined period of time [78].

Finally, a techno-economic and environmental assessment is performed for each HRES configuration. Once all the simulations are done for several different HRES configurations, the optimization is completed, and the software ranks them according to the optimization objectives [78].

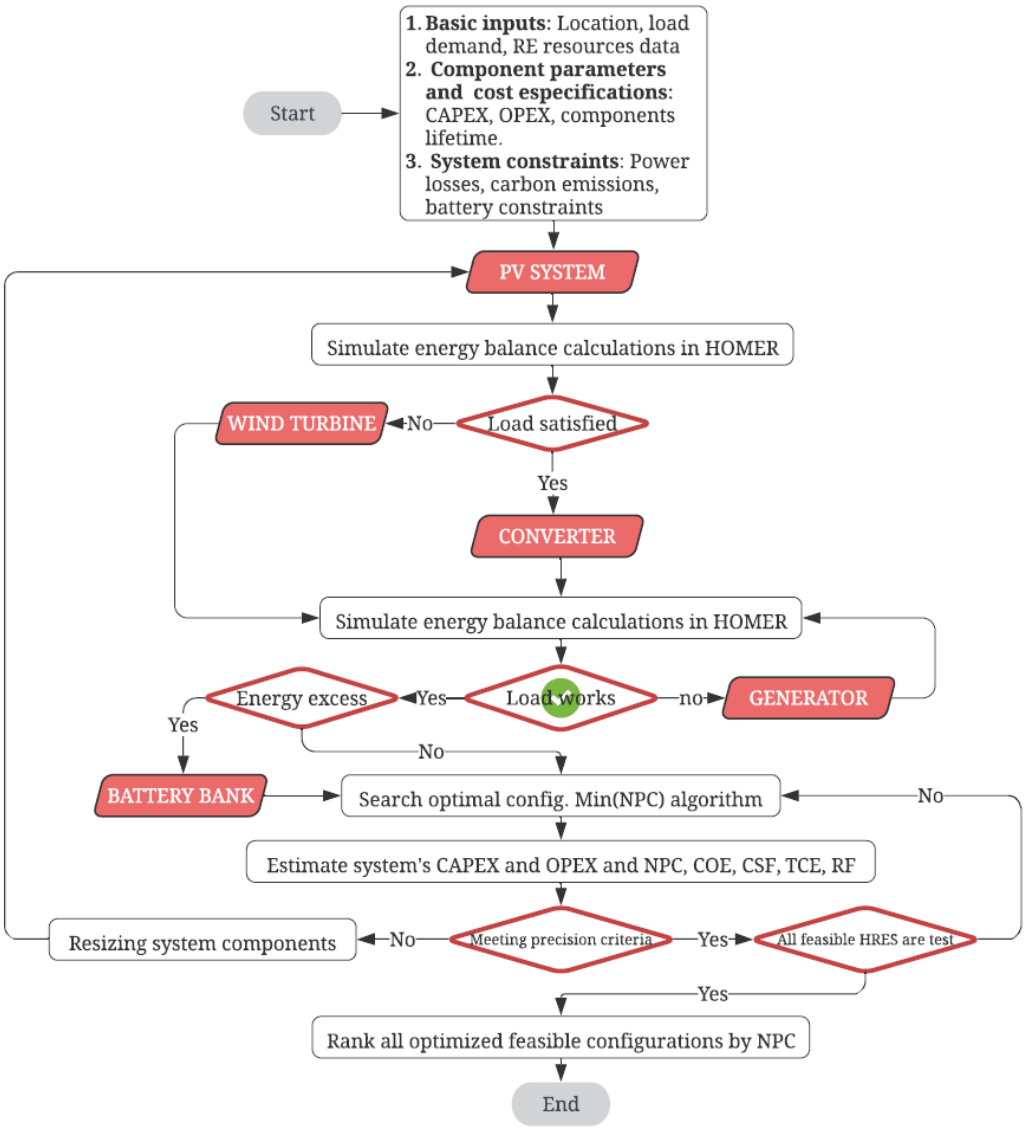

Figure 3.6: Flowchart procedure to select the optimal HRES configuration using HOMER Pro software. Own elaboration.

3.7 Results and Discussions

In this part, the software screen shows several HRES configuration for each variable from the sensitivity analysis. It has been decided to separate the possible configurations into two scenarios: The first HRES configurations are coupled with a diesel generator and the others consist only of renewable technologies to highlight the impact of CO_2 and the performance of the system.

3.7.1 Developed study configurations

A number of ten different off-grid energy configuration were analyzed, compared, and classified into the two scenarios that are mentioned above and are shown in Table 3.4. The schematic diagram in Figure 3.7 shows all the different off-grid configurations provided by HOMER™.

	Diesel	PV	Wind	Converter	Battery
Config.1	Yes	No	Yes	Yes	Yes
Config.2	Yes	Yes	No	Yes	Yes
Config.3	Yes	Yes	Yes	Yes	No
Config.4	Yes	Yes	Yes	Yes	Yes
Config.5	Yes	No	Yes	No	No
Config.6	Yes	Yes	No	Yes	No
Config.7	Yes	No	No	No	No
Config.8	No	Yes	Yes	Yes	Yes
Config.9	No	Yes	No	Yes	Yes
Config.10	No	No	Yes	Yes	Yes

Table 3.4: Off-grid energy configurations according the two scenarios.

3.7.2 Optimization results

Table 3.5 resumes the results of each energy configurations from the techno-economic and environmental analysis to supply the autonomous desalination plant that consumes 4360 kWh/day. All configurations have the same inputs regarding the energy resources, site location, the component types and costs described in Section 3.2, and the project constraints imposed by the user.

In the results table it can be seen the number and quantity of components used in each configuration, a report of the project costs separating the fixed cost and investment from the operating and maintenance costs. It also shows the percentage of renewables, the fuel consumption of the generator in case of being in the first scenario, the energy excess and the energy strategy used in each case. The last column represents the ranking from 1 to 10 starting from the optimal configuration that minimizes the net present cost, although the CO_2 emissions and the percentage of renewables operating in the system have also been assessed. Finally, as can be seen in the table, the optimal configuration that minimizes the net present cost is the one in blue where all the components form the system

		Rated optimal capacities						Evaluation criteria				Cost data		Gen data		Energy	Overall
		Gen Diesel kW	PV CS6X-325P kW	WT EO10 Unit	Batts LI ASM Unit	Conv Generic kW	**NPC** **M€**	COE €/kWh	Excess %	RF %	GHG Ton/y	CAPEX M€	OPEX €/y	Fuel cons L/y	hours L/y	**manage strategy**	**rank**
1	DG/Bt/Cv/WT	550	-	30	490	343	**4.28**	0.227	27.5	73.2	285,971	1.81	208,029	109,249	901	CD	2
2	DG/Bt/Cv/PV	550	1,081	-	3,416	444	**5.66**	0.300	21.0	94.6	67,744	4.14	128,456	25,880	588	LF	5
3	DG/Cv/WT/PV	550	438	36	-	250	**5.45**	0.288	54.4	73.9	314,944	2.16	277,387	120,317	2,304	CD	4
4	DG/Bt/Cv/WT/PV	550	274	28	518	341	**3.97**	0.210	36.0	80.9	204,354	2.10	157,470	78,069	649	CD	1
5	DG/WT	550	-	42	-	-	**5.52**	0.292	48.4	69.3	372,925	1.68	323,709	142,467	2,786	CD	3
6	DG/PV/Cv	550	1,042	-	-	357	**9.57**	0.507	48.5	29.8	832,107	1.86	650,552	317,888	5,593	CD	8
7	DG	550	-	-	-	-	**12.4**	0.658	10.6	0	1,322,389	418,100	1,010,000	505,188	8,760	LF	9
8	Bt/Cv/PV/WT	-	2,297	4	3,696	682	**6.90**	0.366	63.8	100	-	5.61	109,373	-	-	CC	6
9	Bt/Cv/PV	-	2,070	-	4,907	572	**7.57**	0.401	57.1	100	-	5.93	138,384	-	-	CC	7
10	Bt/Cv/WT	-	-	187	16,576	1,595	**22.9**	1.21	82.6	100	-	9.13	282,238	-	-	CC	10

Table 3.5: Optimization results of the different off-grid configurations simulated in HOMER Pro™.

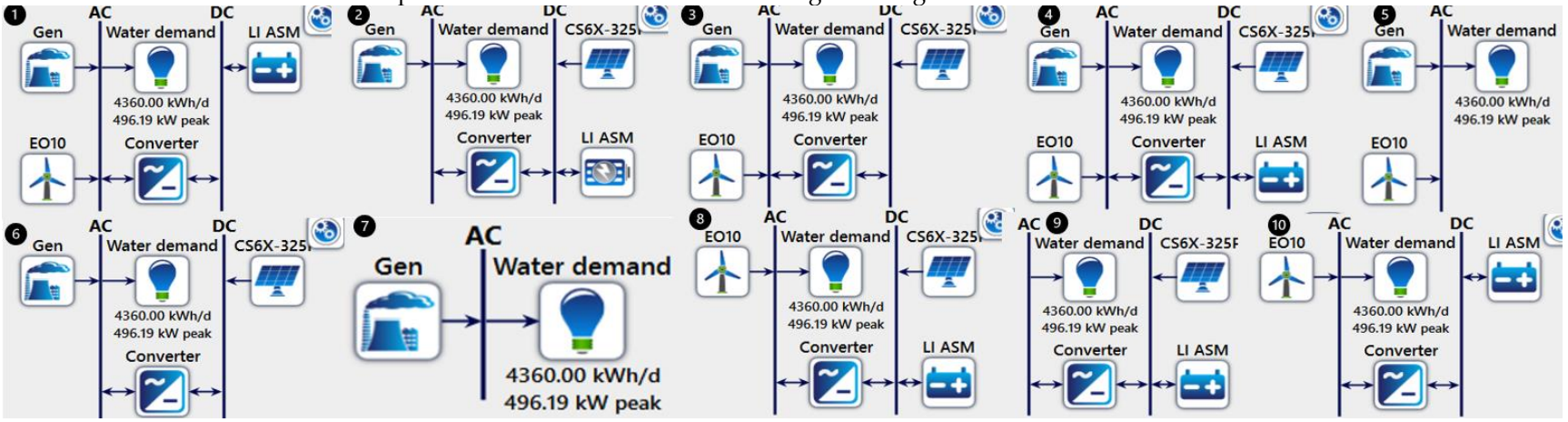

Figure 3.7: Schematic of the hybrid renewable energy configuration systems

3.7.2.1 *Scenario 1. Diesel configurations*

In this scenario, the use of a generic 550 kW diesel generator and an average fuel price of 1 €/L is envisaged. The different configurations with the DG attached are technically and economically analyzed below.

3.7.2.1.1 Diesel/Batteries/Converter/WT configuration

This system is composed of 30 wind turbines, each one with a nominal power of 10 kW, the 550-kW diesel generator operating 901 hours/year, 490 batteries and 70 strings in parallel, and 343 kW of energy converter following a combination dispatch (CD) energy strategy. It ranks the second-best option because the net present cost (NPC) is equal to 4.28 M€ and the levelized cost of the energy (LCOE) is equal to 0.227 €/kWh, and it is practically the same as the best configuration option. The difference is that this system has a lower renewable fraction (73.2%) using more hours the generator during the year and that leads to higher CO_2 emissions (285,971 kg/year). Besides, wind turbines produce 1,852,405 kWh/y, whereas the generator only produces 425,900 kWh/y (18.7%). It has the highest WT electric production in July and August and the lowest in February. This is not a problem because it coincides with the peak and lowest water demand. On the other hand, the AC primary load demand is only 1,591,398 kWh/y, so the system experiments an excess electricity of 627,617 kWh/y (27.5%). Despite this, the system is unable to fully satisfy all the electric demand hour by hour, every day of the year, with an unmet electric load of 2.06 kWh/y (0.0001%). The schematic diagram of this configuration is shown in Figure 3.7.

A drawback of this system is a high enough renewable electricity penetration (RP) to cause stability problems on the system. In the worst period (peak values), the renewable output power divided by load is equal to 1,146% as can be seen in Figure 3.9.

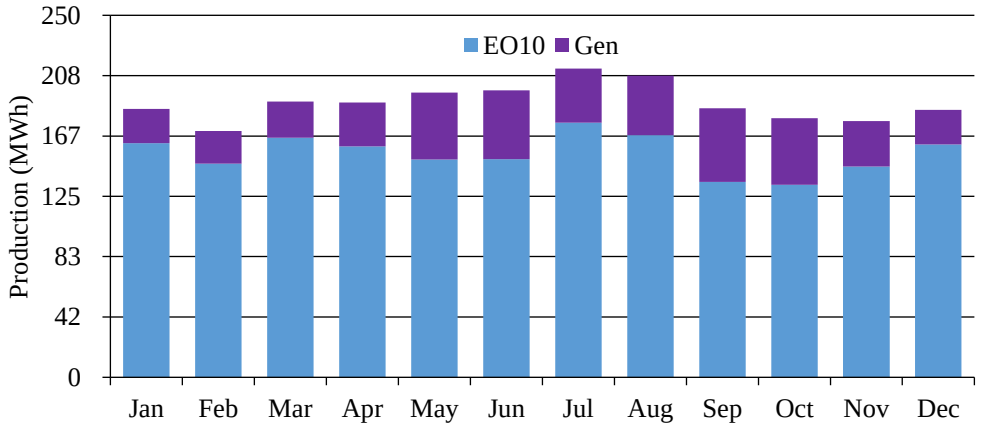

Figure 3.8: Monthly electric production in MWh of the config. 1.

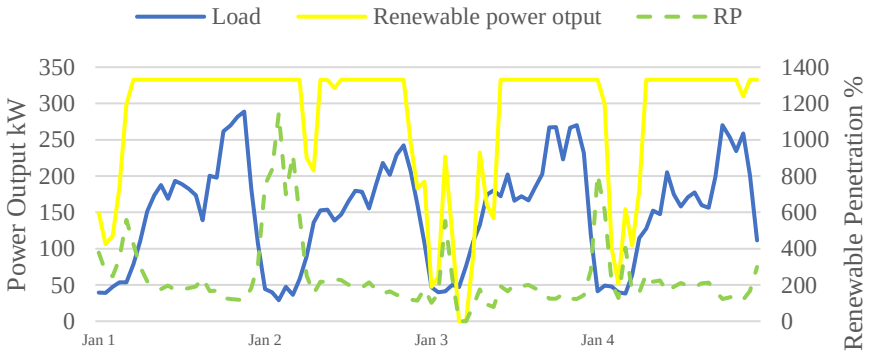

Figure 3.9: Comparison between renewable power output and the lowest load demand on Jan 2 leading to the highest renewable penetration.

3.7.2.1.2 Diesel/Batteries/Converter/PV configuration

This configuration consists of 1,081 PV modules and 3,416 batteries which increases the investment cost considerably resulting in a NPC of 5.66 M€ and LCOE equal to 0.3 €/kWh. The diesel generator (DG) hardly participates in power generator, operating only 588 hrs/y producing 85,485 kWh/y (3.88%) and emitting 67,744 kg CO_2 per year. The rest of the electricity generator is produced by the PV modules and then it is stored into the battery bank. Furthermore, this configuration has the second lowest excess of energy, only a 21% of the energy is not used to supply the electrical demand. The schematic diagram is shown in Figure 3.7.

3.7.2.1.3 Diesel/Converter/PV/WT configuration

This battery-less configuration is composed of 438 PV modules, 36 WTs, and 250 kW of a converter and it follows a CD energy strategy. This is the third best option due to its lower NPC and LCOE, thanks to the battery less investment, but it has the same problem of the first configuration which was the high renewable electricity penetration that could cause stability problems. Another drawback is that DG operates 2,304 hrs/y producing 415,086 kWh/y (11.9%) and emitting 314,944 kgCO_2/y to the environment, much more than the previous cases. The rest of electricity is produced by PV modules 24.5% and mostly WT 63.6% of the total 3,495,703 kWh/y as shown in Figure 3.10.

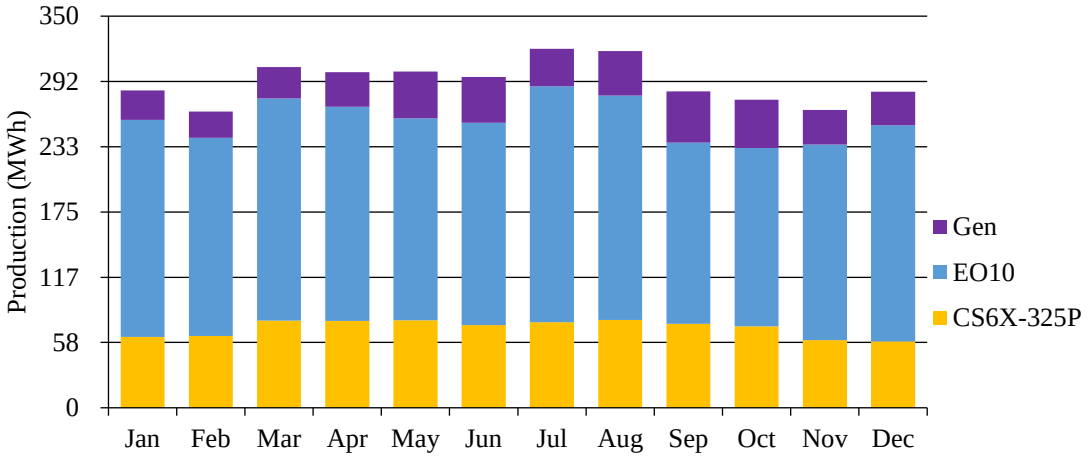

Figure 3.10: Monthly electric production in MWh of the config. 3.

3.7.2.1.4 Diesel/Batteries/Converter/PV/WT configuration

This is the optimal configuration that has been chosen to meet the electrical demand of the desalination plant and is composed of 274 kW of PV modules, 28 WTs, the generic DG, 518 batteries, and 341 kW of converter following a CD energy strategy. This system has the minimum NPC equal to 3.97 M€, and the LCOE equal to 0.21 €/kWh. Moreover, it has a reasonably renewable fraction (80.9%) in order to reduce the dependence on fossil fuel. Thus, the DG only operates 649 hours a year, consuming 78,069 L/y, and emitting 204,354 kgCO_2/y. Wind turbines represent 67.3% of the total electricity production (2,569,176 kWh/y), whereas PV modules 20.9%, and DG only a 11.8% as shown in Figure 3.11. Besides, 926,005 kWh/y or 36% are lost and only 69.7 kWh/y does not meet the electrical demand.

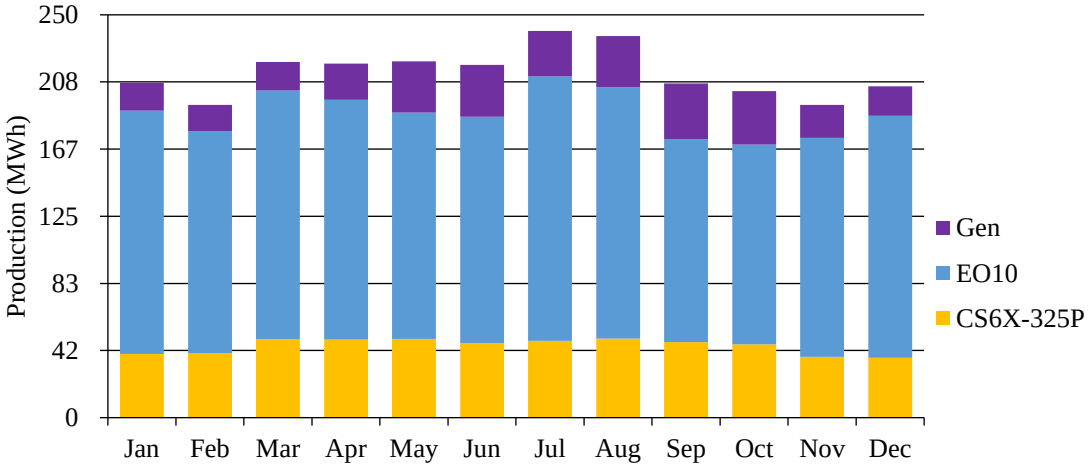

Figure 3.11: Monthly electric production in MWh of the optimal config.

3.7.2.1.5 Diesel/WT configuration

The system consists of 42 wind turbines and the 550-kW diesel generator with a combination dispatch (CD) energy strategy. This configuration has, at the moment, the lowest percentage of renewable energy use (69.3%), meaning that DG works a greater period of time during the year than the previous cases. Anyway, wind turbines still produce a huge percentage (84.1%) of the total electricity production (3,082,492 kWh/y). The total electricity production is almost double what is needed to cover the annual electricity demand, which generates a large excess of energy (48.5%) of the total energy produced, since not having a battery bank means that this energy cannot be stored and is therefore lost. In contrast, all the electricity production meets the electric load demand all over the project lifetime.

3.7.2.1.6 Diesel/Converter/PV configuration

This configuration is composed of 1,042 PV modules, the 550-kW DG, and the DC/AC converter of 357 kW. This system is discarded not only because of its high net present cost (9.57 M€), but also because of the excessive use of the diesel generator since its RF is equal to 29.8%. The electricity production of the PV modules represents a 64.6% of the total energy generation (3,158,172 kWh/y) as shown in Figure 3.12. DG operates 5,593 hrs/y, produces 1,117,030 kWh/y, and emits 832,107 kg/y, which has a penalty cost of 83,210 €/y.

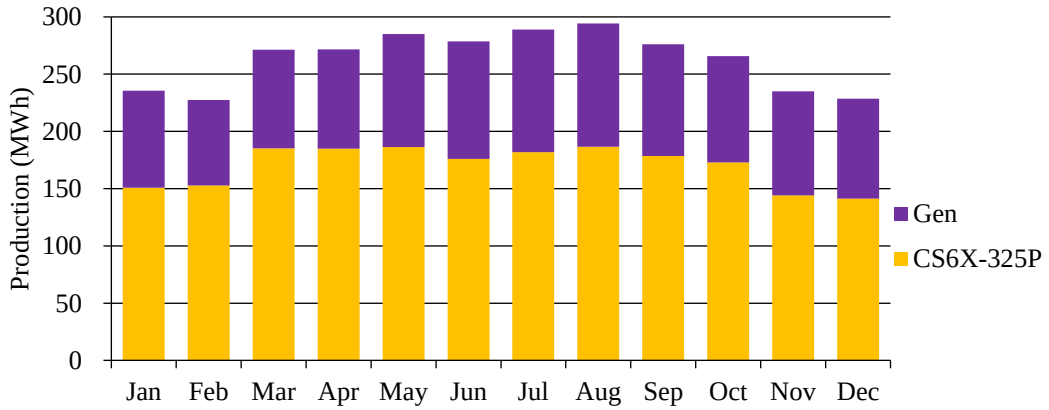

Figure 3.12: Monthly electric production in MWh of the config.6.

3.7.2.1.7 Diesel

This configuration relies 100% on fossil fuels. It is one of the most inefficient systems because the NPC is equal to 12.4 M€ and the LCOE is 0.658 €/kWh. The total load demand is supplied by the diesel generator that produces 1,780,472 kWh/y. In contrast, the excess of electricity represents only 10.6% of the total. But this configuration emits a huge amount of carbon dioxide, specifically 1,322,389 kg/y.

Thus, all of this make the system unfeasible for any period unless minimal excess of energy is desired.

3.7.2.2 Scenario two. Without Diesel configurations

This scenario contemplates three more alternatives without DG that could be useful in the case of seeking to minimize CO_2 emission and to reduce fossil fuel dependence.

3.7.2.2.1 Batteries/Converter/PV/WT configuration

This is the best configuration based only on renewable technologies because it achieves the lowest NPC (6.9 M€) and LCOE (0.366 €/kWh). It consists of 2,297 kW of PV panels, 4 WTs, 3,696 battery units, and 682-kW of converter following a CC energy strategy. It produces a total of 4,747,946 kWh/y leading to a huge amount of energy loss equal to 3,029,594 kWh/y. As shown in Table 3.5 the problem of this system is the high initial capital investment, specifically due to the huge amount of PV panels, and batteries that makes the HRES unfeasible.

3.7.2.2.2 Batteries/Converter/PV configuration

The system is composed of 2,070 PV modules, 4,907 batts, and 572-kW converter. It is similar to the previous case. The difference is that this system is a bit more expensive and has less excess of electricity because it produces less energy and has more batteries to store that energy production.

3.7.2.2.3 Batteries/Converter/WT configuration

This is the last and worst configuration based on NPC. It is the combination of 187 WTs of 10 kW each one, 16,576 batts, and 1,595-kW of converter following a LF energy strategy. The NPC is equal to 22.9 M€ and it produces 11,546,659 kWh/y.

3.7.3 Performance assessment of the optimal configuration

Once all the possible configuration simulated in the Homer Pro™ software have been briefly described, and analyzed, a technical, economic, and environmental analysis is then made of the optimum HRE system that will provide the electrical energy required for the correct operation of the desalination plant to be installed in El Hierro and which will supply the entire island with fresh and drinking water.

3.7.3.1 Energy analysis

As already described in the previous section, the optimal configuration is the one consisting of 274-kW PV modules, 28 WTs, the generic DG, 518 batteries, and 341 kW of converter following a CD energy strategy.

It is worth noting the high share of renewable technologies with a RF equal to 80.9%, as 67.3% of the electricity production is generated by wind turbines and 20.9% using photovoltaic panels, while only 11.8% belongs to the diesel generators. The total system produces 2,569,176 kWh/y covering almost all but 0.0044% of the annual demand and creating an excess of electricity around 36% of the total electricity production. Emphasizing the monthly electricity production as can be seen in Figure 3.11, the energy produced by the wind turbines is maximized in the months of July and August, but in general it is quite similar during all the months of the year, as is the case with solar energy, since the climatic conditions remain practically constant throughout the year. The system rated capacity is 274 kW of solar energy, so the number of PV modules is calculated by the equation (3.15).

$$Nºmod = \frac{P_{tot}^{AC}}{P_{unit}} = \frac{274{,}000\ W}{325\ W} = 843.077 \approx 844\ PV\ modules \qquad (3.15)$$

The solar panels only are able to produce solar energy when resources are available, specifically 4,379 hrs/y with a 33.7% PV penetration, or 5.36 hrs/day. Thus, the total electricity production is equal to 536,129 kWh/y. The figure below shows the rated capacity of the PV system in function of the day of the year and the hour of day. It is clearly seen that the system maximizes its operation when time oscillates between 9:00 a.m-18:00 p.m. The image is also delimitated by distinct colors, from 0 (dark) to 300 kW (intense) and it shows a central line which is intense colored, that means the rated capacity reaches its maximum value between 12:00 a.m. and 17.00 p.m. It also can be seen that the PV power output experiments some stability problems during the months of January and December due to the low radiation. In addition, the system needs more power in those months to supply enough energy to compensate the lack of power resources.

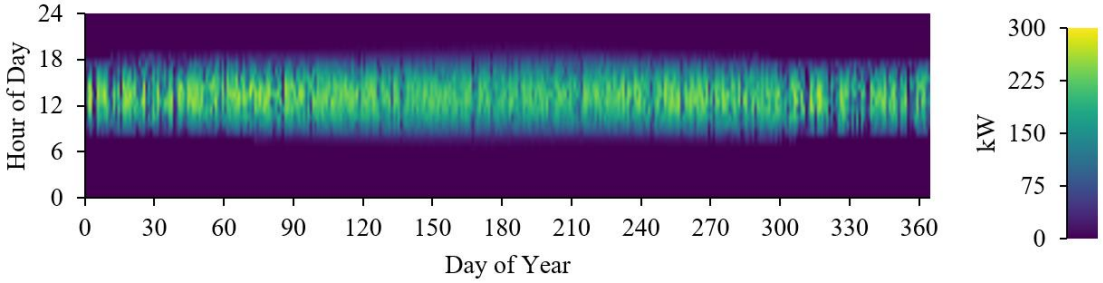

Figure 3.13: PV power output in function of the time simulated in HOMER Pro software.

The total rated capacity of wind turbines is equal to 280 kW, so it is necessary to install 28 units of Eocycle EO10 kW WTs. The total electricity production of WTs is equal to 1,728,912 kWh/y (67.3%) operating 7,591 hrs/y with a maximum power output of 311 kW. As shown in Figure 3.15, the WT power output remains constant

each hour of day during the project lifetime. The mean power output is equal to 197 kW, so it has a higher capacity factor (70.5%) than PV system (22.4%). In Figure 3.14, it can also be seen that the colored diagram appears to be rather more disordered than the previous one, with intense colors predominating. This means that WTs are practically operating close to the maximum capacity all year round thanks to the island's climatic conditions.

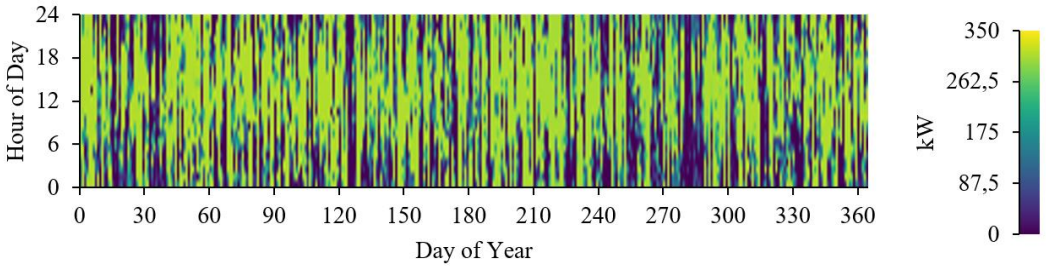

Figure 3.14: WT power output in function of the time simulated in HOMER Pro software.

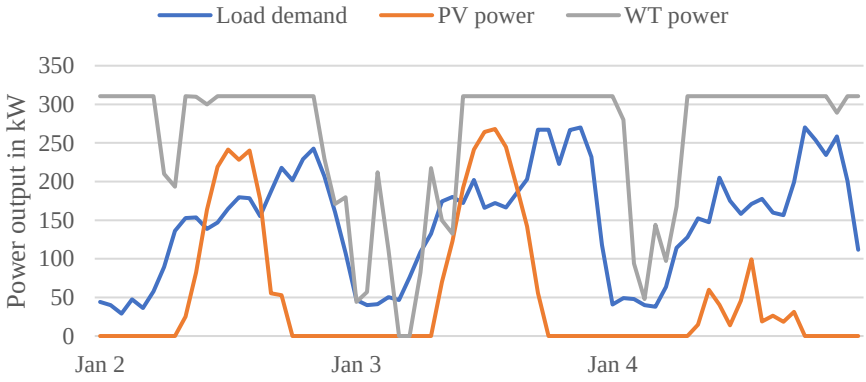

Figure 3.15: Renewable power output and load demand diagram in a three-days period.

A 550-kW of diesel generator is installed in the optimal configuration to support the renewable technologies in order to meet the total electricity demand every time. It consumes 78,069 L/y of diesel, and operates 649 hrs/y to generate 304,135 kWh/y. The box-and-whisker shows the amount of diesel consumption in L/hrs of each month of one year, and it can be seen in the diagram that every month have the same maximum consumption in a determined period with a value of 140 L/h, but with different frequency. For instance, in June the box is the biggest one and ranges from 0 to 95 L/h with high frequency during that month. In contrast, there is a small range of consumption in February (0-50 L/h). Importantly, although each month experiences a different range in the amount of fuel consumption, they all have a line within the boxes, called the median, which represents the value that lies right in the middle of all hourly values for the month. And in this case, it is observed that the median of

each month remains practically constant during the entire year and has a value of less than 10 L/h. This is because the generator is only used at times when it is strictly necessary in order to reduce costs. It can also be seen in Figure 3.17 that the generator power output is maximum from 0 to 6 a.m. and 18 to 24 p.m., when renewable resources are not easily available.

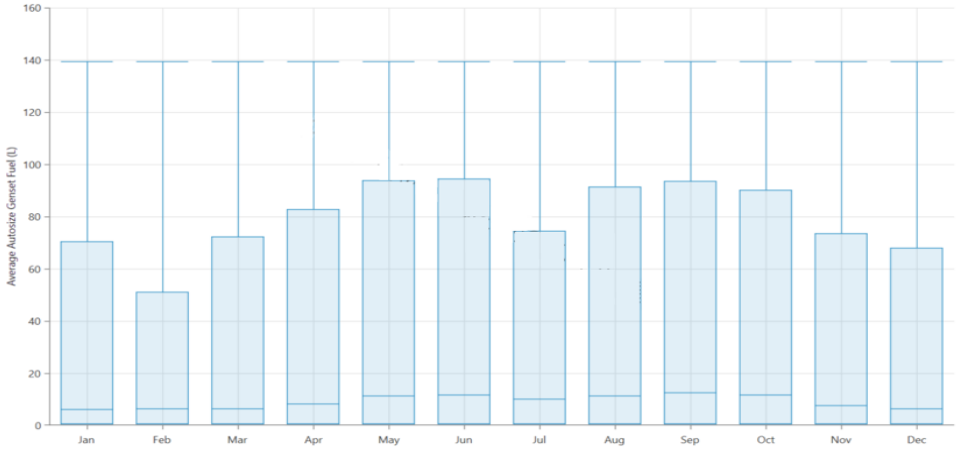

Figure 3.16: Monthly Autosize Genset fuel consumption from the optimal configuration.

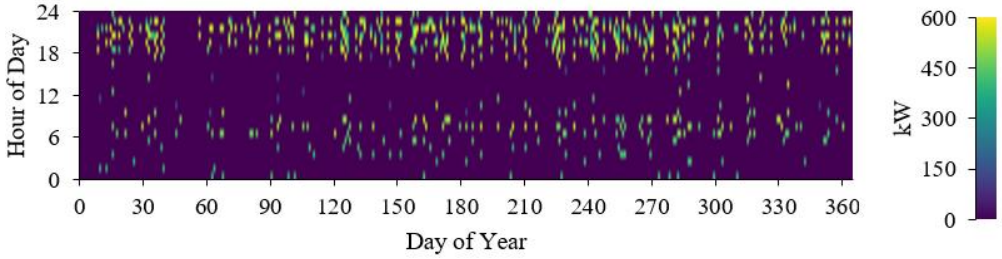

Figure 3.17: Diesel Generator power output in function of the time simulated in HOMER Pro software.

This configuration follows an energy strategy control, called combination dispatch (CD), in which the generator works or not to provide enough energy to meet the daily demand and to store it in the battery bank if it is necessary. In this case, the optimal solution is to install a generic 1 kWh Li-Ion [ASM] storage system with a nominal capacity of 529 kWh. The annual throughput is 229,252 kWh/y. In the color diagram below, it can be seen that the state of charge of the battery has a green color that predominates over the others, which means that it is usually between 70 to 95% charged throughout the year and especially in the daylight hours when the solar energy produced by PV system participates.

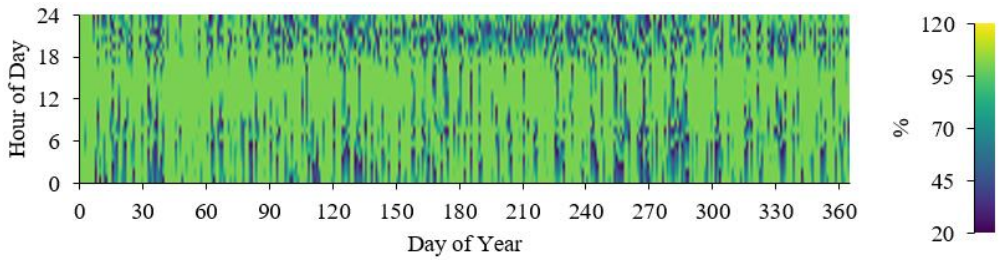

Figure 3.18: Storage state of charge in function of the time simulated in HOMER Pro software.

The following table shows the annual electricity production of each of the components that make up the optimal configuration to provide the necessary energy to the desalination plant and the Figure 3.19 summarizes the energy process it undergoes, i.e., the energy losses, the excess, the unmet demand, and so on.

Component	Annual production (kWh/y)	(%)
PV CS6X-325P	536,129	20.9
WT EO10	1,728,912	67.3
Diesel Gen	304,135	11.8
Total	2,569,176	100

Table 3.6: Annual electricity production of the optimal configuration.

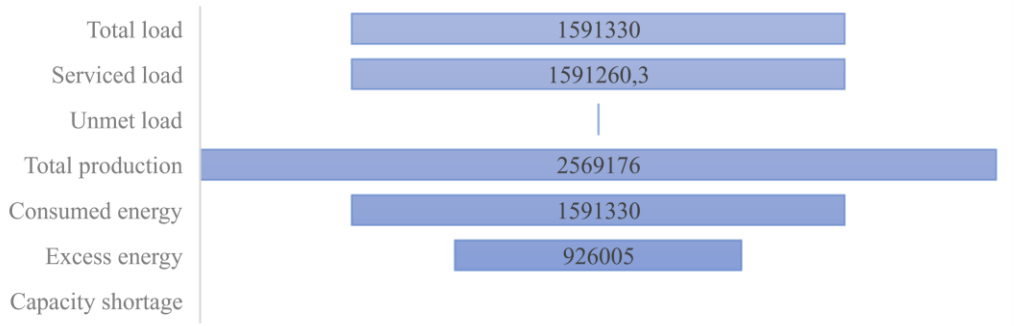

Figure 3.19: Energy contribution of the optimal configuration system in kWh/y.

3.7.3.2 *Economic analysis*

A summary of the total cost results is provided in the Table 3.7 based on the economic results for the optimal configuration simulated in HOMER Pro The total net present cost of the optimal configuration is equal to 3,966,464 € over the project lifetime (25 year) in which the diesel genset represents the 38% of the total NPC accounting 1,488,287.64 €. Lastly, PV and WT represents 9% and 29% of the total (See Figure 3.20). In contrast, if the NPC is divided into the initial capital investment costs

and the operational and maintenance costs, it can be seen in Figure 3.20 that the investment in wind turbines is the largest part, representing 405 of the total project capital cost, which in turn is the largest part of the NPC compared to O&M, and replacement costs. What happens is that the cost of fuel (See Figure 3.21) that feeds the generator is much higher than the previous ones, representing 23.3% of the total NPC, so the total cost of the generator is the highest one.

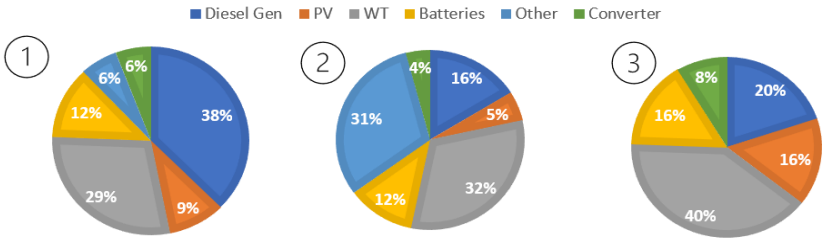

Figure 3.20: 1) Percentage of total NPC by component of the optimal config. 2) Percentage of the O&M cost of the optimal config. 3) Percentage of the total capital cost by component of the optimal config.

It is clear from the figure below that the most relevant factor that has led to a considerable increase in the diesel generator cost is the fuel cost with a value of 926,154.67 € over the project lifetime with an average fuel price of 1 €/L. For further clarification, Figure 3.22 shows a summary of the nominal cash flow for the optimal configuration based on cost type.

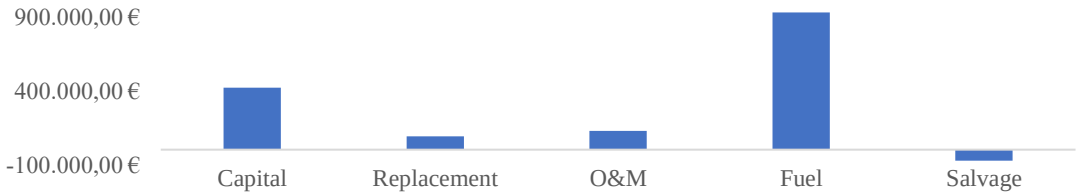

Figure 3.21: Diesel Generator by cost type.

Comp	Capital	O&M	Replace	Fuel	Salvage	Total
Diesel Gen	418,000.00 €	127,038.18 €	90,473.00 €	926,154.67 €	-73,378.22 €	1,488,287.64 €
PV CS6X-325P	328,326.71 €	42,196.26 €	0.00 €	0.00 €	0.00 €	370,522.97 €
WT EO10	840,000.00 €	249,129.37 €	114,862.11 €	0.00 €	-61,989.75 €	1,142,001.73 €
Bat Li ASM	332,038.00 €	92,177.87 €	78,885.90 €	0.00 €	-8,470.35 €	494,631.42 €
Other	100,00 €	242,431.99 €	0.00 €	0.00 €	0.00 €	242,531.99 €
Converter	179,886.55 €	32,395.43 €	19,586.39 €	0.00 €	-3,380.62 €	228,487.74 €
Total	2,098,351.26 €	785,369.09 €	303,807.40 €	926,154.67 €	-147,218.94 €	**3,966,463.48 €**

Table 3.7: Summary of the annual cost analysis of the optimal configuration.

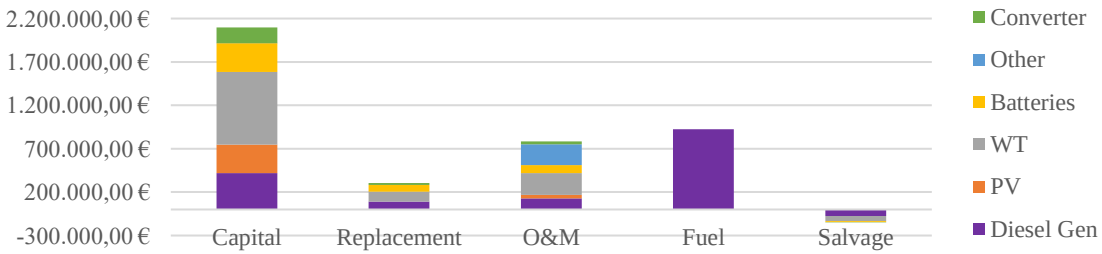

Figure 3.22: Summary of nominal cash flow results for the optimal configuration divided by cost type based on each component.

In addition, to be more accurate, the figure below shows a summary of the nominal cash flow each year of the project lifetime by cost type (above) and by component (below) in order to compare them. It can be seen in the upper image that the capital costs represent more than a half of the total cost of the project and the maximum responsible is the wind turbines investment cost, but also the generator, PV modules, and the battery bank as shown in the lower image. These graphs also show the strong impact of fuel costs from the second year to the last. It is also worth noting that the replacement costs of these technologies increase by more than 100% in the last years of the project's lifetime compared to the previous years.

Finally, the Figure 3.24 shows the cost summary that includes an economic comparison between the optimal configuration with the lowest NPC and the base case with only a diesel generator component. The lines represent the cumulative cost over the years until the project lifetime and consists of the summatory of capital, O&M, replacement, and salvage cost of all components. The intersection of both lines is called the simple payback which is the number of years at which the cumulative cash flow of the difference between the current system and base case system switches from negative to positive, in other words, the payback is an indicator of how long it would take to recover the difference in investment costs between the current system and the base case system. In this case, the simple payback value is 2 years. Other important indicators are the return on investment (ROI), which is the yearly cost savings relative to the initial investment and the internal rate of return (IRR) which is the discount rate at which the base and current cases have the same NPC and the last is equal to 48%. The first one is calculated by the equation (3.16), and it is equal to 47%.

$$ROI = \frac{\sum_{i=0}^{R_{project}} C_{i,ref} - C_i}{R_{project}(C_{cap} - C_{cap,ref})} \quad (3.16)$$

Where $C_{i,ref}$ is the nominal annual cash flow for base case system, C_i is the nominal annual cash flow for the current system, $R_{project}$ is the project lifetime in years, C_{cap} is the capital cost of the current system, and $C_{cap,ref}$ is the capital cost of the base case system.

Figure 3.23: Distribution of nominal cash flow during the project lifetime by cost type (upper) and by component (lower).

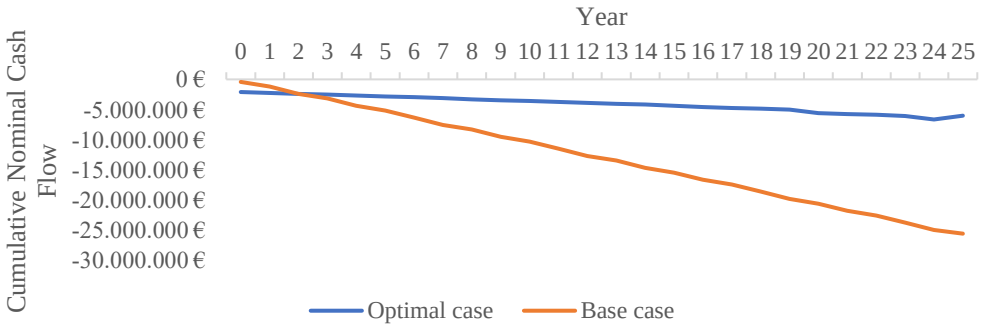

Figure 3.24: Cost summary comparison between the optimal and base case (Only diesel genset)

3.7.3.3 *Environmental analysis*

Homer Pro also calculates the greenhouse gases (GHG) that are emitted into the atmosphere by the diesel combustion process taken in the conventional generator, and which are harmful to humans and pollute the ecosystem. Table 3.8 shows all the GHG involved in the burning of diesel fuel in the optimal case chosen to power the desalination plant. In addition, Figure 3.25 shows the amount of carbon emissions in kg per year produced by all the configurations described in the previous sections, as well as their renewable penetration. It is obvious that the configurations that use only renewable technologies (config. 7-10) do not emit any type of pollutant gas into the atmosphere, while the others (config. 1-7) that are composed of a mixture of renewable technologies and diesel generator do emit pollutant gases, i.e., the value depends solely and exclusively on the use of diesel fuel. The higher the diesel fuel is, the higher is the amount of CO_2 produced.

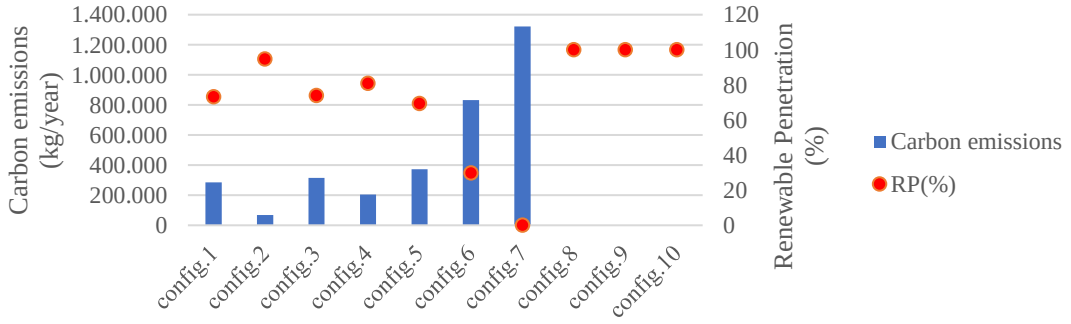

Figure 3.25: CO_2 emissions and renewable penetration of the ten-system configurations.

The optimal configuration (config. 4) ranks the 5th position of emitting less carbon dioxide with a RP approximately 80%.

Quantity	Value (kg/y)
Carbon Dioxide	204,354
Carbon Monoxide	1,288
Unburned Hydrocarbons	56.2
Particulate Matter	7.81
Sulphur Dioxide	500
Nitrogen Oxides	1,210

Table 3.8: GHG emissions expressed in kg/year of the optimal configuration (config.4).

3.8 Sensitivity analysis

It has also been decided to perform a sensitivity analysis between the different variables such as diesel price, daily electricity load demand, solar radiation, and wind speed as they can be easily changeable during the whole life of the project. Therefore, it has been decided to analyze in depth the impact of these external variables as shown in Figure 3.26 and Figure 3.27. HOMER simulates all possible configurations that can meet the load required for the desalination plant for each of the sensitivity values over a period of one year. Then, the software ranks the feasible configurations according to minimize the NPC and discards the unfeasible configurations.

Figure 3.26 shows the optimization results of three system configurations maintaining a constant fuel price equal to 1 €/L. The y-axis corresponds to the daily electricity demand which varies between 1,000 and 7,000 kWh/day while the x-axis represents a range of average wind speed from 3 to 10 m/s keeping constant the average solar radiation which will be equal to 3 kWh/m²/day. In the best case, the PV/WT/Batteries configuration (light blue color) would be adopted as it minimizes the NPC, but this solution would only be feasible if the electricity demand drops more than 77%, i.e., 1,000-2,000 kWh/day and the average wind speed is less than 6 m/s. Therefore, this solution is presented in an extraordinary case that will probably never occur. On the other hand, if the weather conditions change and the average wind speed is in the range of 6 to 10 m/s, the optimal configuration would be dark blue one consisting of Gen/WT/Batteries if it also coincides that the electrical demand is 4,500 kWh/day. As the demand increases, the wind speed should increase exponentially up to 7.2 m/s, or the configuration would no longer be the best. The same is true if the electricity demand decreases. Finally, in the remaining cases, and the one that occupies the largest range of changes, is the configuration consisting of Gen/PV/WT/Batteries and colored in green.

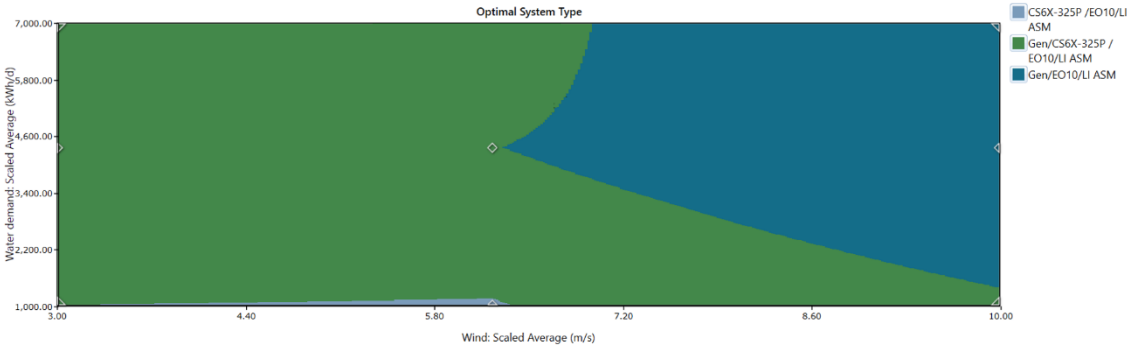

Figure 3.26: Optimal system time plot with constant fuel price which is a result of sensitivity analysis.

Now, if the average solar radiation and wind speed are fixed and are equal to 3 kWh/m²/d and 6.23 m/s and fuel price is that one that is being increased from 0.4 to 3 €/L, it can be seen in Figure 3.27 that the graph is quite different from the previous one. It is observed that as the price of diesel increases, the software proposes a configuration without the diesel generator (PV/WT/Batteries) for a daily electricity demand of between 1,000 and 2,000 kWh/d. The dark blue region consists of a gen/WT/Batteries and obviously a diesel generator is coupled as the price ranges between 0.4 and 0.9 €/L. Thus, the production of electricity by the generator is increased, which decreases the proportion of renewables and therefore the PV system is left out in this configuration. Finally, the optimal configuration covering the largest region of the graph consists of Gen/PV/WT/Batteries.

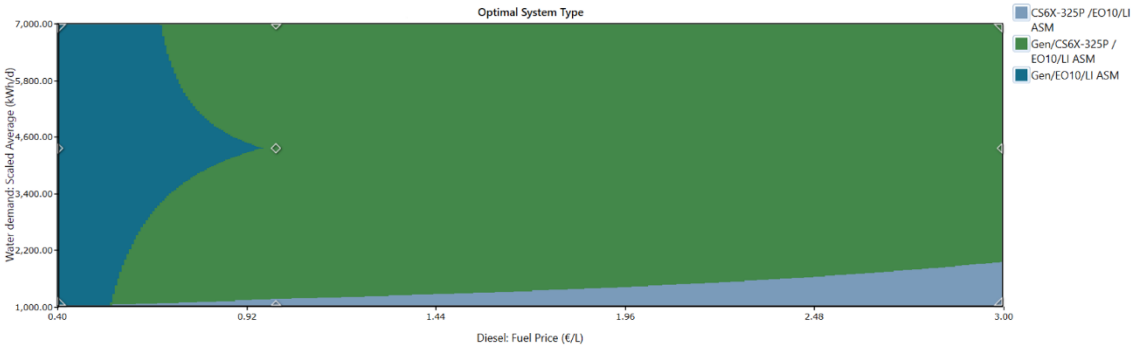

Figure 3.27: Optimal system time plot with variable fuel price which is a result of sensitivity analysis

3.9 Water Storage Tank

In this section , a water storage tank will be considered at the outlet of the ADS (See Figure 3.29). This tank will replace the battery bank of the optimal configuration of the HRES to see if it is more cost effective. The permeate water will be divided into two streams. Whereas one directly meets the water demand, the other will be

charging the water tank. Then, the stored water will be discharged in periods when the peak water demand is so high that the power sources cannot meet it [82].

The injection of water into the tank and also the removal from it shall be carried out by two independent electric motors, charge and discharge water pumps that work similar to those of the battery bank. So, the ADS and the water outlet from the tank, simultaneously supplies the local water demand. Therefore, the water generated per hour by the ADS, the water charged, the water discharged, and the water stored in the tank have been determined from the mathematical calculations of the batteries used in the HOMER Pro™ software to achieve a minimum cost daily schedule. To do so, a mathematical model must be introduced. Equation (3.17) represents the balance between the water consumed and produced by the ADS equipped with water storage system. Equation (3.18) converts the electricity load demand into the water demand per hour by means of SEC. In equation (3.19), the water produced by the ADS at any time is a positive value and cannot exceed the hourly capacity of the water production. In equation (3.20), the hourly water production capacity is a function of the total daily capacity of the ADS. In eq. (3.21), the balance of the water stored in the tank is established and equal to the discharged water minus the charged water.

$$Q_h^{tank} + Q_{prod,h} = Q_{d,h} \; \forall h \, \epsilon \, (0 - 8760) \qquad (3.17)$$

$$Q_{d,h} = E_{d,h}/SEC \; \forall h \, \epsilon \, (0 - 8760) \qquad (3.18)$$

$$0 \leq Q_h^{tank} \leq Q_{prod,h}^{Total} \forall h \, \epsilon \, (0 - 8760) \qquad (3.19)$$

$$Q_{prod}^{Total} = Q_{prod,h}^{Total}/24 \; \forall h \, \epsilon \, (0 - 8760) \qquad (3.20)$$

$$Q_h^{tank} = Q_h^{disch} - Q_h^{Char} \; \forall h \, \epsilon \, (0 - 8760) \qquad (3.21)$$

The batteries are replaced by a water storage tank without modifying the excess of energy produced by renewable energy production of the optimal case. Therefore, a water tank with a capacity of 200 m³ would be needed to satisfy 100% of the total water demand. Fig x shows the capacity of the water tank in m³ per hour for a 4-day sample in summer when the demand is at its maximum. The water tank usually provides water during the night or when renewable energy production is at its lowest and the ADS covers the entire demand, the tank is charged until it reaches its limit.

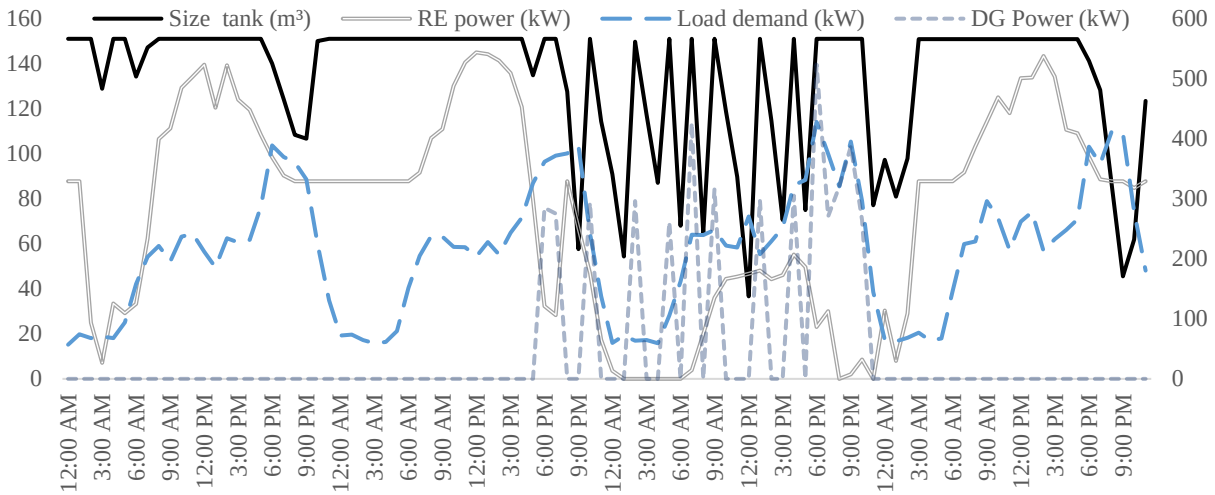

Figure 3.28: Overall electricity production of the HRES and water production of the tank. y-axis left. Water capacity tank in m³/h; y-axis rigth. in kW.

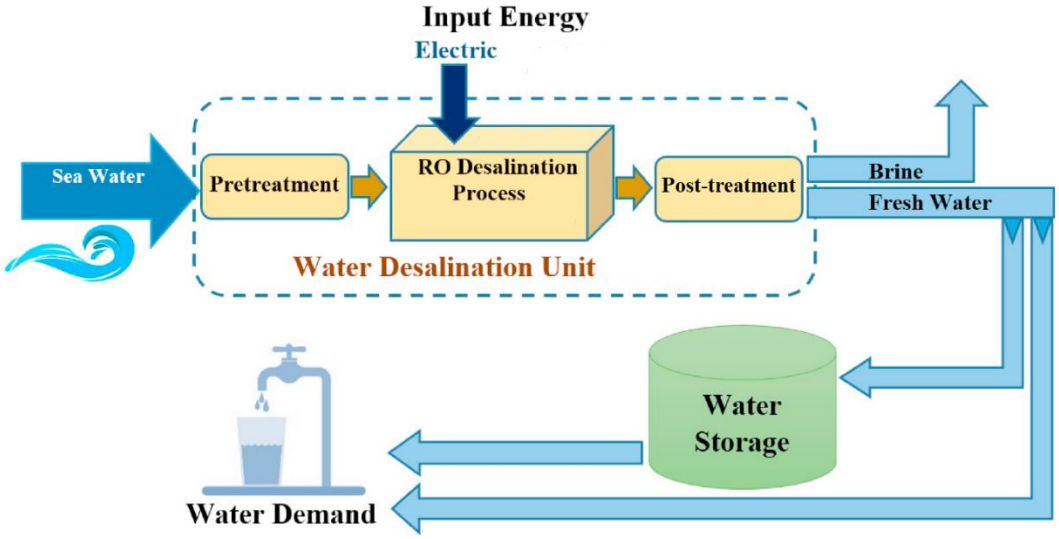

Figure 3.29: Schematic of the ADS with water storage tank [82].

Table 3.9 shows a clear reduction in NPC (9.8%) due to the substitution of electric batteries for the water tank. Capital, O&M, and replacement costs have been considered on the basis of [83]. For the estimation of the costs it has also been necessary to consider some problems that can occur with drinking water tanks. They are related to the water quality and they include:

- Microbiological issues such as pathogenic contamination and bio-fimls [83].
- Chemical issues like leaching of chemicals from tank linings or coatings, loss chlorine residual or precipitates [83].

- Physical issues such as water temperature, turbidity from sediment build-up [83].

All of these problems lead to reduce the water tank lifetime, so it is necessary to add chlorine disinfectant residual, the desinfection of by-products, and avoid ice formation inside the tank.

Comp	Capital	O&M	Replace	Fuel	Salvage	Total
Diesel Gen	418.000,00 €	127.038,18 €	90.473,00 €	926.154,67 €	-73.378,22 €	1.488.287,64 €
PV CS6X-325P	328.326,71 €	42.196,26 €	0,00 €	0,00 €	0,00 €	370.522,97 €
WT EO10	840.000,00 €	249.129,37 €	114.862,11 €	0,00 €	-61.989,75 €	1.142.001,73 €
Water Tank	70.000,00 €	21.000,00 €	13.000,00 €	0,00 €	0,00 €	104.000,00 €
Other	100,00 €	242.431,99 €	0,00 €	0,00 €	0,00 €	242.531,99 €
Converter	179.886,55 €	32.395,43 €	19.586,39 €	0,00 €	-3.380,62 €	228.487,74 €
Total	2.098.351,26 €	785.369,09 €	303.807,40 €	926.154,67 €	-147.218,94 €	**3.575.832,07 €**

Table 3.9: Summary of the annual cost analysis of the optimal configuration.

4. Design of a SWRO plant with a capacity of 2,000 m³/day

In this section, a typical seawater reverse osmosis plant will be designed in order to understand the whole desalination process and compare the results with the energy and economic analysis based on literature.

In a reverse osmosis desalination plant, there are five clearly distinguishable phases clearly differentiated. The first phase consists of collecting and transporting the salt water to the plant, followed by the pre-treatment phase, where the water is adapted to make it suitable for filtration by reverse osmosis. to make it suitable for reverse osmosis filtration. Once the water is in the right conditions, it goes to the next phase where the water is filtered by reverse osmosis filtration. The water is then treated again by post-treatment to ensure that the water is fit for consumption. Finally, it is necessary to return the salt water to the sea by means of submarine outfalls.

The image below represents all essential process steps to desalinate seawater. The aim of this project is to produce fresh water for drinking purpose; therefore, the following steps have been followed; Chlorination, coagulant, Ultrafiltration, dichlorination, antiscalant, reverse osmosis process, remineralization, and disinfection.

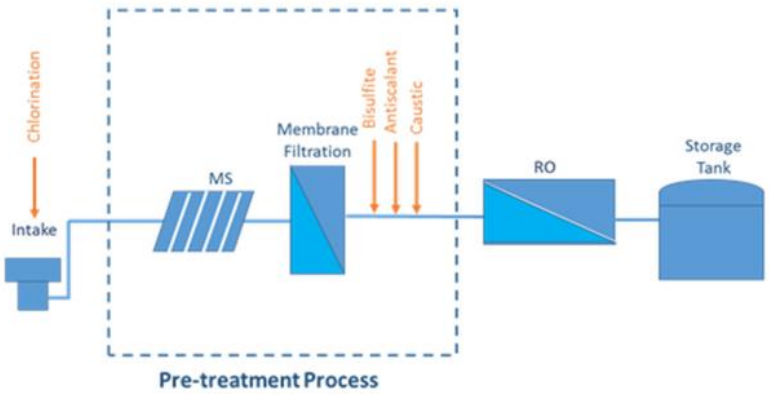

Figure 4.1: Schematic diagram of the RO desalination plant used in the project. Ref. [84].

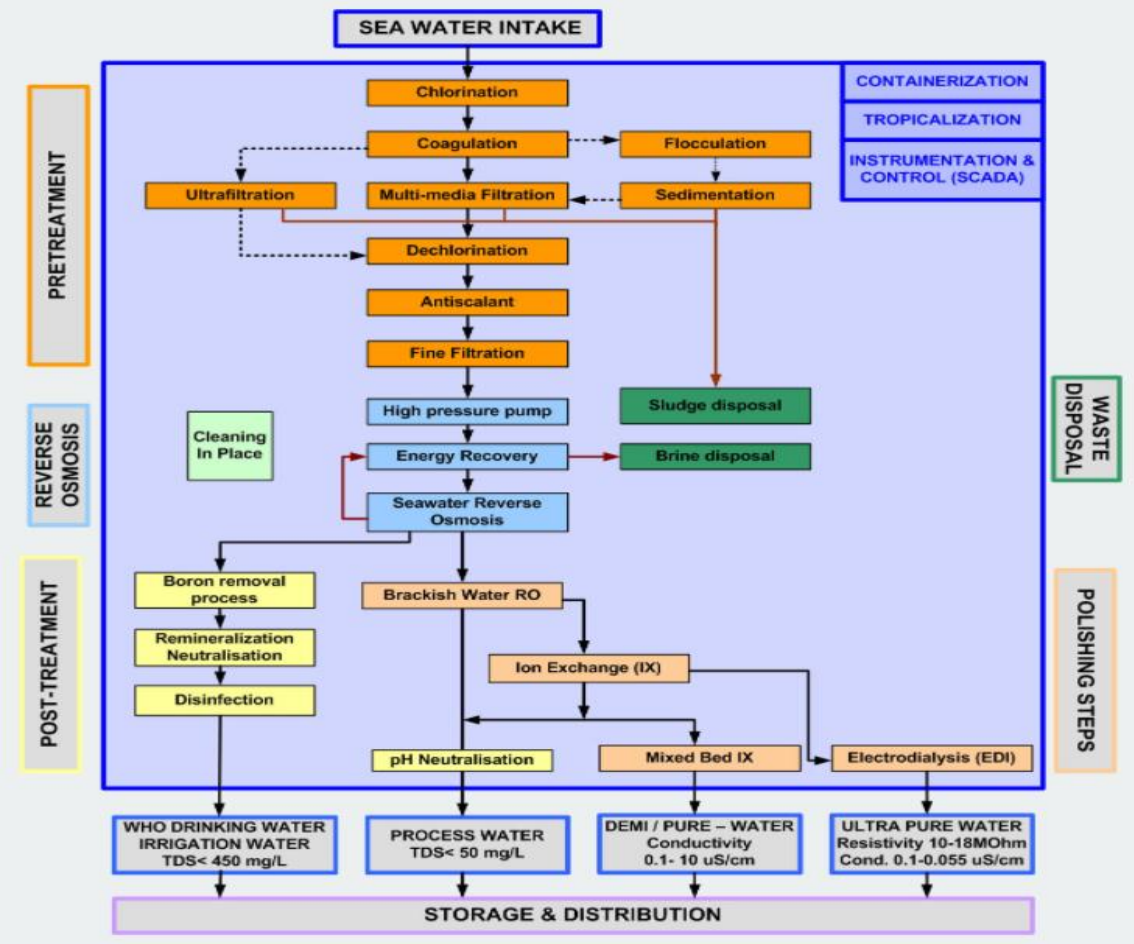

Figure 4.2: Different step processes to desalinate seawater according to permeate quality purposes. Courtesy of *lenntech.com.*

Figure 4.1 shows schematically the process from the seawater entering the plant to the water leaving ready to drink, with emphasis on the pre-treatment used in this project.

In the design of a membrane desalination plant, continuous operation of the plant is necessary. Otherwise, the membranes would dry out, losing their properties and decreasing their permeability. The design of the plant will depend on several factors such as the salinity of the water, chemical composition, micro-organisms present in the water or contaminants.

This project is done with the Water Application Value Engine (WAVE®). It is a powerful software tool that enables the design and modelling of water treatment processes using several techniques, such as ultrafiltration (UF), reverse osmosis (RO), and ion exchange (IX).

El Hierro consists of 10,000 inhabitants. A maximum daily consumption 200 L/d/inhabitant was assumed, also taking future water needs into consideration. Therefore, the maximum total water production needs are 2,000 m³/day. So, for this production capacity, it is necessary to feed the plant with approximately 5,000 m³/day, as the conversion rate of this type of plant is around 40%.

4.1 Water Intake

The first step has been to determine the quality of seawater, as it affects the performance and successful operation of an RO system. The type of feed water constituents can impact the efficiency of the membrane by causing fouling, scaling, or degradation. Table 4.1 lists seawater quality used in this project based on typical seawater quality guidelines.

Species	Units	Value
Colloids	SDI	5.2
Suspended Solids (TSS)	mg/L	42
Turbidity	NTU	5
Organics (TOC)	mg/L	2.5
Dissolved solids (TDS)	mg/L	35,984.108
Conductivity	µS/cm	53,423.87
T_{Min}	ºC	10
T_{Design}	ºC	25
T_{Max}	ºC	36
PH@25ºC	-	8.1

Table 4.1: Feed water quality based on seawater quality guidelines supported by WAVE software.

On the other hand, there are several types of seawater intake systems for desalination plants such as vertical wells, open intakes, horizontal drains, or mixed intakes. In this case an open intake will be used due to its various advantages over the other systems. Open intakes ensure a constant flow regardless of tides and require less maintenance, as the only need to be serviced and cleaned annually on scheduled basis.

It is necessary to place the intake tower at a sufficiently large distance from the coast to ensure a minimum depth of 30 meters. This is necessary to ensure a constant flow to the plant regardless of tidal variation. Furthermore, it is also necessary to take into account the type of terrain where the intake tower will be placed, since sandy

soils or abundant vegetation can block the tower. In this case, a greater filtering of feed water would be necessary. Therefore, the intake tower should be located on a coarse sandy or rocky area.

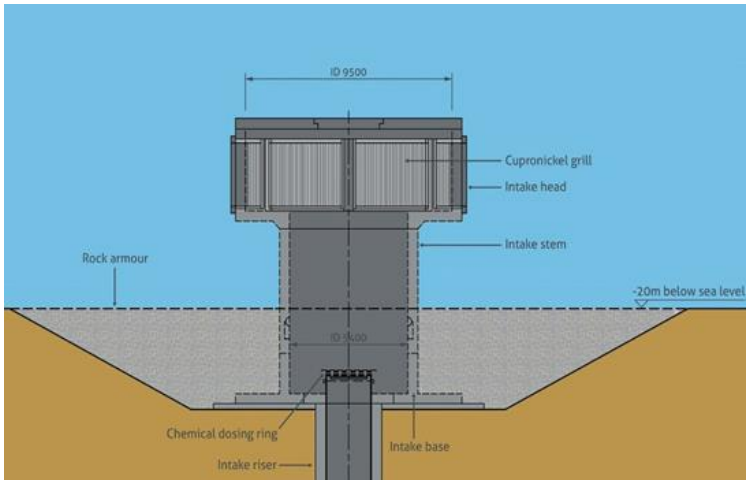

Figure 4.3: Section of an open intake tower. Courtesy of *Arecongroup.com*.

4.2 Pretreatment

Reverse osmosis membranes are subject to fouling and scaling by suspended materials that are present in seawater. The Table 4.2 shows typical seawater RO fouling and their appropriate pretreatment.

Fouling	Cause	Pretreatment
Biological	Bacteria, viruses, microorganisms	Chlorination
Particles	Sand, clay (turbidity and suspended solids)	Filtration
Colloids	Organic and inorganic complexes, colloidal particles, micro-algae	Coagulation + filtration
Organic fouling	Natural organic matter: Humid and fulvic acids	Coagulation + ultrafiltration
Minerals	Calcium, magnesium, barium or strontium sulphates and carbonates	Antiscalant dosing and acidification
Oxidants	Chlorine, ozone	Sodium metabisulfite or granulated activated carbon

Table 4.2: Seawater desalination typical fouling and pretreatment processes.

The processes that have been conducted to remove the particles described above that could damage the membranes in the ultrafiltration and reverse osmosis processes are described below.

4.2.1 Multimedia pressure filter

Once the larger solids have been removed by the intake tower filter, a second filtration is conducted to remove those suspended solids which, to their size, could damage the ultrafiltration (UF) and reverse osmosis (RO) membranes. For this purpose, a screen filter or strainer is used to eliminate particles larger than 100-200 μm [85].

Multimedia pressure filter (also called strainer) is limited to about 10 NTU of turbidity. It contains graduated layers of anthracite of sand on top of sand on top of garnet. Figure 4.4 shows a cross section of a strainer which have three different filters according to the particle size (coarse, medium, and fine).

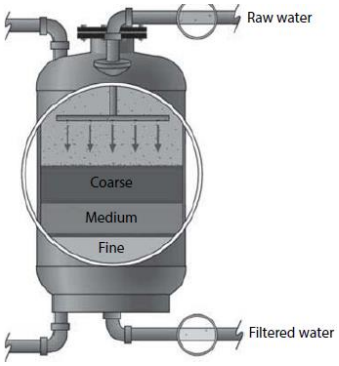

Figure 4.4: Schematic of a multimedia filter showing coarse, medium, and fine filter, typically anthracite, sand, and garnet, respectively. Ref. [16].

The strainer is placed on the feed line of the ultrafiltration (UF) process and after the chemical additions which will be described below. The size of the strainer mesh and its efficacy depend mainly on the feed water quality. Those parameters are designed in the WAVE software and the results are in the Table 4.3.

Parameters	Value
Size	150 μm
Recovery	99,5%

Table 4.3: Strainer specification

4.2.2 Seawater Chlorination

Chlorine is mainly used to kill microbes in a pre-treatment upstream either filter or to break up organics that may foul RO/UF membranes. Killing bacteria and microorganism before entering the membranes will prevent fouling.

Chlorine gas (Cl_2) and sodium hypochlorite (NaOCl) each react with water to form hypochlorous acid, as shown in the equations (4.1) and (4.2), respectively.

$$Cl_2 + 2H_2O \Rightarrow HOCl + H^+ + Cl^- \quad (4.1)$$

$$NaOCl + H_2O \Rightarrow HOCl + NaOH \quad (4.2)$$

In this project, it is used 1 mg/l of NaCl between feed pump and strainer considering that typical chlorine dose is about 3 mg/l for small scale plant. It is important to maintain pH between 7-7.5 to have optimized chlorine disinfection potential.

Therefore, if the average feed flow value is 4,678.6 m³/day and the NaOCl dose is 1 mg/L, the total amount of NaOCl needed to disinfect water is obtained from the equation (4.3).

$$m_{NaOCl} = Q_{in} * concr_{NaOCl} = 194.94 \frac{m^3}{h} * 0{,}001 \ \frac{kg}{m^3} = 0.2 \ kg/h \quad (4.3)$$

Therefore, 0.8 l/h are required in the feed stream. Furthermore, a dose of 350 mg/L (523.6 l/h) in the backwash step and 880 l/h in the CIP (See in detailed in Section 4.2.6) are added in this project.

4.2.3 Coagulation

The main objective of this stage is to facilitate the subsequent removal of those solids which, due to their size, could not be removed in the previous stages This is achieved by the electrical destabilization of colloidal particles to promote their grouping, making their subsequent removal easier. By electrically destabilizing these particles, positive charges are generated to neutralize the repulsive forces between particles.

To electrically destabilize the colloids, it is necessary to add chemical reagents that react with them. In this project, the coagulant used is ferric chloride ($FeCl_3$), generating the reaction (4.4) and (4.5).

$$Fe^{3+} + H_2O \Leftrightarrow Fe(OH)_3 + 3H^+ \quad (4.4)$$

$$HCO_3^- + H^+ \Leftrightarrow H_2O + CO_2 \quad (4.5)$$

The factors which can promote coagulation process are the velocity gradient, the time, and pH. The first two are crucial to increase the probability of the particles to come together and the pH is a key factor in the removal of colloids [86]. The quantity of ferric chloride required shall be calculated based on the flow rate, density of the reagent used, richness and maximum permissible dose as shown in the following table. It is used a maximum dose of 10 mg/L of $FeCl_3$ in this project.

Feed flow	194.94 m³/d
Maximum dose	10 mg/l
Richness	100%
Density	2.4 kg/l

Table 4.4: Coagulation parameters

Once the data has been defined, the amount of coagulant required per day can be obtained. For this purpose, the amount of ferric chloride required is calculated to finally obtain the amount of commercial solution required by the equations (4.6) and (4.7).

$$m_{FeCl_3} = Q_{in} * concr_{NaOCl} = 194.94 \frac{m^3}{h} * 0{,}01 \ \frac{kg}{m^3} = 1.944 \ kg/h \quad (4.6)$$

$$Q_{FeCl_3} = \frac{m_{FeCl_3}}{\rho_{FeCl_3}} * \frac{1}{richness} = 0.8 \ l/h \quad (4.7)$$

4.2.4 Antiscalant

In membrane desalination plants, there is a risk of scale formation in the membranes, which reduces their performance and can even damage them irreversibly. These incrustations are due to the precipitation of salts in the water, forming crystals. Crystals, in turn, favor the addition of more particles increasing their size to the point of not being able to be filtered by the membranes, becoming encrusted and obstructing them.

Due to the different ionic composition of sea water, there are several types of fouling. The most common types are calcium carbonate crystals, silica, sodium

sulphate, calcium phosphate, barium sulphate, strontium sulphate or precipitates of magnesium hydroxide. Therefore, to avoid these problems, antiscalants are added.

Antiscalants or scale inhibitors are used to reduce the potential for forming scale on the surface of an RO/UF membrane. They can work by one of the following methods:

- Crystal modification, which is the ability to change crystal shapes into sift and non-adherent scales.
- Threshold inhibition. It is the ability to keep supersaturated salts in solution.
- Dispersion which is the ability to impart a highly negative charge to the crystal while keeping them separated and preventing propagation.

The main function of antiscalants is to reduce the pH in order to control SDI[4] for calcium carbonate scale and to control calcium phosphate and calcium fluoride scales. Acid is added to drop the LSI down to zero to control calcium carbonate scale. In this project, addition of hydrochloric acid (HCl) is preferred for pH reduction rather than sulfuric acid (H_2SO_4) due to the last can increase the potential for forming sulphate-based scales.

The table below shows the water properties before and after adjusting the pH level from 8.1 to 7 by means of a hydrochloric acid dose of 16 mg/l (9.4 L/h). In the results it can be seen how the scale measurement coefficients (LSI and SDI) become zero as well as how this pH reduction manages to reduce the concentration of HCO_3^- and $Mg(OH)_2$. However, it also leads to a rise in CO_2 concentration. While the TDS remains constant, as these smaller particles will be removed by reverse osmosis membranes.

[4] Stiff & Davis Index (SDI) is a parameter that measures the degree of saturation of water with respect to calcium carbonate. Generally used when TDS>10,000 ppm. The desired value is when SDI=0. When it is lower than zero (negative) water can be corrosive and when it is higher than zero, the membranes can promote scaling.

Measurement	Before adjustment	After ↓pH
pH	8.1	7
LSI	1.04	-0.02
SDI	0.06	-0.03
TDS (mg/l)	35,985	36,001
Ionic strength (molal)	0.73	0.73
HCO_3^- (mg/l)	104.7	113.41
CO_2 (mg/l)	0.42	5.67
CO_3^- (mg/l)	17.21	1.48
$CaSO_4$(%)	22.34	22.34
$SrSO_4$(%)	15.49	15.49
CaF_2(%)	17.15	17.15
SiO_2(%)	0.7	0.8
$Mg(OH)_2$(%)	2.3	0.01

Table 4.5: Water Properties before and after pH regulation.

4.2.5 Dichlorination

After the ultrafiltration process and before reverse osmosis process, it is necessary to reduce the oxidizing load that the water may have. As mentioned above in the disinfection stage (chlorination), it is necessary to eliminate the free chlorine present in the water due to the action of the sodium hypochlorite used in this stage. The presence of oxidants can irreversibly damage the membranes used in the reverse osmosis process, making the process and therefore the desalination of the water more expensive.

For the elimination of oxidants, it is necessary to add chemicals to neutralize their effect. In this project, sodium metabisulphite ($Na_2S_2O_5$) will be used. Sodium metabisulphite is a solid product that dissolves in water and dissociates according to the reactions (4.8) and (4.9).

$$Na_2S_2O_5 + H_2O \Leftrightarrow 2HSO_3^- + 2Na^+ \quad (4.8)$$

$$2HSO_3^- + 2Na^+ \Leftrightarrow 2NaHSO_3 \quad (4.9)$$

For the dosage of sodium metabisulphite, it is necessary to prepare an initial solution and then mix it with water. The initial solution of the mixture will have a concentration of 250 g/L. For the calculation of the required product, the data presented in the following table shall be considered. As in the previous sections, a six-hour shock treatment shall be applied.

Feed flow	185.2 m³/d
Maximum dose	10 mg/l
Richness	40%
Density	1.3 kg/L

Table 4.6: Calculation basis for the dichlorination process.

Therefore, the quantity of sodium metabisulphite required is obtained according to the following formula (4.10):

$$m_{Na_2S_2O_5} = Q_{in} * concr_{Na_2S_2O_5} = 185.2 \frac{m^3}{h} * 0.01 \frac{kg}{m^3} = 1.852\ kg/h \quad (4.10)$$

4.2.6 Ultrafiltration (UF) process

The next pre-treatment stage is ultrafiltration. As the name suggests, ultrafiltration consists of filtering the water to separate the solid particles from the water. In this membrane filtration stage, water is pumped at high pressure to filter through the pores of the membranes. The size of these pores varies between 0.1 µm and 0.001 µm [85].

In this stage, although polyvalent ions or dissolved salts are not eliminated as in reverse osmosis, it can eliminate bacteria, viruses, endotoxins, and suspended solids, making it the ideal pre-treatment for the reverse osmosis stage, since in this last stage it would only be necessary to eliminate nanoparticles, ions, and dissolved salts, reducing the need to wash the membranes and extending their useful life. Figure 4.5 shows how UF perm-selectivity compares to many other membrane-based and conventional filtration techniques. As shown in the figure, RO offers the finest

filtration currently available, rejecting most dissolved solids as well as suspended solids [16]. In contrast, UF membranes does not eliminate the smallest particles.

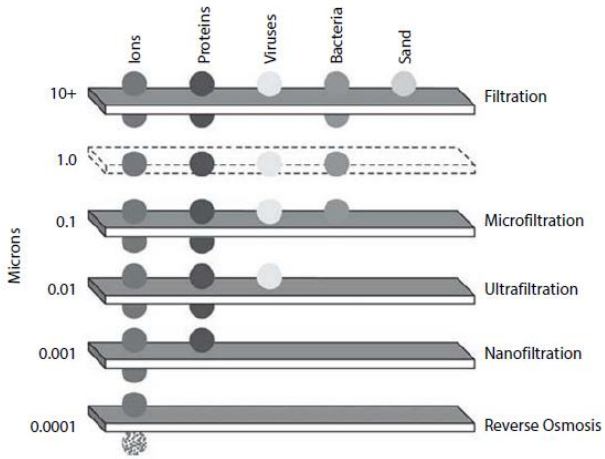

Figure 4.5: Schematic view of distinct size filtration comparing their rejection capabilities. Ref [16].

The following is a description of the ultrafiltration process devices used for the design of this project using WAVE software. Figure 4.7 shows the detailed schematic of this process with the different components used.

- **Strainer.** The strainer is described in 4.2.1 Section. It is placed on the feed line and is designed to remove large aggregates from the feed water before they can reach the UF membrane modules in order to prevent fouling and damage the system.
- **Membrane module.** In the Figure 4.7 it is placed in the middle. The membrane module is the most critical component of the process and generally it can be grouped more than one forming a skid which is a prefabricated assembly of modules, often mounted on a modular pallet. It can be arranged in sequence or in parallel. Finally, a train is complete self-contained arrangement of skids with accompanying equipment such as pump and tanks to meet the treatment goals [87].
- **Filtrate Tank.** It is placed on the filtrate line leaving behind the UF membrane module. The tank is used to store water in order to backwash the membrane and also acts as a swing tank. *Backwashing* is frequently removing foulants and debris on or inside the membrane by forcing a short stream of water at high pressure backwards through the membrane. Also, a chemically-enhanced backwash (CEB) can be added to the system where a cleaning chemical is added to the backwash water in order to help scour and solubilize foulants and scale [87].

- **Air scour.** It is used to break up and clean out solid debris accumulated within the membrane modules.
- **Cleaning-In-Place Tank.** As shown in Figure 4.7, this tank is placed upper on the left and is linked to the membrane. This tank holds chemicals dissolved in water and it is used to remove foulants.
- **Pumps and valves.** Several pumps in the feed, backwash and CIP are required to operate each membrane train. Valves are also required to operate a single module [87].

The filtration process is divided into four clearly differentiated stages: filtration, aeration, backwashing and rinsing. The design of the aeration, backwashing and rinsing stages is defined according to the characteristics of the membranes and the actions defined by the manufacturer. Before installing the membranes, it is necessary to wash the ultrafiltration modules to remove possible residual materials and chemicals from the manufacturing process.

1. **Filtration**

   The filtration process starts when the feed water is pumped through the membrane and then it is converted to filtrate (See 1) Figure 4.6). All feed is converted to filtrate in what is referred as dead-end filtration (See 1.5.1.2 Section) as opposed to crossflow filtration where a fraction of the feed leaves the system as reject. Filtration cycles typically oscillates between 20 and 90 minutes, depending on the water source and quality.

2. **Air Scour**

   This step is used to loosen particles deposited on the outside of the membrane surface. Oil-free air is introduced through the bottom of the module creating a stream of ascending bubbles which help to scour material off the membrane. Displaced water volume is allowed to discharge through the top port of the modules for disposal, as shown in 2) Figure 4.6. After a minimum of 20/30 seconds of continuous air scour, the module is drained by gravity.

3. **Gravity Drain**

   Once the air scour step is finished, the module must be drained by gravity in order to flush out of the system the fouled material from the membrane surface by the preceding air scour stage (See 3) Figure 4.6). It typically has a duration of 30/60 seconds. If gravity drain is not possible due to the system configuration, it can be substituted by a forced flush through the bottom outlet of the membrane using the backwash system. A drawback of using the backwash mode is the higher water and energy consumption.

4. **Backwash Top**

   Backwash system configuration is included in the project. Filtrate water is pumped backwards. Then, it is flushed out to the waste through the top module outlet as shown in 4) Figure 4.6. The backwash flux ranges from 100 to 120 LMH, and it lasts 30/45 seconds. In this project, chlorine is added to the backwash stream to remove foulants or microbes and air scour is combined with the backwash top step to increase cleaning effectiveness.

5. **Backwash bottom**

   After the backwash top stage, the filtrate continues to flow from the inside of the fiber to outside but now it is flushed out through the bottom outlet of the module in order to ensure the cleaning of the entire length of fibers [See 5) Figure 4.6]. The duration of this step is around 30/45 seconds.

6. **Forward flush**

   The last step is the forward flush in which feed water is used to rinse the system to remove the remaining solids and the air that might have got trapped in the system during the previous steps. Water flows on the outside of fibers with the filtrate valve closed, and exits through the module top outlet, as shown in 6) Figure 4.6. This step usually lasts 30/60 seconds. After this, the system returns to filtration mode and the cycle starts again.

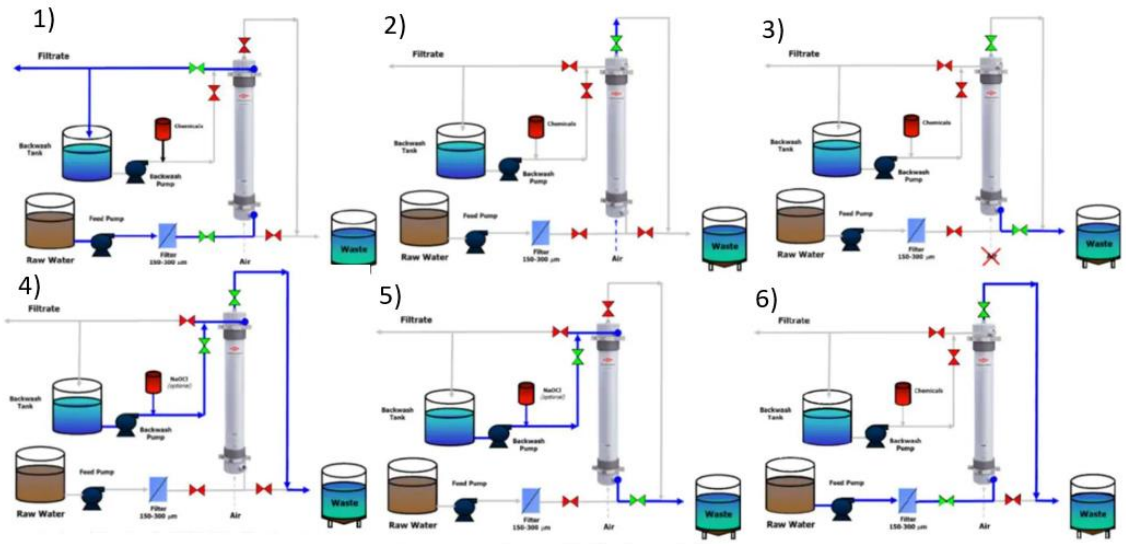

Figure 4.6: Schematic of the cleaning and filtrating steps in ultrafiltration process. Courtesy of *DOW™ Ultrafiltration membranes.*

For the design of the plant, WAVE provide only membranes from its company (DuPont™ UF module IntegraFlux™ SFD-2880XP) was selected to operate the system. SFD means that the module is for drinking applications. The first number "2" is the product material code which corresponds to PVDF, the next two correspond to

the product module diameter and the rest "80" is the product length of the module. XP means that the module has a higher permeability fiber. This module is an ideal choice for systems with capacities greater than 1,000 m³/day. It offers a high effective membrane area combined with high permeability that provides the most economical and efficient membrane system design. The table below shows the module of the membrane characteristics chosen in this project. The number of modules and trains was optimized by the software to select the most suitable and economic configuration.

Membrane Area	77 m²
Length	2.36 m
Diameter	0.225 m
Weight (empty)	61 kg
Weight (water filled)	100 kg
Water volume	30 L
Total trains	1
Modules/train	72
Total modules	72

Table 4.7: UF system size and module details

Therefore, considering the input data shown in Table 4.1 and specifying UF characteristics which are all shown in Table 4.8, the results are obtained by simulating the UF process in WAVE as shown in the Figure 4.7.

Strainer Specification		**Design flux and flow rates**		**Design Cycle intervals**	
Recovery	99.5%	**Filtrate flux**	40.9 LMH	**Filtration duration**	30 min
Strainer size	150µm	**Backwash flux**	100 LMH	**Acid CEB**	168 h
		CEB flux	100 LMH	**Oxidant CEB**	80 h
		Forward flush flow	75.62 m³/d/mod	**CIP**	90 d
		Air flow	12 m³/d/mod		
		CIP recycle flow rate	36 m³/d/mod		

Table 4.8: specifications of the ultrafiltration process design.

In the figure below, the size of the CIP and filtrate tank has been calculated. The software also determined the UF system recovery 89.4% and the operating flux 41 LMH which is a correct value for seawater desalination plants. The overall UF results are shown in the Table 4.9.

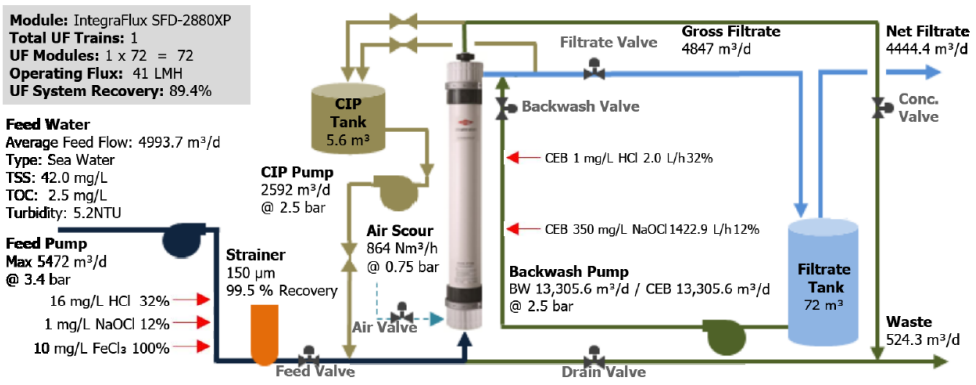

Figure 4.7: Schematic of a UF process and design of the study case of the project. WAVE Software.

	Feed	UF product
Temperature (ºC)	25	25
TSS (mg/L)	42	-
Turbidity (NTU)	5.2	<0.1
TOC (mg/L)	2.5	2.2
SDI	5.2	<2.5
TDS (mg/L)	35,985	36,001
pH@25ºC	8.1	7

Table 4.9: UF Water quality

As shown in the table above, TDS practically remains the same concentration. Besides, UF process achieved a total rejection of TSS and turbidity which was the main objective of this technique.

On the other hand, several simulations have been made in the program to obtain the best combination and type of UF membranes. In the Figure 4.8 and Figure 4.9 the two integraFlux™ membranes and the number of modules to be installed have been compared to select the most economical option. The operating costs of the UF system are divided into chemical, service water (waste), and electrical costs. The energy consumption and chemical cost in both membrane types remains practically equal and the first one is by far the smallest cost of the three with a value of 0.06 €/m³. That

is because the system does not require much pressure to overcome in the feed stream. Comparing both graphs, the **IntegraFlux™ SFD-2880XP** membrane has been chosen as it has the lowest specific cost of water produced with a value of 0.113 €/m³.

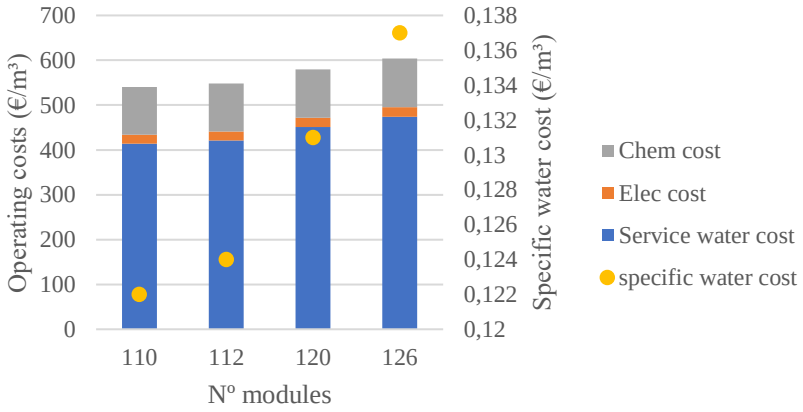

Figure 4.8: Operation and water production cost of UF process with IntegraFlux™ SFD-2860XP.

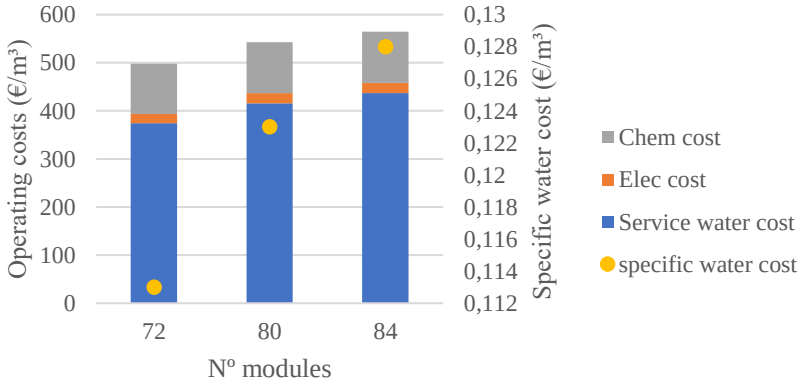

Figure 4.9: Operation and water production cost of UF process with IntegraFlux™ SFD-2880XP

4.3 Reverse Osmosis (RO) process

Following the UF process designed above, it is necessary to install an RO system to retain the largest number of dissolved solids. As explained in Section 1.5.1, the reverse osmosis stage consists of pumping water at high pressure and filtering it through semi-permeable membranes that prevent the filtration of dissolved salts, finally obtaining desalinated water. In the reverse osmosis process, unlike ultrafiltration, not 100% of the feed water is filtered. The conversion rate of this type of plant can vary around 40-60% depending on the type of membrane and the performance of the installation as a whole.

To model the RO process, the IMS Design™ software from the company Hydranautics Nitto Group has been used, since WAVE program used to design UF process does not include the option of installing an energy recovery device which will be discussed later. Before presenting the final design of this process, it is necessary to describe the variables that affect the performance of the membranes.

- **Element.** It is the smallest membrane unit in a RO process. It is like a module of the UF process.
- **Pressure vessel (PV).** It is a coaxial tube that contains one or more elements which are arranged in series [87].
- **Train.** It is the same as UF train. They are self-contained arrangements pressure vessels with the necessary accompanying pumps, tanks, valves, etc.
- **Stages.** If a system is coupled with two or more stages, then the first stage retentate becomes the second stage feed, and so on. They are used to further purify concentrate water and/or obtain higher recovery rates [87].
- **Passes.** In a multiple-pass system, permeate water from the first pass becomes the feed in the second pass, and so on. They are used to improve the permeate water quality [87]. An example of passes and stages is shown in Figure 4.10.

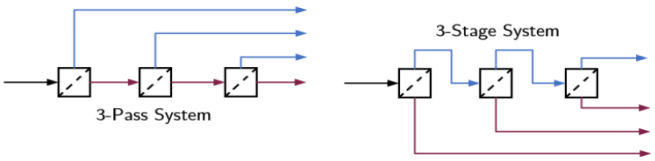

Figure 4.10: Examples of multiple-pass and multiple-stage RO systems. Concentrate streams are colored in blue and permeate are in red. ref. [87].

The first step in designing the RO process is to select the module model that best suits the system with the given characteristics. Therefore, the different models proposed by the software have been evaluated by means of several simulations and it has been concluded that the SWC6 MAX model is the optimal one for a correct operation and to reduce costs. The characteristics and configuration of the module are shown in the Table 4.10.

Membrane Area	40,9 m²
Length	1.016 m
Configuration	Spiral Wound
Membrane polymer	Composite Polyamide
Total trains	1
Modules/train	126
Total modules	126

Table 4.10: RO system size and module details (SWC6 MAX).

The next step is to select the permeate recovery of the system in function of the product water quality desired. It ranges to 40-60%. Once again, several aspects were analysed, such as the permeate water quality and the total cost of water produced as the recovery rate varied. In the diagram below it can be seen that as the recovery increases, the total dissolved solids (TDS) in the permeate also increases. This is due to the higher the recovery is, the more permeate is produced and therefore the membrane can retain less dissolved salts. On the other hand, the total cost of produced water is inversely proportional to the recovery up to 55% of it. Above this value the cost starts to rise. Thus, a value of 45% has been chosen for this case since the production of 300 mg/L of TDS has been set as a limit.

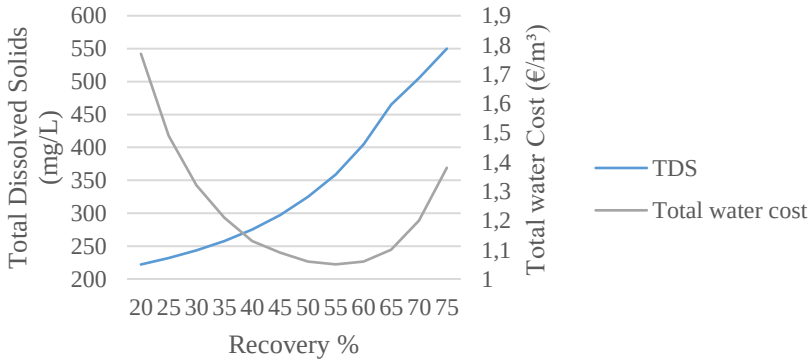

Figure 4.11: Difference between TDS/levelized water cost and recovery rate of the RO process with no ERD.

Finally, in order to maximize the performance of the installation and minimize energy consumption, an energy recovery device (ERD) will be installed. The ERD of seawater desalination system can be divided into two categories:

The positive displacement (volumetric) and centrifugal type [88]. According to different working parts equipment, the positive displacement is divided into piston type (DWEER™) and ceramic rotary (PX™). On the other hand, centrifugal type is mainly divided into Pelton turbine, hydraulic turbocharger, hydraulic booster and reverse centrifugal pump [89].

The positive displacement ERDs recover the energy of high-pressure concentrated seawater by directly transferring liquid pressure. Its operating mechanism is simple, the device is highly efficient, and it is currently used in massive quantities [89]. Therefore, a pressure exchange system will be installed to transfer the residual pressure of the dead salt to the feed water without the need to pump some of the water with the high-pressure pump. The following image shows the final flow diagram used in the simulation of the stage.

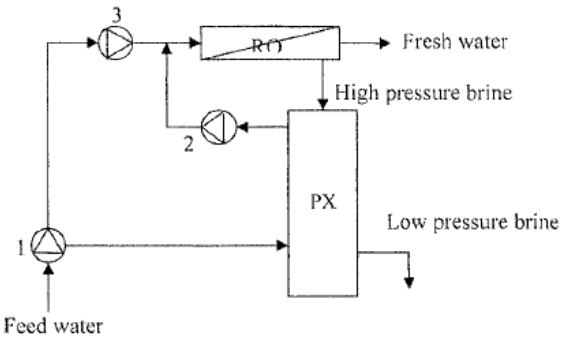

Figure 4.12: Floating Diagram of the RO process proposed coupled with an energy recovery device. Ref. [90].

According to [91], which did an exhaustive techno-economic evaluation of ERDs installed in the Canary Islands desalination plants, concluded that PX has been the predominant device installed in the archipelago, it is the ideal ERD for small, medium and large scale plants due to its robustness and modularity since they can install several of them in parallel. Besides, quite low energy consumption is achieved with this device (close to 2.2 kWh/m³) [91].

Pressure exchanger	
Leakage	1%
Volumetric mixing	6%
H.P differential	0.5 bar
Boost pressure	1.62 bar

Table 4.11: PX characteristic design

4.4 Post-Treatment

After the main treatment of filtration by reverse osmosis, the water is not suitable for human consumption or other uses due to its low alkalinity, low pH, and low hardness. Therefore, the water must be treated in such a way that it finally possesses the properties necessary for its use. The table below shows the permeate water quality of the reverse osmosis process with no post-treatment compared to the recommended characteristics of the water quality for drinking purposes.

Reverse osmosis is not a selective ion removal process. After the first pass RO process, permeate water is poor in minerals and low mineralized water have the following adverse effects:

- High corrosion potential.
- Dietary deficiency causing risks of heart and cerebrovascular disease [92].

For this purpose, it is necessary to remineralize the water by various processes. The following table shows the recommended characteristics that desalinated water should have after a remineralization process.

Measurement	EU standards 1998	After RO
pH	6.5-8.5	5.7
TDS (mg/l)	500	300
CO_2		5.74
HCO_3		1.806
NH_4	0.5	-
Ba	0.3	-
B	1	2.02
F	1.5	0.033
NO_3	50	-
Ca	104.7	0.046
Mg^+	0.005	0.142
Na^+	200	114.32
Cl^-	250	175.8
NO_2^-	0.5	-
SO_4^{2-}	250	6.22

Table 4.12: Comparison between EU drinking water standards and permeate of the RO process [92].

Measurement	Range
pH	6.5-8.5
SDI	± 0.15
HCO_3	68 ± 3
CO_2	0.5
Mg	10 ± 2
Ca	30 ± 2
$CaCO_3$	56 ± 3

Table 4.13: Water properties after remineralisation process. ref. [92].

According to World Health Organization (WHO), dose of 10 mg/L and 30mg/L of Mg and Ca are recommended for drinking water. For the remineralization of water from reverse osmosis, it was decided to use calcite beds with CO_2 dosing. It is essential to achieve a correct remineralization of the calcite beds. For this purpose, low-pressure CO_2 dosing devices are used. These dosers incorporate the CO_2 in a counter current in such a way as to facilitate the mixing of the water with the bubbles of the injected compound.

On the other hand, it has been decided to use calcite beds and no other systems due to the advantages that this system offers. By using calcite beds, a greater number of bicarbonates is obtained with the same amount of CO_2 and at the same time, the balance is reached automatically, regulating the pH, and consuming only the necessary amount of calcium carbonate, without the use of control and monitoring equipment. The amount of reagent necessary for the remineralization of the water is consumed according to the following equation:

$$CO_2 + CaCO_3 + H_2O \Leftrightarrow Ca(HCO_3)_2 \qquad (4.11)$$

In order to calculate the required amount of CO2 and calcite, it is necessary to consider the final properties of the water to be obtained. The final concentration of calcite in the water should be 80 mg/l [86]. Therefore, considering the permeate flow rate and the required concentration is obtained:

$$m_{CaCO_3} = Q_{permeate} * concr_{CaCO_3}$$
$$= 83.33 \frac{m^3}{h} * 80 \frac{mg}{L} * \frac{1{,}000\ L}{1\ m^3} * \frac{1\ kg}{1x10^6 mg} = 6.7\ kg/h \qquad (4.12)$$

By calculating the stoichiometric coefficients (SI) in equation (4.11) and with the amount of reagent obtained in equation (4.12), the amount of CO_2 to be added is obtained:

$$m_{CO_2} = m_{CaCO_3} * SI = 6.7 \frac{kg}{h} * 0.44 = 2.95\ kg/h \qquad (4.13)$$

4.5 Results

This section describes the results obtained from the simulations of the seawater desalination plant design. First, the results obtained from the energy analysis of the ultrafiltration and reverse osmosis processes are discussed, as well as the usefulness of installing the energy recovery device.

Practically all the plant's energy consumption goes to the high-pressure pump of the RO process due to the high pressure required to retain the maximum number of TDS. The total power required to achieve a correct operation of the RO process is 176.5 kW whose value also depend largely on the characteristics of the pumps. Whereas in the UF process only 38.27 kW of peak power will be required, or what is the same, in the RO process 2.12 kWh/m³ will be consumed while in UF process only 0.06 kWh/m³ will be consumed. Therefore, the total energy consumption of the plant is equal to 2.18 kWh/m³thanks to the installation of the energy recovery device, otherwise the energy consumption would be much higher, approximately 4.36 kWh/m³.

It is assumed that the specific investment cost of the desalination plant is 950 €/m³/day, i.e., a total of 1,9 M€, considering that the production capacity of the plant is 2,000 m³/day. Considering a plant lifetime of 25 years, membranes lifetime of 5 years, membrane cost of 800 €/element, the chemical costs, interest rate of 4.5%, plant factor of 41%, power consumption of 2.18 kWh/m³, and a maintenance cost of a 3% of the investment cost, the levelized cost of the water (LCOW) is then calculated and it is equal to 0.87 €/m³ and the net present cost of the desalination plant is equal to 7,536,472.7 €. The Figure 4.13 represents the percentage of each type of cost in terms of €/m³ and the power cost or energy consumption cost represents a half of the total water cost.

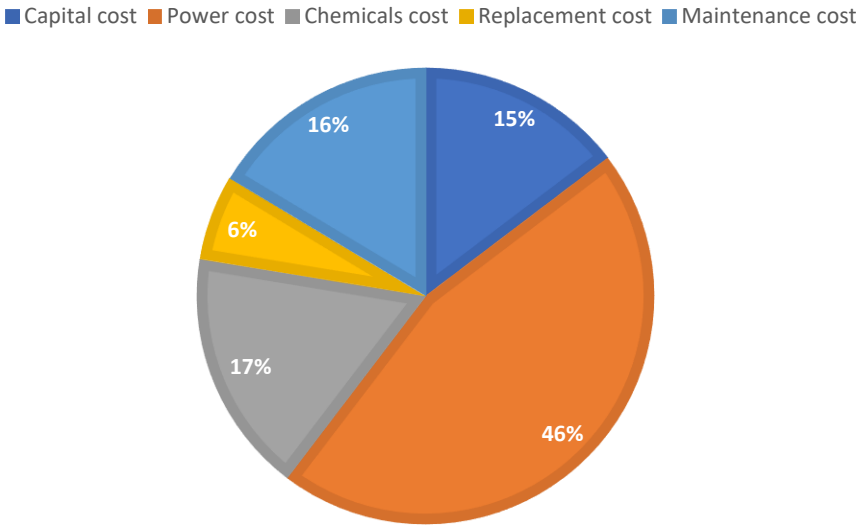

Figure 4.13: Different type of cost per m³ of permeate water produced.

4.6 Comparison of simultaneous energy and water production costs among the commercial DES-RE technologies

The aim of this section is to show the levelized cost of the energy (LCOE) and the levelized cost of the water (LCOW) of the whole project (HRES+ADS) as this is the optimal way to compare them to similar RE-DES projects. Table 4.14 shows the result of these parameters in two possible scenarios of the optimal HRES configuration. The first scenario consists of the HRES config.4 (550-kW diesel gen, 274-kW PV, 28 WT, 518 batteries, and 341-kW converter). The other scenario also comprises HRES config 4. but replaces the energy storage (batteries) by a water storage tank that was modelled in Section 3.9. It is noted that the addition of the water tank will result in a lower LCOE (3.4%) and LCOW (3.5%) and will therefore be a better alternative to the use of batteries.

	LCOE (€/kWh)	**LCOW (€/m³)**
Batteries. Energy Storage	0.61	1.328
Water Storage Tank	0.59	1.283

Table 4.14: LCOE and LCOW of the optimal configuration HRES-ADS. 1)With batteries. 2)With Water Storage Tank.

To compare the different RE-DES technologies, it was necessary to look up the cost of drinking water production in the literature. In Table 4.15, the technologies that are most widely used are selected, and only seawater has been considered as the cost varies greatly from brackish water. On the other hand, the capacity of the desalination plants is limited based on the type of technology used.

Once the LCOW has been determined, it is possible to estimate the LCOE by simply dividing by the total energy consumption of the RE-DES plant in question. Therefore, it can be observed that the LCOW is similar in many of the technologies exposed below, ranging between 1 to 5 €/m³. Although there are some, such as PV-RO or Solar membrane distillation, that present values higher than 10 €/m³. Thus, any option implemented in this project, either with batteries or with the water tank, is more profitable than the technologies described in the table. Only the cost of water produced per m³ is lower in modern technologies such as Solar pond-RO and Solar pond-MED which reaches values from 0.6 to 0.8. The same is true for the LCOE, which will vary according to the energy produced per year from renewables and this will be directly linked to the energy consumption of the desalination plant.

		Size capacity (m³/d)	LCOW (€/m³)	LCOE (€/kWh)	ref
Membrane technologies	PV-RO	<100	9.9-13.3	2.21-2.5	[35]
	Solar Pond-RO	20,000-200,00	0.6-0.8	0.13-0.15	[35]
	PV-EDR	<100	8.8-9.8	2.45-5.9	[35]
	WT-RO	<100	5-7	1.2-1.25	[35]
		1,000-10,000	1.95-5.4	0.9-1.1	[35]
Thermal technologies	Solar Still	<100	1.1-5.5	-	[35]
	Solar MEH	<100	2.2-5.5	1.5-3.7	[51]
	Solar MD	<10	8.9-16.6	-	[35]
	Solar Pond-MED	20,000-200,000	0.6-0.75	0.25-0.3	[35]
	Solar CSP-MED	>5,000	2.1-2.4	0.8-1.05	[93]
	WT-MVC	<100	4.4-6.6	-	[93]
	Geothermal-MED	<80	1.7-2.4	0.8-0.85	[93]

Table 4.15: Water and energy production cost of RE-coupled desalination plants.

5. Conclusion and future development

The Canary Island, El Hierro is experienced with the lack of grid electrification in the past; To exploit the seawater resources, a seawater desalination reverse osmosis desalination plant was designed in this project, as it was found in literature to be cheapest and most advanced desalination technology. This plant consists of several stages including pre-treatment, reverse osmosis membrane process, and post-treatment to make it a high-quality water for drinking purposes (TDS<300 mg/l) with a capacity of 2,000 m^3/day. Furthermore, an energy recovery device was incorporated to lower costs and reduce the energy consumption of the desalting process from 4.3 to 2.18 kWh/m^3.

Once this data has been obtained, electricity consumption is estimated with a value 4360 kWh/day based on the daily water consumption per inhabitant and monthly profiles with peak demand in July. The objective is to install an autonomous desalination system (ADS) using hybrid renewable energy systems (HRES). A software called HOMER Pro™ is used to simulate a techno-economic and environmental assessment of different hybrid configurations to identify the optimal one. Several considerations have been evaluated to discover the best solution that minimizes the NPC, LCOE, and TCE. The most relevant discoveries of the analysis can be highlighted as follows:

- The economic evaluation proved that the config 4. was the most profitable, with the minimum NPC=3.97 M€ and COE=0.21 €/kWh compared to all other configurations. Comparing the optimal case with the base case (Diesel Genset only), a 68% reduction in NPC and COE is achieved.
- The optimal sizing of the components from the optimal configuration were found to be of a 550-kW diesel generator, 274-kW PV system, 28 wind turbines of 10 kW each, 518 batteries of 1.02 kWh Li-on [ASM], and 341-kW DC/AC converter based on the site power resources and the profile load demand.
- Additionally, a water storage tank has been considered at the outlet of the ADS to replace the battery bank of the HRES optimal configuration in order to reduce costs. With this solution, the NPC of the HRES would be reduced by 10%.
- An environmental analysis of the 10-configurations was performed to compare the carbon emissions produced by electricity generation. The last three consisted only of renewable technologies, thus producing zero CO_2

emissions but instead a large excess of energy and therefore a considerable increase in NPC. The optimal configuration ranks the 5th position in terms of lowest carbon emissions but considering the above it is not of an immense importance because it still achieves a reduction of 84.5% compared to the base case.

- Finally, the optimal configuration was also characterized by a ridiculously small unmet demand of a 0.0044% leading to a continuous ensure of the electricity required for the SWRO desalination plant.

This Project has compared all current seawater water renewable energy desalination technologies found in the most recent literature. From this techno-economic analysis of the HRES-DES, it has been obtained a water production cost equal to 1.328 €/m³ (with batteries) and 1.283 €/m³ (with water tank), a lower value compared to the other technologies thanks to the lower RO energy consumption and the addition of several renewable power sources.

This work is crucial for future water projects on these technologies as they promote the use of clean and sustainable energy and contribute to the reduction of climate change which is so important at this time of year. As time progresses, so does the world's population, and consequently water demand, so it is inevitable to damage the planet using conventional energies. By using reverse osmosis with an energy recovery device, it is possible to reduce most of the energy consumed, and if it is coupled with renewable energy, the process becomes sustainable over time and with zero carbon emissions.

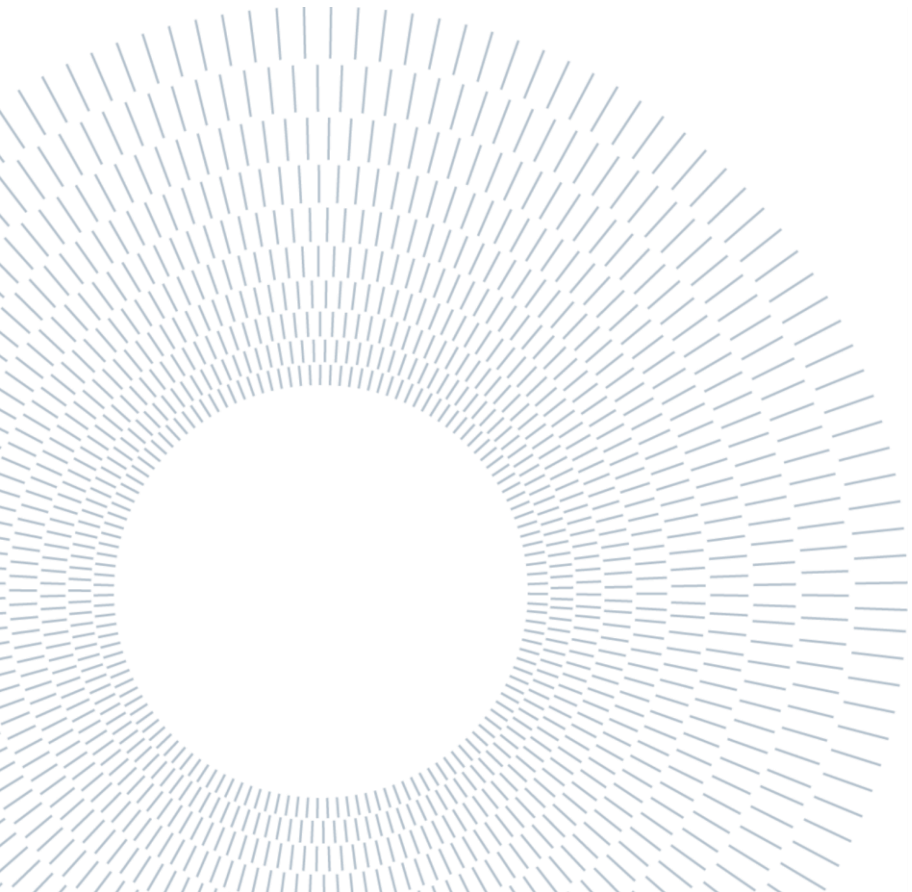

6. Bibliography

[1] G. Fiorenza, V. K. Sharma, and G. Braccio, "Techno-economic evaluation of a solar powered water desalination plant," *Energy Convers. Manag.*, vol. 44, no. 14, pp. 2217–2240, 2003, doi: 10.1016/S0196-8904(02)00247-9.

[2] D. Molden, *Water for food water for life: A Comprehensive assessment of water management in agriculture*. 2013.

[3] T. Hayasaki, "Coping with water scacity: Challenge of the twenty-first century," *World Water Day 2007*, vol. 71, no. 4, pp. 53–57, 1999, [Online]. Available: http://ci.nii.ac.jp/naid/40005232449/.

[4] W. Blomquist *et al.*, "Desalination and water Purification technology roadmap: A report of the executive committee," *Desalin. Solut. Roadmap an Improv. Water Supply*, pp. 87–179, 2012.

[5] C. Heather, G. Peter H, and W. Gary, *Desalination, with a grain of salt. A California Perspective*, vol. 35, no. June. 2006.

[6] K. V. Reddy and N. Ghaffour, "Overview of the cost of desalinated water and costing methodologies," *Desalination*, vol. 205, no. 1–3, pp. 340–353, 2007, doi: 10.1016/j.desal.2006.03.558.

[7] IDA & GWI, "International Desalination Association and Global Water Intelligence Release New Data in 30th Worldwide Desalting Inventory - Idadesal." [Online]. Available: https://idadesal.org/international-desalination-association-and-global-water-intelligence-release-new-data-in-30th-worldwide-desalting-inventory/.

[8] M. Nair and D. Kumar, "Water desalination and challenges: The Middle East perspective: A review," *Desalin. Water Treat.*, vol. 51, no. 10–12, pp. 2030–2040, 2013, doi: 10.1080/19443994.2013.734483.

[9] J. E. Miller, "Review of water resources and desalination techniques," no. May, 2003, doi: 10.2172/809106.

[10] P. Palomar and I. J. Losada, "Desalination in Spain: Recent developments and recommendations," *Desalination*, vol. 255, no. 1–3, pp. 97–106, 2010, doi: 10.1016/j.desal.2010.01.008.

[11] A. S. Rybar, M. Vodnar, F. L. Vartolomei, and P. S. Rybar, "Experience with Renewable Energy Source and SWRO Desalination in Gran Canaria," *SP05-100. Int. Desalin. Assoc. World Congr.*, pp. 1–11, 2005.

[12] AMTA, "Water Desalination Processes," *American Membrane Technology Association*. p. 1, 2007, [Online]. Available: https://www.amtaorg.com/Water_Desalination_Processes.html.

[13] American Water Works Association, *M61 Desalination of Seawater*. 2011.

[14] S. Miller, H. Shemer, and R. Semiat, "Energy and environmental issues in desalination," *Desalination*, vol. 366, pp. 2–8, 2015, doi: 10.1016/j.desal.2014.11.034.

[15] Puretec Industrial Water, "Puretec Industrial Water | What is Reverse Osmosis?" 2018, [Online]. Available: https://puretecwater.com/reverse-osmosis/what-is-reverse-osmosis.

[16] Luz Yolanda Toro Suarez, *Reverse Osmosis: Design, Processes, and Applications for Engineers*. 2015.

[17] E. O. Ezugbe and S. Rathilal, "Membrane technologies in wastewater treatment: A review," *Membranes (Basel).*, vol. 10, no. 5, 2020, doi: 10.3390/membranes10050089.

[18] F. Calise, F. L. Cappiello, R. Vanoli, and M. Vicidomini, "Economic assessment of renewable energy systems integrating photovoltaic panels, seawater desalination and water storage," *Appl. Energy*, vol. 253, Nov. 2019, doi: 10.1016/j.apenergy.2019.113575.

[19] P. A. Davies, "A solar-powered reverse osmosis system for high recovery of freshwater from saline groundwater," *Desalination*, vol. 271, no. 1–3, pp. 72–79, 2011, doi: 10.1016/j.desal.2010.12.010.

[20] R. S. Silver, "The developement on multi-stage flash distillation," vol. II, 1956.

[21] O. K. Buros, "The ABCs of Desalting," *Int. Desalin. Assoc. Mass*, no. 2, pp. 1–32, 2000, [Online]. Available: http://www.water.ca.gov/pubs/surfacewater/abcs_of_desalting/abcs_of_desalting.pdf.

[22] I. C. Karagiannis and P. G. Soldatos, "Water desalination cost literature: review and assessment," *Desalination*, vol. 223, no. 1–3, pp. 448–456, 2008, doi: 10.1016/j.desal.2007.02.071.

[23] *Green Energy and Technology*. 2006.

[24] R. A. M. A.M.Shams El Din, "Brine and scale chemistry in MSF distillers, Desalination." p. Volume 99, Issue 1, 1994.

[25] A. M. Shams El Din, M. E. El-Dahshan, and H. H. Haggag, "Carbon-induced corrosion of MSF condenser tubes in Arabian Gulf water," *Desalination*, vol. 172, no. 3, pp. 215–226, 2005, doi: 10.1016/j.desal.2004.06.202.

[26] M. A. Eltawil, Z. Zhengming, and L. Yuan, "A review of renewable energy technologies integrated with desalination systems," *Renew. Sustain. Energy Rev.*, vol. 13, no. 9, pp. 2245–2262, 2009, doi: 10.1016/j.rser.2009.06.011.

[27] H. Cooley, P. H. Gleick, and G. Wolff, "Appendix A Desalination Technologies," pp. 1–9, 2006.

[28] "Multi-effect distillation plants- state of the art.pdf." .

[29] F. Mandani, H. Ettouney, and H. El-Dessouky, "LiBr-H2O absorption heat pump for single-effect evaporation desalination process," *Desalination*, vol. 128, no. 2, pp. 161–176, 2000, doi: 10.1016/S0011-9164(00)00031-X.

[30] International Energy Agency, "Energy Policy Review Spain 2021," 2021, [Online]. Available: www.iea.org/t&c/.

[31] IRENA, "Water Desalination Using Renewable Energy ENERGY TECHNOLOGY SYSTEMS ANALYSIS PROGRAMME," *Int. Renew. Energy Agency*, no. March, pp. 1–28, 2012, [Online]. Available: www.etsap.org-www.irena.org.

[32] F. E. Ahmed, R. Hashaikeh, and N. Hilal, "Solar powered desalination – Technology, energy and future outlook," *Desalination*, vol. 453, no. November 2018, pp. 54–76, 2019, doi: 10.1016/j.desal.2018.12.002.

[33] N. Ghaffour, J. Bundschuh, H. Mahmoudi, and M. F. A. Goosen, "Renewable energy-driven desalination technologies: A comprehensive review on challenges and potential applications of integrated systems," *Desalination*, vol. 356, pp. 94–114, 2015, doi: 10.1016/j.desal.2014.10.024.

[34] F. Azevedo, "Renewable Energy Powered Desalination Systems: Technologies and Market Analysis," p. 68, 2014.

[35] A. Al-Karaghouli and L. L. Kazmerski, "Energy consumption and water production cost of conventional and renewable-energy-powered desalination processes," *Renew. Sustain. Energy Rev.*, vol. 24, pp. 343–356, 2013, doi: 10.1016/j.rser.2012.12.064.

[36] S. A. Avlonitis, K. Kouroumbas, and N. Vlachakis, "Energy consumption and membrane replacement cost for seawater RO desalination plants," *Desalination*, vol. 157, no. 1–3, pp. 151–158, 2003, doi: 10.1016/S0011-9164(03)00395-3.

[37] S. M. Shalaby, "Reverse osmosis desalination powered by photovoltaic and solar Rankine cycle power systems: A review," *Renew. Sustain. Energy Rev.*, vol. 73, no. February, pp. 789–797, 2017, doi: 10.1016/j.rser.2017.01.170.

[38] A. J. Karabelas, C. P. Koutsou, M. Kostoglou, and D. C. Sioutopoulos, "Analysis of specific energy consumption in reverse osmosis desalination processes," *Desalination*, vol. 431, no. February 2017, pp. 15–21, 2018, doi: 10.1016/j.desal.2017.04.006.

[39] E. Cabrera, T. Estrela, and J. Lora, "Pasado, presente y futuro de la desalación en España," *Ing. del agua*, vol. 23, no. 3, p. 199, 2019, doi: 10.4995/ia.2019.11597.

[40] R. Semiat, "Energy issues in desalination processes," *Environ. Sci. Technol.*, vol. 42, no. 22, pp. 8193–8201, 2008, doi: 10.1021/es801330u.

[41] J. Koschikowski, M. Wieghaus, and M. Rommel, "Solar thermal driven desalination plants based on membrane distillation," *Water Sci. Technol. Water Supply*, vol. 3, no. 5–6, pp. 49–55, 2003, doi: 10.2166/ws.2003.0149.

[42] J. B. Tonner and J. Tonner, "Desalination and Energy Use," *Encycl. Energy*, vol. 1, pp. 791–799, 2004, doi: 10.1016/b0-12-176480-x/00403-4.

[43] M. Shatat and S. B. Riffat, "Water desalination technologies utilizing conventional and renewable energy sources," *Int. J. Low-Carbon Technol.*, vol. 9, no. 1, pp. 1–19, 2014, doi: 10.1093/ijlct/cts025.

[44] V. G. Gude, N. Nirmalakhandan, and S. Deng, "Renewable and sustainable approaches for desalination," *Renew. Sustain. Energy Rev.*, vol. 14, no. 9, pp. 2641–2654, 2010, doi: 10.1016/j.rser.2010.06.008.

[45] W. Lai, Q. Ma, H. Lu, S. Weng, J. Fan, and H. Fang, "Effects of wind intermittence and fluctuation on reverse osmosis desalination process and solution strategies," *Desalination*, vol. 395, pp. 17–27, 2016, doi: 10.1016/j.desal.2016.05.019.

[46] A. del Villar García, "El coste energético de la desalinización en el Programa A.G.U.A.," *Investig. Geográficas*, no. 62, p. 101, 2014, doi: 10.14198/ingeo2014.62.07.

[47] A. Wahed, M. Bieri, T. K. Kui, and T. Reindl, "Levelized Cost of Solar Thermal System for Process Heating Applications in the Tropics," in *Transition Towards 100{\%} Renewable Energy: Selected Papers from the World Renewable Energy Congress WREC 2017*, A. Sayigh, Ed. Cham: Springer International Publishing, 2018, pp. 441–450.

[48] A. M. Delgado-Torres, L. García-Rodríguez, B. Peñate, J. A. de la Fuente, and G. Melián, "Water Desalination by Solar-Powered RO Systems," *Curr. Trends Futur. Dev. Membr. Renew. Energy Integr. with Membr. Oper.*, pp. 45–84, 2019, doi: 10.1016/B978-0-12-813545-7.00003-9.

[49] V. R. Patil, V. I. Biradar, R. Shreyas, P. Garg, M. S. Orosz, and N. C. Thirumalai, "Techno-economic comparison of solar organic Rankine cycle (ORC) and photovoltaic (PV) systems with energy storage," *Renew. Energy*, vol. 113, pp. 1250–1260, 2017, doi: 10.1016/j.renene.2017.06.107.

[50] F. Trieb and M. Moser, "Combined Solar Power and Desalination Plants : Techno-Economic Potential in Mediterranean Partner Countries and Desalination Configurations adapted for Application in the Southern and Eastern Mediterranean Region," *Technol. Rev.*, no. June, pp. 1–117, 2009.

[51] E. Tzen and M. Papapetroub, "Promotion of renewable energy sources for water production through desalination," *Desalin. Water Treat.*, vol. 39, no. 1–3, pp. 302–307, 2012, doi: 10.1080/19443994.2012.669232.

[52] S. W. Sharshir, N. Yang, G. Peng, and A. E. Kabeel, "Factors affecting solar stills productivity and improvement techniques: A detailed review," *Appl. Therm. Eng.*, vol. 100, no. February, pp. 267–284, 2016, doi: 10.1016/j.applthermaleng.2015.11.041.

[53] B. Peñate and L. García-Rodríguez, "Current trends and future prospects in the design of seawater reverse osmosis desalination technology," *Desalination*, vol. 284, pp. 1–8, 2012, doi: 10.1016/j.desal.2011.09.010.

[54] D. Manolakos, E. S. Mohamed, I. Karagiannis, and G. Papadakis, "Technical and economic comparison between PV-RO system and RO-Solar Rankine system. Case study: Thirasia island," *Desalination*, vol. 221, no. 1–3, pp. 37–46, 2008, doi: 10.1016/j.desal.2007.01.066.

[55] Q. Ma and H. Lu, "Wind energy technologies integrated with desalination

systems: Review and state-of-the-art," *Desalination*, vol. 277, no. 1–3, pp. 274–280, 2011, doi: 10.1016/j.desal.2011.04.041.

[56] B. S. Richards, D. P. S. Capao, and A. I. Schafer, "The effect of energy fluctuations on performance of a photovoltaic hybrid membrane system," *Environ. Sci. Technol.*, vol. 42, no. 12, pp. 4563–4569, 2008.

[57] G. L. Park, A. I. Schäfer, and B. S. Richards, "Renewable energy-powered membrane technology: Supercapacitors for buffering resource fluctuations in a wind-powered membrane system for brackish water desalination," *Renew. Energy*, vol. 50, pp. 126–135, 2013, doi: 10.1016/j.renene.2012.05.026.

[58] A. M. Gilau and M. J. Small, "Designing cost-effective seawater reverse osmosis system under optimal energy options," *Renew. Energy*, vol. 33, no. 4, pp. 617–630, 2008, doi: 10.1016/j.renene.2007.03.019.

[59] I. Padrón, D. Avila, G. N. Marichal, and J. A. Rodríguez, "Assessment of Hybrid Renewable Energy Systems to supplied energy to Autonomous Desalination Systems in two islands of the Canary Archipelago," *Renew. Sustain. Energy Rev.*, vol. 101, no. February 2018, pp. 221–230, 2019, doi: 10.1016/j.rser.2018.11.009.

[60] J. Schallenberg-Rodríguez, J. M. Veza, and A. Blanco-Marigorta, "Energy efficiency and desalination in the Canary Islands," *Renew. Sustain. Energy Rev.*, vol. 40, pp. 741–748, 2014, doi: 10.1016/j.rser.2014.07.213.

[61] H. C. Gils and S. Simon, "Carbon neutral archipelago – 100% renewable energy supply for the Canary Islands," *Appl. Energy*, vol. 188, pp. 342–355, 2017, doi: 10.1016/j.apenergy.2016.12.023.

[62] A. González, J. C. Pérez, J. P. Díaz, and F. J. Expósito, "Future projections of wind resource in a mountainous archipelago, Canary Islands," *Renew. Energy*, vol. 104, pp. 120–128, 2017, doi: 10.1016/j.renene.2016.12.021.

[63] EU, "ADIRA Handbook. A guide to autonomous desalination system concepts," *Euro-Mediterranean Reg. Program. Water Manag.*, 2008, [Online]. Available: http://wrri.nmsu.edu/conf/conf11/2008_adira_handbook.%5Cnpdf.

[64] V. Khare, S. Nema, and P. Baredar, "Solar-wind hybrid renewable energy system: A review," *Renew. Sustain. Energy Rev.*, vol. 58, pp. 23–33, 2016, doi: 10.1016/j.rser.2015.12.223.

[65] "NASA. Prediction of Worlwide Energy Resources." https://power.larc.nasa.gov/ (accessed Sep. 06, 2021).

[66] T. Lambert, P. Gilman, and P. Lilienthal, "Micropower System Modeling with Homer," *Integr. Altern. Sources Energy*, pp. 379–418, 2006, doi: 10.1002/0471755621.ch15.

[67] US Energy Information Administration, "Cost and Performance Characteristics of New Generating Technologies," *Annu. Energy Outlook 2020*, vol. 2020, no. January, pp. 1–4, 2020, [Online]. Available: https://www.eia.gov/outlooks/aeo/assumptions/pdf/table_8.2.pdf.

[68] R. Fu, D. Feldman, and R. Margolis, "110. U.S. Solar Photovoltaic System Cost Benchmark: Q1 2018," *Nrel*, no. Novmnber, pp. 1–47, 2018, [Online]. Available: https://www.nrel.gov/docs/fy19osti/72399.pdf.

[69] E. Vartiainen, G. Masson, C. Breyer, D. Moser, and E. Román Medina, "Impact of weighted average cost of capital, capital expenditure, and other parameters on future utility-scale PV levelised cost of electricity," *Prog. Photovoltaics Res. Appl.*, vol. 28, no. 6, pp. 439–453, 2020, doi: 10.1002/pip.3189.

[70] "Gaia 133 - 11kW Wind Turbine price," *Renugen renewable generation*, 2021. https://www.renugen.co.uk/gaia-wind-11kw-wind-turbine/ (accessed Sep. 07, 2021).

[71] "Candor Gaia Turbine Report," *Wadebridge Renew. energy Netw.*, pp. 1–30, 2012, [Online]. Available: https://www.wren.uk.com/.

[72] M. Ramesh and R. P. Saini, "Dispatch

strategies based performance analysis of a hybrid renewable energy system for a remote rural area in India," *J. Clean. Prod.*, vol. 259, p. 120697, 2020, doi: 10.1016/j.jclepro.2020.120697.

[73] W. and central A. Technical assistant facility, sustainable energy for all, *Sustainable Energy Handbook. Simplified Financial Models*, no. 6.1. 2016.

[74] V. Schyns, "Greenhouse gas emissions trading," *2008 AIChE Spring National Meeting, Conference Proceedings*, 2008. https://www.inforse.org/europe/eu_em-trad.htm (accessed Sep. 10, 2021).

[75] "Spain - Economic Indicators," *Trading Economics*, 2021. https://tradingeconomics.com/spain/indicators (accessed Sep. 14, 2021).

[76] D. Somwanshi and A. Chaturvedi, "Design and Optimization of a Grid-Connected Hybrid Solar Photovoltaic-Wind Generation System for an Institutional Block," no. January, pp. 319–326, 2020, doi: 10.1007/978-981-15-1059-5_36.

[77] UL.LCC, "Total Net Present Cost," *HOMER Pro 3.14*, 2020. https://www.homerenergy.com/products/pro/docs/latest/total_net_present_cost.html (accessed Sep. 09, 2021).

[78] K. Elmaadawy *et al.*, "Optimal sizing and techno-enviro-economic feasibility assessment of large-scale reverse osmosis desalination powered with hybrid renewable energy sources," *Energy Convers. Manag.*, vol. 224, no. August, 2020, doi: 10.1016/j.enconman.2020.113377.

[79] L. Cost, W. Resources, and E. N. Records, "Appendix A : Levelized Cost Methodology," no. October, pp. 1–6, 2016, [Online]. Available: http://pacinst.org/wp-content/uploads/2016/10/PI_TheCostofAlternativeWaterSupplyEfficiencyOptionsinCA_AppendixA.pdf.

[80] T. Tezer, R. Yaman, and G. Yaman, "Evaluation of approaches used for optimization of stand-alone hybrid renewable energy systems," *Renew. Sustain. Energy Rev.*, vol. 73, no. February, pp. 840–853, 2017, doi: 10.1016/j.rser.2017.01.118.

[81] K. M. Kotb, M. R. Elkadeem, M. F. Elmorshedy, and A. Dán, "Coordinated power management and optimized techno-enviro-economic design of an autonomous hybrid renewable microgrid: A case study in Egypt," *Energy Convers. Manag.*, vol. 221, no. March, p. 113185, 2020, doi: 10.1016/j.enconman.2020.113185.

[82] H. Mehrjerdi, "Modeling and integration of water desalination units in thermal unit commitment considering energy and water storage," *Desalination*, vol. 483, no. March, p. 114411, 2020, doi: 10.1016/j.desal.2020.114411.

[83] Government of Newfoundland & Labrador Department of Environment & Conservation, "Evaluation of Potable Water Storage Tanks in Newfoundland and Labrador and their Effect on Drinking Water Quality," no. July, p. 152, 2011, [Online]. Available: https://www.mae.gov.nl.ca/waterres/reports/drinking_water/Tank_Report_July_12_2011.pdf.

[84] M. Badruzzaman, N. Voutchkov, L. Weinrich, and J. G. Jacangelo, "Selection of pretreatment technologies for seawater reverse osmosis plants: A review," *Desalination*, vol. 449, no. August 2018, pp. 78–91, 2019, doi: 10.1016/j.desal.2018.10.006.

[85] A. Sánchez Alcaide, "Estudio comparativo de los principales procesos de desalación y diseño de una planta de osmosis inversa con una capacidad de 10,000 m^3/d," Universidad Pontifica de comillas Madrid, 2017.

[86] "Desalination Post-treatment : Boron Removal Process." 2017, [Online]. Available: https://www.lenntech.com/processes/desalination/post-treatment/post-treatments/boron-removal.htm.

[87] R. J. Larue, B. E. Mgmt, D. R. Latulippe, and D. Ph, "Industrial Separations Processes Introduction to the WAVE Design Software Custom Courseware," 2019.

[88] M. Wilf and C. Bartels, "Optimization of seawater RO systems design," *Desalination*, vol. 173, no. 1, pp. 1–12, 2005, doi: 10.1016/j.desal.2004.06.206.

[89] B. Huang, K. Pu, P. Wu, D. Wu, and J. Leng, "Design , Selection and Application of Energy," 2020.

[90] E. S. Mohamed and G. Papadakis, "Design, simulation and economic analysis of a stand-alone reverse osmosis desalination unit powered by wind turbines and photovoltaics," *Desalination*, vol. 164, no. 1, pp. 87–97, 2004, doi: 10.1016/S0011-9164(04)00159-6.

[91] S. Arenas Urrea, F. Díaz Reyes, B. Peñate Suárez, and J. A. de la Fuente Bencomo, "Technical review, evaluation and efficiency of energy recovery devices installed in the Canary Islands desalination plants," *Desalination*, vol. 450, no. July 2018, pp. 54–63, 2019, doi: 10.1016/j.desal.2018.07.013.

[92] C. Laprise, K. Cole, V. S. Sridhar, C. Crimi, L. West, and B. J. Foster, "WHO : World Health Organization," no. 514. pp. 1–32, 2019.

[93] A. Mollahosseini, A. Abdelrasoul, S. Sheibany, M. Amini, and S. K. Salestan, "Renewable energy-driven desalination opportunities – A case study," *J. Environ. Manage.*, vol. 239, no. January, pp. 187–197, 2019, doi: 10.1016/j.jenvman.2019.03.044.

A. Appendix A

PV modules MXPOWER C6X-325 P Datasheet

ENGINEERING DRAWING (mm)

Rear View

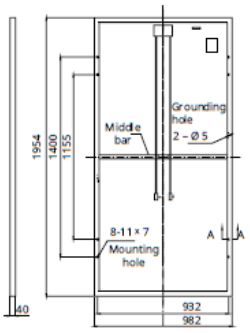

Frame Cross Section A-A

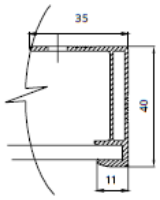

Mounting Hole

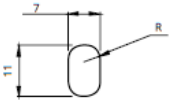

CS6X-320P / I-V CURVES

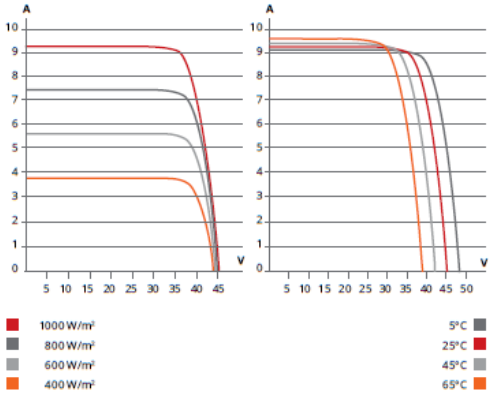

ELECTRICAL DATA | STC*

CS6X	310P	315P	320P	325P
Nominal Max. Power (Pmax)	310 W	315 W	320 W	325 W
Opt. Operating Voltage (Vmp)	36.4 V	36.6 V	36.8 V	37.0 V
Opt. Operating Current (Imp)	8.52 A	8.61 A	8.69 A	8.78 A
Open Circuit Voltage (Voc)	44.9 V	45.1 V	45.3 V	45.5 V
Short Circuit Current (Isc)	9.08 A	9.18 A	9.26 A	9.34 A
Module Efficiency	16.16%	16.42%	16.68%	16.94%
Operating Temperature	-40°C ~ +85°C			
Max. System Voltage	1000 V (IEC) or 1000 V (UL)			
Module Fire Performance	TYPE 1 (UL 1703) or CLASS C (IEC 61730)			
Max. Series Fuse Rating	15 A			
Application Classification	Class A			
Power Tolerance	0 ~ + 5 W			

* Under Standard Test Conditions (STC) of irradiance of 1000 W/m², spectrum AM 1.5 and cell temperature of 25°C.

MECHANICAL DATA

Specification	Data
Cell Type	Poly-crystalline, 6 inch
Cell Arrangement	72 (6 × 12)
Dimensions	1954 × 982 × 40 mm (76.9 × 38.7 × 1.57 in)
Weight	22 kg (48.5 lbs)
Front Cover	3.2 mm tempered glass
Frame Material	Anodized aluminium alloy
J-Box	IP67, 3 diodes
Cable	4 mm² (IEC) or 4 mm² & 12 AWG 1000V (UL), 1150 mm
Connector	T4-1000V or PV2 series
Per Pallet	26 pieces, 620 kg (1366.9 lbs)
Per Container (40' HQ)	624 pieces

ELECTRICAL DATA | NOCT*

CS6X	310P	315P	320P	325P
Nominal Max. Power (Pmax)	225 W	228 W	232 W	236 W
Opt. Operating Voltage (Vmp)	33.2 V	33.4 V	33.6 V	33.7 V
Opt. Operating Current (Imp)	6.77 A	6.84 A	6.91 A	6.98 A
Open Circuit Voltage (Voc)	41.3 V	41.5 V	41.6 V	41.8 V
Short Circuit Current (Isc)	7.36 A	7.44 A	7.50 A	7.57 A

* Under Nominal Operating Cell Temperature (NOCT), irradiance of 800 W/m², spectrum AM 1.5, ambient temperature 20°C, wind speed 1 m/s.

TEMPERATURE CHARACTERISTICS

Specification	Data
Temp. Coefficient (Pmax)	-0.41 % / °C
Temp. Coefficient (Voc)	-0.31 % / °C
Temp. Coefficient (Isc)	0.053 % / °C
Nominal Operating Cell Temperature	45±2 °C

PERFORMANCE AT LOW IRRADIANCE

Outstanding performance at low irradiance, average relative efficiency of 96.0 % from an irradiance of 1000 W/m² to 200 W/m² (AM 1.5, 25°C).

Ultrafiltration modules Datasheet

DUPONT

Product Data Sheet

IntegraFlux™ Ultrafiltration Modules

Model SFP-2860XP, SFD-2860XP, SFP-2880XP and SFD-2880XP

Description

IntegraFlux™ Ultrafiltration (UF) modules with XP fiber are made from high permeability, high mechanical strength, hollow fiber PVDF membranes. The modules provide excellent performance, industry leading membrane area with low energy and chemical consumption. IntegraFlux™ modules have the following general properties and characteristics:

- Up to 35% higher permeability than previous generation modules helping to improve operating efficiencies and productivity
- 0.03 µm nominal pore diameter for removal of bacteria, viruses, and particulates including colloids to protect downstream processes such as RO
- PVDF polymeric hollow fibers for high mechanical strength with excellent chemical resistance providing long membrane life and reliable operation
- Outside-In flow configuration allowing a wide range of solids in the feed water minimizing the need for pretreatment processes and reducing the backwash volume compared to Inside-Out configurations

These modules are an excellent choice for systems with capacities greater than 50 m^3/hr (220 gpm). The shorter SFP-2860XP or SFD-2860XP modules are well suited for installations with limited height. Larger and longer, 8 inch diameter and 80 inch in length, the SFP-2880XP or SFD-2880XP modules offer a high effective membrane area combined with high permeability that provides the most economical and efficient membrane system design.

IntegraFlux™ Ultrafiltration Modules can be used for a wide variety of treatment applications such as industrial and municipal wastewaters, surface water, and seawater.

Typical Properties

		Membrane Area		Volume		Weight (empty/water filled)	
Product	Type	m^2	ft^2	liters	gallons	kg/lbs	kg/lbs
SFP-2860XP	Industrial	51	549	35	9.3	48/83	106/183
SFD-2860XP	NSF/ANSI 61 and 419	51	549	35	9.3	48/83	106/183
SFP-2880XP	Industrial	77	829	39	10.3	61/100	135/220
SFD-2880XP	NSF/ANSI 61 and 419	77	829	39	10.3	61/100	135/220

Dimensions

SFP-2860XP, SFD-2860XP, SFP-2880XP, and SFD-2880XP (8-inch diameter)

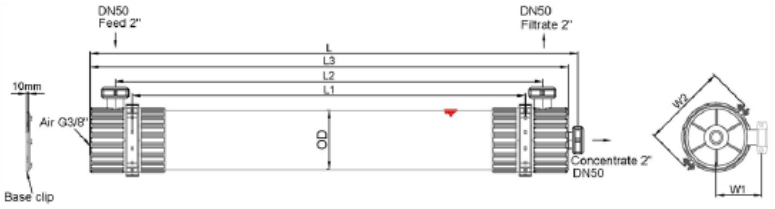

Product	Units	Length				Diameter	Width	
		L	L1	L2	L3	D	W1	W2
SFP-2860XP and SFD-2860XP	SI (mm)	1860±3	1500	1630±3	1820±3	225	180	342
	US (inch)	73.2±0.1	59.1	64.2±0.1	71.7±0.1	8.9	7.1	13.5
SFP-2880XP and SFD-2880XP	SI (mm)	2360±3	2000	2130±3	2320±3	225	180	342
	US (inch)	92.9±0.1	78.7	83.9±0.1	91.3±0.1	8.9	7.1	13.5

Suggested Operating Conditions

	SI Units	US Units
Filtrate Flux (25°C)	40 – 110 l/m^{2}hr	24 – 65 gfd
Flow Range Per Module[1]	2.0 – 8.5 m^3/hr	8.8 – 37.4 gpm
Temperature	1 – 40°C	34 – 104°F
Maximum Inlet Module Pressure (20°C)	6.25 bar	90.65 psi
Maximum Inlet Module Pressure (40°C)	4.75 bar	68.89 psi
Maximum Operating TMP	2.1 bar	30.5 psi
Maximum Operating Air Scour Flow	12 Nm^3/hr	7.1 scfm
Maximum Backwash Pressure	2.5 bar	36 psi
Operating pH	2 – 11	
Maximum NaOCl	2,000 mg/L	
Maximum Particle Size	300 µm	
Flow Configuration	Outside in, dead end flow	
Expected Filtrate Turbidity	≤ 0.1 NTU	
Expected Filtrate SDI	≤ 2.5	

[1] Flow range represents DUPONT™ Ultrafiltration SFP-2860XP, SFD-2860XP, SFP-2880XP, and SFP-2880XP Modules for filtrate flux range shown

Important Information

Proper start-up of an ultrafiltration system is essential to prepare the membranes for operating service and to prevent membrane damage. Following the proper start-up sequence also helps ensure that system operating parameters conform to design specifications so that system water quality and productivity goals can be achieved.

Before initiating system start-up procedures, membrane pretreatment, installation of the membrane modules, instrument calibration and other system checks should be completed.

Please refer to the Ultrafiltration Technical Manual (Form No. 45-D00874-en).

Reverse Osmosis membrane module Datasheet

SWC6 MAX

Specified Performance*

	Low Pressure:	High Flow:
Permeate Flow:	6,600 gpd (25 m^3/d)	13,200 gpd (50 m^3/d)
Salt Rejection:	99.6% (99.4% minimum)	99.8% (99.7% minimum)
Applied Pressure:	600 psi (4.1 MPa)	800 psi (5.4 MPa)

Test Conditions:
32000 ppm NaCl solution
600 psig (4.1 MPa) Applied Pressure
77 °F (25 °C) Operating Temperature
10% Permeate Recovery
6.5 - 7.0 pH Range

*The Specified Performance is based on data taken after a minimum of 10 minutes of operation. Actual testing of elements may be done at conditions which vary from these exact values; in which case, the performance is normalized back to these standard conditions. Permeate flow for individual elements may vary +25 / -15 percent from the value specified.

General Product Description**

Configuration:	Spiral Wound
Membrane Polymer:	Composite Polyamide
Membrane Active Area**:	440 ft^2 (40.9 m^2)

Packaging: All membrane elements are supplied with a brine seal, interconnector, and O-rings. Elements are enclosed in a sealed polyethylene bag containing less than 1.0% sodium meta-bisulfite solution, and then packaged in a cardboard box.

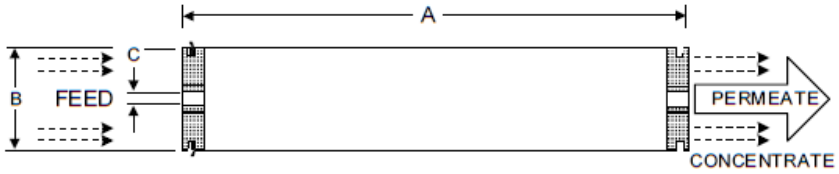

Element Details**

A, inches (mm)	B, inches (mm)	C, inches (mm)
40.0 (1016)	7.89 (200)	1.125 (28.6)

**Values listed are indicative, not specified. For more detailed specifications, see our Technical Service Bulletin documents or contact Hydranautics Technical Department.

Product Use and Restrictions^

Maximum Applied Pressure:	1200 psig (8.27 MPa)
Maximum Chlorine Concentration:	< 0.1 ppm
Maximum Operating Temperature:	113 °F (45 °C)
pH Range, Continuous (Cleaning):	2-11 (1-13)
Maximum Feedwater Turbidity:	1.0 NTU
Maximum Feedwater SDI (15 mins):	5.0
Maximum Feed Flow:	75 gpm (17.0 m^3/h)
Minimum Brine Flow:	12 gpm (2.7 m^3/h)
Maximum Pressure Drop for Each Element:	15 psi (0.10 MPa)

^ The limitations shown here are for general use. For specified projects, operation at more conservative values may ensure the best performance and longest life of the membrane. See Hydranautics Technical Bulletins for more details.

List of Figures

List of Tables

List of Symbols

Variable	Description	SI unit
TDS	Total dissolved solids	mg/l; ppm
Cf	Influent concentration of a specific component	-
Cp	Permeate concentration of a specific component	-
J	Flux of water membrane	
K	Water transport coefficient, equal to permeability/thickness of the membrane	-
ΔP	Pressure variation across the membrane.	
ΔΠ	Osmotic pressure variation across the membrane.	
SWRO	Seawater Reverse Osmosis	
BWRO	Brackish Water Reverse Osmosis	
ED	Electrodialysis	
MSF	Multi-Stage Flash	
MED	Multiple Effect Distillation	
MVC	Mechanical Vapor Compression	
TVC	Thermal Vapor Compression	
TPES	Total Primary Energy Supply	ktoe
TFC	Total Final Consumption	ktoe
ERD	Energy Recovery Device	
SEC	Specific Energy Consumption	kWh/m^3
GOR	Gain Output Ratio	

$\dot{m}_{distillate}$	Mass of distillate	kg
$\Delta hevap$	Latent heat of evaporation	kJ/kg
$\dot{Q}_{in}$	Mass of the input steam	kJ
PR	Performance Ratio	
TBT	Maximum Operating Brine Temperature	ºC
GHG	Green House Gas emissions	kgco2/m³ H2O
$CAPEX$	Total Capital Costs	€
$OPEX$	Operation and Maintenance Costs	€/y
$LCOE$	Levelized Cost of Energy	€/kWh
ORC	Organic Rankine Cycle	
CSP	Concentrating Solar Panels	
$LCOW$	Levelized Cost of Water	€/m³
RES	renewable Energies	
ADS	Autonomous Desalination System	
$HRES$	Hybrid Renewable Energy System	
$HOMER$	Hybrid Optimization of Multiple Energy Resources Software	
$PMPP$	Power Output of the PV system	kW
G	Global Solar Radiation (Beam and diffuse)	kW/m²
G_{Ref}	Maximum Global Solar Radiation	W/m²
$P_{SC,ref}$	Rated Capacity of the PV array	kW
f_{PV}	PV derating factor	
T_C	Cell Temperature	ºC

$T_{C,ref}$	Cell Reference Temperature	ºC
T_{amb}	Ambient Temperature	ºC
$NOCT$	Maximum cell Temperature	ºC
T_{NOCT}	Nominal operating cell Temperature	ºC
G_{NOCT}	Maximum solar radiation	W/m²
$ICCPV$	PV system initial capital costs	€
$RCPV$	PV system Replacement Costs	€
$OMCPV$	PV system Operation and Maintenance Costs	€/y
P_{wind}	average wind turbine power	kW
p	determined period of time	h
ρ	Density of air	kg/m³
C_p	capacity factor of the wind turbine	
A	Rotor surface of the wind turbine	m²
$f_{(v)}$	Weibull distribution	
v_x^3	velocity of the wind	m/s
$ICCWT$	WT system initial capital costs	€
$RCWT$	WT system Replacement Costs	€
$OMCWT$	WT system Operation and Maintenance Costs	€/y
E	Battery bank size capacity	kWh
n	efficiency of the batteries	
D_d	determined period in which the battery can store electrical energy	h
V_0	output voltage of the battery bank	V

C_N	capacity of the battery bank	Ah
CC	Cycle Charging energy strategy	
LF	Load Following energy strategy	
CD	Combined Dispatch energy strategy	
F	Fuel curve of the diesel generator	L/h
Y_{gen}	nominal capacity of the diesel generator	kW
P_{gen}	power output of the generator	kW
F_0	fuel curve y-intercept coefficient	
F_1	fuel curve slope	
$C_{gen,fixed}$	Fixed cost of energy of the generator	€
$C_{om,fixed}$	operational and maintenance cost of the diesel generator	€/h
$C_{rep,gen}$	Replacement cost of the diesel generator	€
R_{gen}	Lifetime of the diesel generator	y
F_0	fuel curve y-intercept coefficient	L/h/kW
$C_{fuel,eff}$	effective price of fuel	€/L
$C_{gen,margin}$	Marginal cost of energy of the diesel generator	€
NPC	Net Present Cost	€
CSF	Capacity shortage Fraction	
RP	Renewable Penetration	
TCE	Total Carbon Emissions	
CRF	Capital Recovery Factor	
d_r	real discount rate	
d_r'	interest rate	

C_{tot}	Total cost per year	€/y
f_r	inflation rate	
ROI	Return on Investment	
$C_{i,ref}$	nominal annual cash flow for base case system	
C_i	nominal annual cash flow for the current system	
WAVE®	Water Application Value Engine Software	
LSI	Langelier Saturation Index	
SDI	Silt Density Index	
CIP	Cleaning in place tank of the ultrafiltration process	
TOC	Total Organic Carbon (mg/l)	
TSS	Total Suspended solids (NTU)	
IMS Design®	Software from the company Hydronautics Nitto Group	
SI	Stoichiometric coefficients	

Acknowledgements

First and foremost, I have to thank my thesis supervisor, Mr. Giampaolo Manzolini, who gave me the opportunity to do a project related to renewable technologies and sustainable development that I am so passionate about.

It has been a pleasure to have done this work that I have enjoyed and worked so hard on, even though it has been a very complicated year due to the pandemic and not having had closer contact with my thesis supervisor.

Secondly, I also thank all my friends who accompanied me during the Master of Science in Energy Engineering at Politecnico di Milano, who made it the best experience of my life and for having constantly motivated me in the most difficult moments.

Most importantly, none of this could have happened without my family. I must express my very profound gratitude to my parents and my girlfriend for providing me with unfailing support and continuous encouragement throughout my years of study and through the process of researching and writing this thesis. This accomplishment would not have been possible without them.

I also place on record, my sense of gratitude to one and all, who directly or indirectly, have lent their hand in this venture.

Author

Alberto Pilato Colomar